

Electronic Thesis and Dissertation Repository

1-8-2013 12:00 AM

Development of Novel Nano-structured Materials with Low-Cost and High Stability for PEM Fuel Cell

Dongsheng Geng
The University of Western Ontario

Supervisor
Dr. Andy (Xueliang) Sun
The University of Western Ontario

Graduate Program in Mechanical and Materials Engineering
A thesis submitted in partial fulfillment of the requirements for the degree in Doctor of Philosophy
© Dongsheng Geng 2013

Follow this and additional works at: <https://ir.lib.uwo.ca/etd>

 Part of the [Nanoscience and Nanotechnology Commons](#)

Recommended Citation

Geng, Dongsheng, "Development of Novel Nano-structured Materials with Low-Cost and High Stability for PEM Fuel Cell" (2013). *Electronic Thesis and Dissertation Repository*. 1071.
<https://ir.lib.uwo.ca/etd/1071>

This Dissertation/Thesis is brought to you for free and open access by Scholarship@Western. It has been accepted for inclusion in Electronic Thesis and Dissertation Repository by an authorized administrator of Scholarship@Western. For more information, please contact wlsadmin@uwo.ca.

Development of Novel Nano-structured Materials with Low-Cost and High Stability
for PEM Fuel Cell

(Spine title: Nano-structured cathode Materials for fuel cell)

(Thesis format: Integrated Article)

by

Dongsheng Geng

Graduate Program in Mechanical and Materials Engineering

A thesis submitted in partial fulfillment
of the requirements for the degree of
Doctor of Philosophy

The School of Graduate and Postdoctoral Studies
The University of Western Ontario
London, Ontario, Canada

© Dongsheng Geng 2013

THE UNIVERSITY OF WESTERN ONTARIO
School of Graduate and Postdoctoral Studies

CERTIFICATE OF EXAMINATION

Supervisor

Examiners

Dr. Xueliang (Andy) Sun

Dr. Robert J. Klassen

Supervisory Committee

Dr. Liying Jiang

Dr. Liying Jiang

Dr. Paul A. Charpentier

Dr. Jun Yang

Dr. Aiping Yu

The thesis by

Dongsheng Geng

entitled:

**Development of Nano-structured Materials with Low-cost and High
Stability for PEM Fuel Cell**

is accepted in partial fulfillment of the
requirements for the degree of
Doctor of Philosophy

Date

Chair of the Thesis Examination Board

Abstract

Polymer electrolyte membrane fuel cells (PEMFCs) are non-polluting and efficient energy conversion devices that are expected to play a dominant role in energy solutions of the future. However, due to high cost and known degradation issue of Pt electrocatalyst, more durable, efficient, and inexpensive electrocatalysts are required before fuel cells can become commercially viable. This research is revolving around the development of electrocatalysts such as non-noble metal oxygen reduction reaction (ORR) catalyst, new alternative supports, and novel Pt nanostructures to address the above-mentioned challenges in PEMFCs.

Firstly, we report the synthesis of nitrogen doped carbon nanotubes (CN_x) and nitrogen doped graphene (N-graphene) with the various nitrogen contents. The relationship between structures and ORR activity is investigated in detail. We identified the real active site by the study. Most importantly, CN_x and N-graphene have the comparable ORR activity even the improved durability compared with a platinum-based catalyst, showing the potential to replace costly Pt/C catalyst in alkaline fuel cells.

Secondly, due to the advantages of N-graphene as not only a support of Pt but the non-noble metal ORR catalyst, we developed three different methods to prepare it: (i) post-treatment of graphene with ammonia (ii) from CN_x to N-graphene directly (iii) one-step solvothermal process. Especially, by the solvothermal method, for the first time, nanoflower-like N-graphene was obtained with pure sp² hybridized carbon and the controllable nitrogen types. Importantly, the synthesized materials exhibit much higher durability as Pt support for fuel cells than commercial carbon powder.

Thirdly, previous results have shown that star-like Pt nanowires have both good catalytic activity and durability for ORR. However, there is a limitation in scale up and controlling length and shape of Pt nanowire for previous method. Here we report a universal method to address the challenge. It is a very simple, green and efficient wet chemical route without any surfactant and template to produce urchin-shaped Pt nanostructures in high yield.

In summary, the discoveries in this thesis contribute to development of fuel cell cathode electrocatalysts and make the improvement in electrocatalyst cost and stability.

Keywords

Polymer electrolyte membrane Fuel cells, Oxygen reduction reaction, Durability, Electrocatalyst, Non-noble metal catalyst, Nitrogen doped carbon nanotubes, Graphene, Nitrogen doped graphene, Pt nanoparticles, Solvothermal method, Dendritic Pt nanostructures.

Co-Authorship Statement

1.

Title: Non-Noble Metal Oxygen Reduction Electrocatalysts Based on Carbon Nanotubes with Controlled Nitrogen Contents

Authors: Dongsheng Geng, Hao Liu, Yougui Chen, Ruying Li, Xueliang Sun, Siyu Ye, and Shanna Knights

All the experimental and theoretical work was carried out by Dongsheng Geng under the guidance of Dr. Xueliang Sun. Hao Liu did previous research work on the synthesis of nitrogen doped carbon nanotubes. Siyu Ye revised the manuscript. The other coauthors contributed to the formation of the final version with discussion and related characterization. The final version of this manuscript has been published in *Journal of Power sources*, 2011, **196**, 1795-1801.

2.

Title: Nitrogen Doping Effects on the Structure of Graphene

Authors: Dongsheng Geng, Songlan Yang, Yong Zhang, Jinli Yang, Jian Liu, Ruying Li, Tsun-Kong Sham, Xueliang Sun, Siyu Ye, and Shanna Knights

Dongsheng Geng designed and conducted experiments, collected data, and wrote the manuscript. The initial draft and the followed modifications of this manuscript were conducted by Dongsheng Geng under the supervision of Dr. Xueliang Sun. Songlan Yang did the experiment of near-edge X-ray absorption fine structure (NEXAFS). Tsun-Kong Sham revised the data analysis of NEXAFS and the manuscript. The other coauthors contributed to the formation of the final version with discussion and related characterization. The final version of this manuscript has been published in *Applied Surface Science*, 2011, **257**, 9193-9198.

3.

Title: High Oxygen-Reduction Activity and Durability of Nitrogen-doped Graphene

Authors: Dongsheng Geng, Ying Chen, Yougui Chen, Yongliang Li, Ruying Li, Xueliang Sun, Siyu Ye, and Shanna Knights

Dongsheng Geng designed and conducted experiments, collected data, and wrote the manuscript. The initial draft and the followed modifications of this manuscript were conducted by Dongsheng Geng under the supervision of Dr. Xueliang Sun. Siyu Ye revised the manuscript. The other coauthors contributed to the formation of the final version with discussion and related characterization. The final version of this manuscript has been published in *Energy & Environmental Sciences*, 2011, **4**, 760-764.

4.

Title: Nitrogen doped graphene oxide nanoribbons from Nitrogen doped carbon nanotubes

Authors: Dongsheng Geng, Yuhai Hu, Jian Liu, Ruying Li, Xueliang Sun, Siyu Ye, and Shanna Knights

Dongsheng Geng designed and conducted experiments, collected data, and wrote the manuscript. Jian Liu did previous research work on the synthesis of nitrogen doped carbon nanotubes. The other coauthors contributed to the formation of the final version with discussion and related characterization. The final version of this manuscript is to be submitted for publishing.

5.

Title: One-pot Solvothermal Synthesis of Doped Graphene with the Designed Nitrogen Type Used as a Pt Support for Fuel Cells

Authors: Dongsheng Geng, Yuhai Hu, Yongliang Li, Ruying Li, and Xueliang Sun

Dongsheng Geng designed and conducted experiments, collected data, and wrote the manuscript. The initial draft and the followed modifications of this manuscript were conducted by Dongsheng Geng under the supervision of Dr. Xueliang Sun. The other coauthors contributed to the formation of the final version with discussion and related

characterization. The final version of this manuscript has been published in *Electrochemistry Communications*, 2012, **22**, 65-68.

6.

Title: A universal method to synthesize urchin-shaped Pt nanostructures

Authors: Dongsheng Geng, Shuhui Sun, Jinli Yang, Ruying Li, and Xueliang Sun

Dongsheng Geng designed and conducted experiments, collected data, and wrote the manuscript. The initial draft and the followed modifications of this manuscript were conducted by Dongsheng Geng under the supervision of Dr. Xueliang Sun. The other coauthors contributed to the formation of the final version with discussion and related characterization. The final version of this manuscript will be submitted for publishing.

Acknowledgments

This PhD work was carried out in Dr. Sun's group at the University of Western Ontario. It is my pleasure to convey my sincere acknowledgements to every individual who contributed to my research and made this thesis possible.

At this moment, I would like to express my deep gratitude first to my supervisor, Dr. Xueliang Sun, the Canada Research Chair in Nanomaterials for Clean Energy, a professor in the Department of Mechanical & Materials Engineering at UWO, for providing me the opportunity to come to Canada and work under his guidance. His profound knowledge, rigorous attitude and enthusiasm in research benefit me for life long.

I am very grateful to Ms. Ruying (Kathy) Li, Dr. Sun's wife and a research engineer in the group. She arranges everything perfect in our lab and enables us to do research smoothly. I would like to express my acknowledgements to Dr. Siyu Ye at Ballard and Prof. Tsun-Kong Sham at Department of chemistry, the University of Western Ontario, for their kind guidance and fruitful discussion on my work.

I also would like to thank Dr. Paul Charpentier, a professor in the Department of Biochemical and Chemical Engineering at UWO, Dr. Robert Klassen, Dr. Liying Jiang, the professors in MME at UWO, and Dr. Aiping Yu, a professor in chemical engineering at the University of Waterloo. As examiners of my defense, they all provided many helpful suggestions to improve my thesis.

Many thanks to all my group members in Dr. Xueliang (Andy) Sun's group, Dr. Yong Zhang, Dr. Xiangbo (Henry) Meng, Dr. Shuhui Sun, Dr. Gaixia Zhang, Dr. Jiajun Wang, Dr. Mohammad Norouzi Banis, Dr. Yougui Chen, Dr. Hao Liu, Dr. Yu Zhong, Dr. Yuhai Hu, Dr. Xifei Li, Dr. Liang Li, Harmid Norouzi Banis, Yongliang Li, Dongniu Wang, Jinli Yang, Jian Liu, Dr. Mihnea Ioan Ionescu, Dr. Niancai Cheng, Dr. Dawei Wang, Dr. Kun Chang, and Dr. Ying Chen. It was a so much pleasure to work with so many nice people. Without their collaboration, generous help, my project could not have been done so smoothly.

I would also like to thank the help from Tim Stephens, the technician in the Department of Civil and Environmental Engineering with the characterization of inductive coupled plasma-

optical emission spectroscopy (ICP-OES). I also appreciate Mr. Fred Pearson at McMaster University, who assisted me with HRTEM observation. My thanks also go to Mark C. Biesinger, a senior research scientist in surface science western, who helped me finish x-ray photoelectron spectroscopy (XPS) test and analysis.

Specially, I would like to express my sincere gratitude towards my parents and parents-in-law, for their understanding, support and encouragement, especially my heartiest thanks to my wife (Xiaohui Liu) for her love and dedication. I would also like to say “thanks” to my lovely daughter, Zichun for her contributions to our family with so much happiness.

Dongsheng Geng
1796 Devos Dr.
London, ON, Canada, N5X 4H9
January 09, 2013

Table of Contents

CERTIFICATE OF EXAMINATION	ii
Abstract	iii
Keywords	iv
Co-Authorship Statement.....	v
Acknowledgments.....	viii
Table of Contents	x
List of Tables	xv
List of Figures	xvi
List of Abbreviations	xxi
Chapter 1	1
1 Introduction	1
1.1 Fundamentals of PEM fuel cells.....	1
1.2 Challenges of PEM fuel cells.....	3
1.3 Solutions for catalyst development.....	5
1.3.1 Modifying Pt main catalyst.....	6
1.3.2 Looking for the novel supports	7
1.3.3 Developing non-precious metal ORR catalyst.....	8
1.4 Objectives of thesis	10
1.5 Thesis structure	11
References	14
Chapter 2	21
2 Experimental and characterization techniques.....	21
2.1 Experimental.....	21

2.1.1	Synthesis of carbon nanotubes with the controlled nitrogen contents via a floating catalyst chemical vapour deposition method.....	21
2.1.2	Synthesis of graphene by modified Hummers' method.....	22
2.1.3	Synthesis of nitrogen doped graphene	22
2.1.4	Synthesis of S, P doped graphene	24
2.1.5	Synthesis of dendritic Pt nanostructures via a universal chemical method	24
2.2	Characterization techniques	25
2.2.1	Physical characterization (SEM, TEM, XPS, XRD, BET, and Raman spectra).....	25
2.2.2	Electrochemical characterization	27
	References	31
	Chapter 3.....	34
3	Non-Noble Metal Oxygen Reduction Electrocatalysts Based on Carbon Nanotubes with Controlled Nitrogen Contents	34
3.1	Introduction.....	36
3.2	Experimental.....	37
3.2.1	Preparation of CN _x	37
3.2.2	Physical characterizations	37
3.2.3	Electrochemical characterization	37
3.3	Results and discussion	38
3.3.1	SEM, TEM and XPS analysis.....	38
3.3.2	ORR activities of CN _x in acid solution	40
3.3.3	ORR activities of CN _x in alkaline solution	44
3.4	Conclusions.....	49
	Acknowledgments.....	49
	References	50
	Chapter 4.....	54

4	Nitrogen doping effects on the structure of graphene	54
4.1	Introduction.....	56
4.2	Experimental.....	57
4.2.1	Preparation of graphene and N-graphene	57
4.2.2	Physical characterizations.....	58
4.3	Results and discussion	58
4.4	Conclusions.....	67
	Acknowledgments.....	68
	References	68
	Supporting information	73
	Chapter 5.....	74
5	High Oxygen-Reduction Activity and Durability of Nitrogen-doped Graphene.....	74
5.1	Introduction.....	76
5.2	Experimental.....	77
5.3	Results and discussion	77
5.4	Conclusions.....	84
	Acknowledgments.....	84
	References	84
	Chapter 6.....	88
6	Nitrogen doped graphene oxide nanoribbons from Nitrogen doped carbon nanotubes88	
6.1	Introduction.....	89
6.2	Experimental.....	90
6.3	Results and discussion	90
6.4	Conclusions.....	95
	Acknowledgments.....	95
	References	96

Chapter 7.....	99
7 One-Pot Solvothermal synthesis of doped graphene with the designed nitrogen type used as a Pt support for fuel cells.....	99
7.1 Introduction.....	101
7.2 Experimental.....	102
7.2.1 Sample preparation and characterization.....	102
7.2.2 Electrochemical test.....	103
7.3 Results and discussion.....	103
7.4 Conclusions.....	109
Acknowledgements.....	109
References.....	109
Supporting information.....	113
Chapter 8.....	115
8 A universal method to synthesize urchin-shaped Pt nanostructures.....	115
8.1 Introduction.....	117
8.2 Experimental.....	118
8.2.1 Materials.....	118
8.2.2 Typical synthesis of urchin-shaped Pt nanostructures.....	118
8.2.3 Characterization.....	119
8.2.4 Electrochemical test.....	119
8.3 Results and discussion.....	120
8.4 Conclusions.....	125
Acknowledgements.....	125
References.....	125
Supporting information.....	129
Chapter 9.....	133

9 Conclusions and Suggestions.....	133
9.1 Conclusions.....	133
9.2 Suggestions	135
APPENDICES	136
CURRICULUM VITAE.....	143

List of Tables

Table 3-1 Surface composition (at. %) determined with XPS experiments.	40
Table 3-2 The onset electrode potentials for the ORR on various CN_x electrodes.....	42
Table 4-1 Specific surface area of graphene and N-graphene determined by BET method...	59
Table 4-2 X-ray structural parameters of graphene and N-graphene from plane (002).	62
Table 5-1 Distribution of N species obtained from the de-convolution of the N1s peaks by XPS.	80

List of Figures

Figure 1-1 Maximum H ₂ fuel cell efficiency at standard pressure, with reference to higher heating value. The Carnot limit is shown for comparison, with a 50 °C exhaust temperature.	1
Figure 1-2 Schematic of the working principle for PEMFCs.	2
Figure 1-3 Low temperature fuel cell losses.	3
Figure 1-4 Pie chart of stack baseline cost.	4
Figure 1-5 Degradation processes of Pt nanoparticles on carbon support.	5
Figure 1-6 Summary of the progress over recent years with respect to transition metal oxide, carbide and nitride based materials as ORR electrocatalysts [56].	9
Figure 1-7 Research topic of PEM fuel cell catalyst.	10
Figure 2-1 The schematic drawing of our synthesis stratagem of nitrogen doped carbon nanotubes.	21
Figure 2-2 The schematic process for graphene synthesis.	22
Figure 2-3 Schematic of CVD synthesis of N-graphene.	23
Figure 2-4 A photo of our SEM (Hitachi S-4800).	25
Figure 2-5 A photo of our TEM (Philips CM10).	26
Figure 2-6 Autolab potentiostat/galvanostat (Model, PGSTAT-30, Ecochemie, Brinkman Instruments) with rotation control (MSR, Pine Instruments).	28
Figure 2-7 Sketch of a rotating ring-disk electrode apparatus [11].	28
Figure 2-8 Analysis of a linear sweep voltammogram (Pt/C, 0.05 – 1.20 V vs. SHE, 5 mV s ⁻¹ , 1600 rpm, saturated O ₂ , 0.5 M H ₂ SO ₄ , room temperature).	29

Figure 2-9 Analysis of cyclic voltammogram (Pt/C, 0.05 – 1.20 V vs. SHE, 50 mV s ⁻¹ , saturated N ₂ , 0.5 M H ₂ SO ₄ , room temperature).....	31
Figure 3-1 (a) SEM image of CN _x prepared with 200 mg of melamine; (b) the magnified images.	38
Figure 3-2 TEM images of CN _x prepared with various amount of melamine: (a) 50 mg, (b) 200 mg, (c) 400 mg, (d) 2000 mg.	39
Figure 3-3 (a) Typical CV curves of CN _x (7.7%) in 0.5 M H ₂ SO ₄ . Scan rate: 5 mVs ⁻¹ ; rotation speed: 900 rpm. (b) ORR polarization curves at a rotation speed of 900 rpm for the different CN _x with the loading of 160 μg cm ⁻²	41
Figure 3-4 Oxygen reduction currents for CN _x (7.7%) in 0.5 M H ₂ SO ₄ with saturated O ₂ . Scan rate: 5 mV s ⁻¹	43
Figure 3-5 I _{Disk} , I _{Ring} , n (the apparent number of electrons transferred during ORR), and %H ₂ O ₂ measured by RRDE in O ₂ saturated H ₂ SO ₄ at room temperature for CN _x (7.7%). ...	43
Figure 3-6 Measured ORR currents of CN _x (7.7%) catalyst at different electrode rotation speed (a) and different catalyst loading (b). Scan rate: 5 mV s ⁻¹ , electrolyte: 0.1 M KOH....	45
Figure 3-7 The polarization curves of oxygen reduction on CN _x catalysts with different nitrogen content. Electrolyte: 0.1 M KOH, scan rate: 5 mV s ⁻¹ , and rotation speed: 1600 rpm.	47
Figure 3-8 RRDE voltammograms of CN _x (7.7%) and Pt/C with different loading in 0.1 M KOH solution saturated with O ₂ . The ring-disk electrode rotation rate was 1600 rpm, and the Au ring electrode was held at 0.7 V.....	47
Figure 4-1 SEM and TEM images of graphene (a, c) and N-graphene samples (b, d).....	59
Figure 4-2 Raman spectra of graphene and N-graphene samples.....	60
Figure 4-3 XRD patterns of graphene and N-graphene samples.	61
Figure 4-4 Infrared spectra of graphene and N-graphene samples.	63

Figure 4-5 XPS spectra of graphene and N-graphene samples. The inset: the high resolution N1s spectra of N-graphene sample: The pink and black lines are the raw and fitted spectra. The red, green, and blue lines correspond to pyridine-like N (398.1 eV), pyrrole-like N (399.9 eV), and quaternary N (401.3 eV), respectively.....	64
Figure 4-6 (a) and (b) TEY of the C K-edge and N K-edge XANES spectra of graphene and N-doped graphene, (c) FLY of the XANES spectra of the N-doped graphene, and (d) TEY of the O K-edge XANES spectra of graphene and N-doped graphene.....	66
Figure 4-7 (a) Typical TEM image of S-graphene; (b) XPS survey scan spectra of S-graphene; (c) Deconvoluted XPS spectrum of the S-2p-orbital for S-graphene.	73
Figure 5-1 The linear-sweep voltammograms of graphene and N-graphene under different temperatures. Electrolyte: O ₂ -saturated 0.1 M KOH, scan rate: 5 mV s ⁻¹ , and rotation speed: 1600 rpm.	78
Figure 5-2 The typical SEM (a) and TEM (b) images for N-graphene (900). (c) The Raman spectrum of graphene and N-graphene (900). (d) The XPS survey for three samples; (e) the high-resolution N1s spectrum for N-graphene: the black and purple lines are the raw and fitted spectra; the red, green, and blue lines correspond to pyridine-like N (398.1 eV), pyrrole-like N (399.9 eV), and quaternary N (401.3 eV), respectively.	79
Figure 5-3 (a) Measured ORR currents of N-graphene (900) catalyst at different electrode rotation speed and (b) Koutecký-Levich plot at -0.5 V using the data obtained from (a). (c) and (d): The current density of ring and disk measured by RRDE for N-graphene (900). Scan rate: 5 mV s ⁻¹ , electrolyte: 0.1 M KOH.	82
Figure 5-4 (a) The polarization curves of oxygen reduction on N-graphene (900) and Pt/C (E-TEK) catalysts. Electrolyte: 0.1 M KOH, scan rate: 5 mV s ⁻¹ , and rotation speed: 1600 rpm. (b) Cyclic voltammograms of N-graphene (900) in N ₂ -saturated 0.1 M KOH (the black line) and O ₂ -saturated 0.1 M KOH after 50, 500, 1000, 2000, 3000, 4000, and 5000 potential cycles, respectively. Potential Sweep rate: 100 mV s ⁻¹ . (c) Dependence of the current density for the ORR at 0.05 V on the potential cycles evaluated from the cyclic voltammograms....	83

Figure 6-1 (a) The SEM image of the pristine carbon nanotubes (b, c) the TEM pictures of graphene oxide nanoribbons; (d) the TEM of home-made CN_x , and (e, f) the TEM images of nitrogen doped graphene oxide nanoribbons.	91
Figure 6-2 The HRTEM images of (a) the pristine CN_x and (b) nitrogen doped graphene oxide nanoribbons.	92
Figure 6-3 The Raman spectra of MWCNTs and CN_x	93
Figure 6-4 (a) XPS spectra of CN_x and NGON. (b) the high resolution N1s spectra of CN_x and NGON	94
Figure 7-1 (a), (b) SEM and TEM images of the synthesized NG. (c) A high-resolution TEM micrograph of NG. (d) Electron diffraction pattern of NG.	104
Figure 7-2 The high-resolution N1s spectrum for NG: the black and cyan lines are the raw and fitted spectra; the red and green lines correspond to pyridine-like N (398.5 eV) and quaternary N (401.3 eV), respectively.	105
Figure 7-3 (a) and (b): TEM images of Pt/NG and Pt/C (homemade). (c) CV curves of Pt/NG for the different cycles. Scan rate: 50 mV/s. (d) Normalized ECSA of Pt/NG, Pt/C (homemade), and commercial Pt/C.	106
Figure 7-4 Raman spectra of NG and Vulcan XC-72.	107
Figure 7-5 Schematic description of NG formation process.	108
Figure 7-6 (a) SEM and (b) TEM images of Pt/graphene; (c) SEM and (d) TEM images of Pt/N-graphene. Graphene and N-graphene samples from Hummers' method (please see Chapter 4), Pt nanoparticles deposition is done based on reference 24 in this chapter.	113
Figure 7-7 Cyclic voltammograms of: (a) Pt/C (E-TEK), (b) Pt/graphene, (c) Pt/N-graphene (2.8 at.% N) after 50, 500, 1000, 1500, 2000, 2500, 3000, 3500, 4000 cycles, and (d) the comparison of the degradations of the thee catalysts. Scan rate: 50 mV/s.	114
Figure 8-1 TEM images of urchin-shaped Pt nanostructures from the various reductants: (a) methanol (b) ethanol (c) 2-propanol (d) ethylene glycol (e) formaldehyde (f) formic acid.	122

Figure 8-2 HRTEM images of urchin-shaped Pt nanostructures from the different reductants: (a) methanol (b) ethanol (c) ethylene glycol (d) formaldehyde. The insets are the corresponding SAED pictures.....	123
Figure 8-3 Normalized ECSA of urchin-like Pt nanostructures and commercial Pt/C.	124
Figure 8-4 TEM images of Pt nanostructures from the various reductants and under pH = 2: (a) methanol (b) formaldehyde (c) formic acid.....	129
Figure 8-5 TEM images of Pt nanostructures from the various reductants under the existence of NO_3^- ($[\text{Pt}]:[\text{NO}_3^-] = 1 : 10$): (a) methanol (b) ethanol (c) 2-propanol (d) ethylene glycol (e) formaldehyde (f) formic acid.	130
Figure 8-6 TEM images of Pt nanostructures from the various reductants under the existence of Fe^{3+} ($[\text{Pt}]:[\text{Fe}^{3+}] = 1 : 10$): (a) methanol (b) ethanol (c) 2-propanol (d) ethylene glycol (e) formaldehyde (f) formic acid.	131
Figure 8-7 Urchin-shaped Pt nanostructures growth on carbon black (Vulcan XC-72); the reductant is formaldehyde.....	132

List of Abbreviations

2D: two-dimensional

3D: three-dimensional

A

ADT: Accelerated durability test

B

BET: Brunauer, Emmett, and Teller

C

CN_x: nitrogen doped carbon nanotubes

CV: Cyclic voltammograms

CVD: chemical vapour deposition

D

DOS: density of state

E

ECSA: electrochemical active surface area

F

FLY: fluorescence yield mode

FT-IR: Fourier transform-infrared

G

GC: glassy carbon

GON: graphene oxide nanoribbon

H

HRTEM: High-resolution transmission electron microscopy

I

ICP-OES: inductive coupled plasma-optical emission spectroscopy

K

K-L: Koutecky-Levich

M

MEA: Membrane electrode assembly

MOR: methanol oxidation reaction

MWNTs: multiwall carbon nanotubes

N

N-graphene: nitrogen doped graphene

NEXAFS: near-edge X-ray absorption fine structure

NGON: N-graphene oxide nanoribbons

NSTF: nanostructured thin film

O

ORR: oxygen reduction reaction

P

PEMFCs: Polymer electrolyte membrane fuel cells

R

RRDE: rotating ring disk electrode

S

SAED: selected area electron diffraction

SEM: scanning electron microscopy

SGM: Spherical Grating Monochromator

SHE: standard hydrogen electrode

SWCNTs: single-wall carbon nanotubes

T

TEM: transmission electron microscopy

TEY: total electron yield

THH: tetrahedral

TPP: triphenylphosphine

TSA: toluenesulfonic acid

X

XANES: X-ray Absorption Near Edge Structure

XPS: x-ray photoelectron spectroscopy

XRD: X-ray diffraction

Chapter 1

1 Introduction

1.1 Fundamentals of PEM fuel cells

Energy shortages and environmental pollution are serious challenges that humanity will face for the long-term. The world power demand is expected to double from 14 terawatts (TW) in the year 2000 to 28 TW by the year 2050 [1]. Fuel cells are innovative energy conversion devices that, with the help of catalysts, convert chemical energy to electrical energy [2]. As long as fuel is supplied, the fuel cell will continue to generate power. Since the conversion of the fuel to energy takes place via an electrochemical process, not combustion, the process is clean, quiet, and highly efficient—two to three times more efficient than fuel burning (see Fig.1-1) [3]. At about 200 °C, fuel cell can have 77% efficiency, whereas the efficiency limit is only 30% for heat engine such as steam or gas turbines. Therefore, fuel cells have the potential to solve both energy crisis and pollution problems.

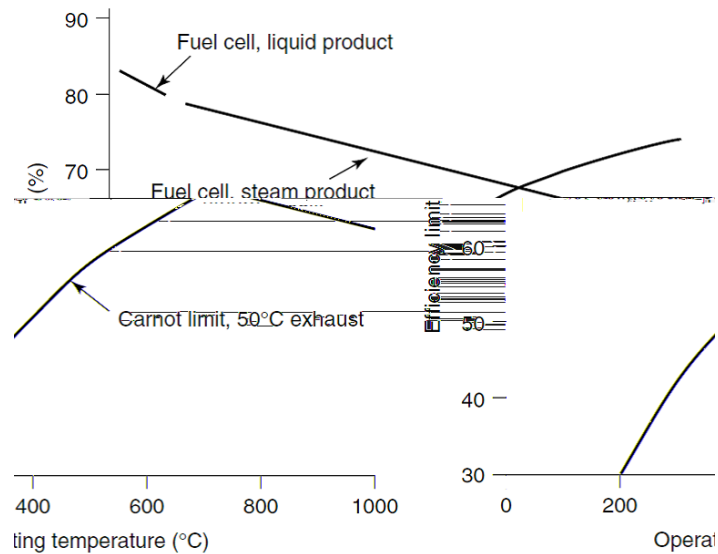


Figure 1-1 Maximum H₂ fuel cell efficiency at standard pressure, with reference to higher heating value. The Carnot limit is shown for comparison, with a 50 °C exhaust temperature.

Among various types of fuel cells [3], Proton Exchange Membrane Fuel Cells (PEMFCs) are attracting much more attention, and may, eventually, become a choice for power production due to their many advantages. They are all solid-state and compact, and can thus provide high power density. Their low operating temperature should also lead to quick start up and shut down. The tolerance of PEM fuel cells to the presence of CO₂ is attractive in comparison with other fuel cells, which can also exhibit high power density and fast start up.

Membrane electrode assembly (MEA) is the heart of a single PEMFC, which consists of two electrodes (anode and cathode) and a separating proton exchange membrane (usually Nafion[®]). The schematic of MEA is shown in Fig.1-2. A stream of hydrogen is delivered

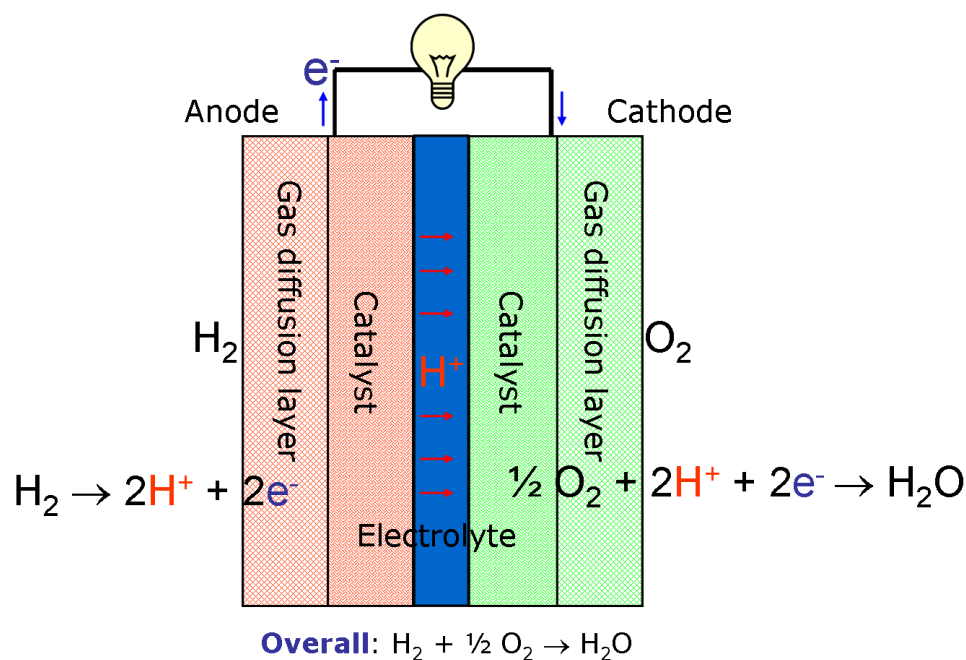


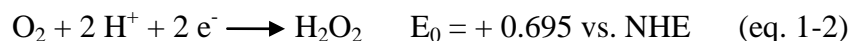
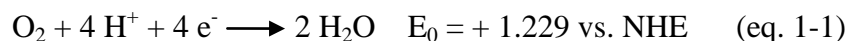
Figure 1-2 Schematic of the working principle for PEMFCs.

to the anode side of the MEA. It is catalytically split into protons and electrons. The newly formed protons permeate through the polymer electrolyte membrane to the cathode side. The electrons travel along an external load circuit to the cathode side of the MEA, thus creating the current output of the fuel cell. Meanwhile, a stream of oxygen is delivered to the cathode side of the MEA. At the cathode side oxygen molecules react with the protons permeating through the polymer electrolyte membrane and the electrons

arriving through the external circuit to form water molecules. In the whole process, only electricity and water is produced. Therefore it is an environmentally friendly device. Each individual cell produces a voltage of about 0.6-0.7 V. To provide a suitable voltage, individual cells are stacked to form a fuel cell stack [4].

1.2 Challenges of PEM fuel cells

As introduced above, the oxygen reduction reaction (ORR) is the cathode reaction for PEMFCs. The oxygen reacts on the cathode side of the PEMFCs with protons and electrons to form water or hydrogen peroxide according to the half-cell redox process (eq. 1-1 and 1-2).



The direct four electron process of oxygen reduction to form water is the preferred and desired reaction pathway. Hydrogen peroxide formation via direct two electron process is the competitive reaction and leads to significant cell voltage and overall efficiency losses in PEMFCs due to the sluggish rate limiting reaction [5]. Figure 1-3 showed the detailed

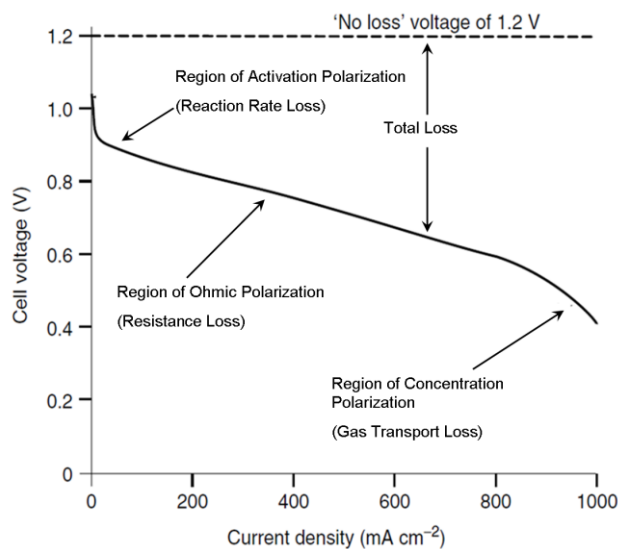


Figure 1-3 Low temperature fuel cell losses.

fuel cell losses, which can be broken up into four different types. These are activation losses, fuel crossover/internal current losses, ohmic losses, and mass transport/concentration losses. These losses each have a different effect on the theoretical voltage of the fuel cell [3]. To decrease the reaction rate loss, new developed and designed PEM fuel cell cathode catalysts need a maximum reducing of the hydrogen peroxide formation. Therefore, one of challenges for PEM fuel cells we are facing is still the activity of cathode catalysts. In addition, the higher cost is another barrier for the commercialization of fuel cell. Figure 1-4 shows the stack cost breakdown pie chart [6]. The electrodes represent approximately 77% of the fuel cell stack cost due to the most common, but expensive, platinum electrocatalyst. As the demand for Pt grows, the price of Pt has increased by almost three times from \$520 per oz in 2002 to \$1500 per oz in 2012 over the last decade [7]. Currently, the amount of platinum catalyst required per kilowatt to power a fuel cell engine is about 0.5 to 0.8 grams, or 0.018 to 0.028 ounces, which means the platinum catalyst alone would cost between \$2,300 to \$3,700 to operate a small, 100-kilowatt two- or four-door vehicle. To make the transition to fuel cell-powered vehicles possible, it is necessary to reduce the utilization of Pt and keep higher performance.

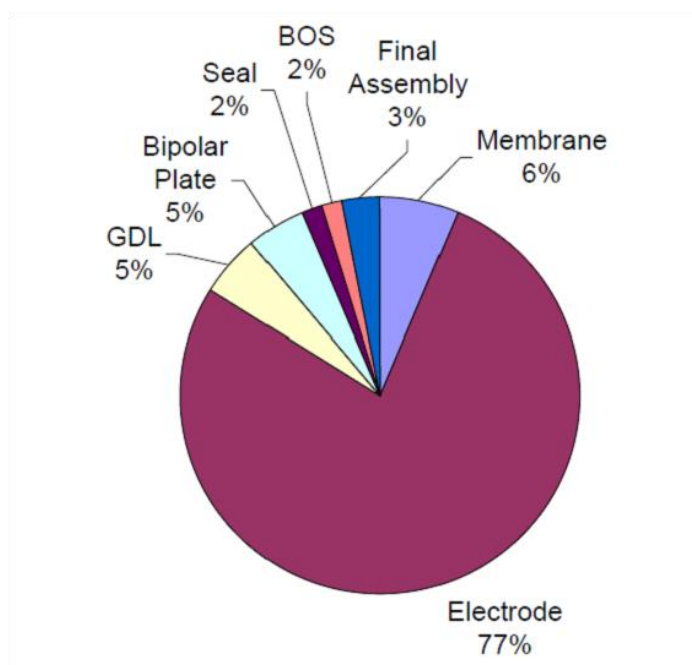


Figure 1-4 Pie chart of stack baseline cost.

Another bottleneck problem in PEMFCs development is the limited electrochemical stability of the current catalysts (Pt nanoparticles supported on porous carbon). Figure 1-5 showed the detailed schematic for the degradation of Pt/C catalyst [8]. During the duty cycles of repeated start-ups and shut-downs, the fuel cell undergoes high potentials that lead to carbon and Pt degradation processes. Pt is dissolved and/or sintered into bigger agglomerates. Meanwhile, the agglomeration process is accelerated by carbon corrosion in oxidative conditions. As a consequence, Pt particles are detached from their support and tend to gather together, which results in the lower fuel cell performance. The degradation of Pt/C has been recognized as one of the main contributors to the long-term degradation of fuel cell performance [9-11].

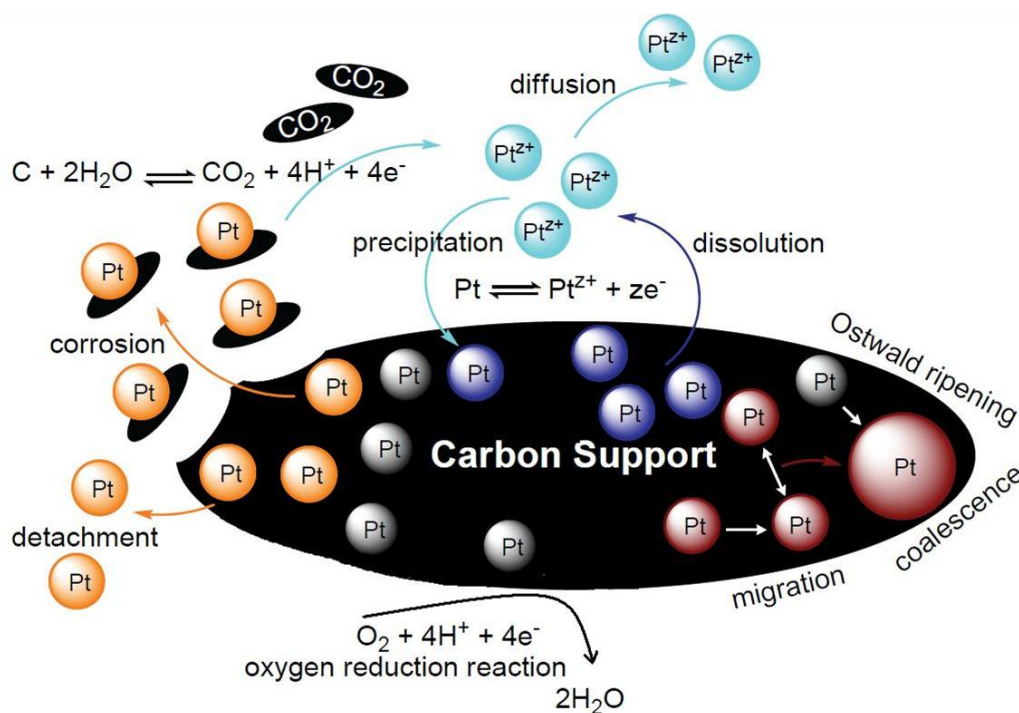


Figure 1-5 Degradation processes of Pt nanoparticles on carbon support.

More durable, efficient, and inexpensive fuel cell electrocatalysts are desperately required before fuel cells can become commercially viable.

1.3 Solutions for catalyst development

Much of the current research on catalysts for PEM fuel cells can be classified into three categories [12]: (I) modifying Pt main catalyst--lower platinum content and improve its

activity and durability by changing catalyst particle, morphology and crystal structure; even alloy Pt with less expensive metals such as Fe, Co, Mn, Ni, Cu and others (II) looking for the novel support such as novel carbon supports, alternative carbon structures, and non-carbon supports (III) developing non-precious metal ORR catalyst.

1.3.1 Modifying Pt main catalyst

The size, shape and dispersion uniformity of Pt nanoparticles on supporting materials have significant effects on the catalytic activity. Great effort has been made to control the size of Pt nanoparticles in order to increase their catalytic activities. The maximum mass activity could be achieved at a particle size of 3-4 nm for ORR [13]. Recent studies demonstrated that the Pt nanoparticles with a diameter of 3 nm have better electrochemical stability than those of size 1.8 nm. Because the adsorption behaviors of species involved in the electrochemical reaction appears differently on various facets of the nanocrystals, platinum nanocrystals having well-defined shapes, such as cubes, octahedrons, tetrahedrons, and their overgrown forms, have been achieved and studied [14-16]. Some unconventional shapes, for instance, Pt tetrahedral (THH) nanocrystals, have also been achieved by electrochemical treatment. And it is several times more efficient per unit surface area for the oxidation of small organic molecules, compared to Pt nanospheres and commercial Pt/C catalysts [17]. Interestingly, 1D nanostructures (nanowires and nanotubes) and nanostar of Pt also show increase in both catalytic activity and stability for fuel cell applications [18-20]. In addition, Pt alloy and bimetals, or trimetals nano-catalysts have been developed to remarkably reduce Pt loading while enhancing the catalytic performance [21-27]. Typically, Stamenkovic et al. demonstrated that the Pt₃Ni(111) surface is 10-fold more active for the ORR than the corresponding Pt(111) surface and 90-fold more active than the current state-of-the-art Pt/C catalysts for PEMFCs [22]. The Pt₃Ni(111) surface has an unusual electronic structure (*d*-band center position) and arrangement of surface atoms in the near-surface region. Under operating conditions relevant to fuel cells, its near-surface layer exhibits a highly structured compositional oscillation in the outermost and third layers, which are Pt-rich, and in the second atomic layer, which is Ni-rich. The weak interaction between the Pt surface atoms and nonreactive oxygenated species increases the number of active

sites for O₂ adsorption. Xia et al. developed Pd-Pt bimetallic nanodendrites consisting of a dense array of Pt branches on a Pd core, which are two and a half times more active on the basis of equivalent Pt mass for the ORR than the state-of-the-art Pt/C catalyst and five times more active than the first-generation supportless Pt-black catalyst due to relatively large surface areas and particularly active facets [23]. Adzic et al. demonstrated that platinum oxygen-reduction fuel-cell electrocatalysts can be stabilized against dissolution under potential cycling regime by modifying Pt nanoparticles with gold clusters [27].

1.3.2 Looking for the novel supports

Carbon black has been extensively used as a support for PEMFCs due to its fine properties and low cost. However, carbon black is known to undergo electrochemical oxidation to surface oxides and, finally, to CO₂ at the cathode in the fuel cell, where it is subjected to low pH, high potential, high humidity, and high temperatures (~80 °C). As carbon black corrodes, Pt supported on carbon black will detach from the electrode and possibly aggregate to larger particles, resulting in Pt surface area loss, which subsequently lowers the performance of PEMFCs [9, 28]. Therefore, many efforts have been made to develop more stable, high-surface-area carbon supports or other alternative carbon structures in an attempt to improve the durability of PEMFCs electrocatalysts [29]. Various carbon nanostructures such as single walled nanotubes [30], multiwalled nanotubes [31], stacked nanocups [32], graphitic nanofibers [33], graphene [34, 35], and mesoporous carbon materials [36] have been investigated as catalyst supports for PEMFCs. It has been shown that the structures and properties of the carbon supports, such as surface functional groups, graphitizing structure, and surface area, have a large effect on the activity and durability of the catalysts. The graphitic carbon (e.g. carbon nanotubes) is more stable than the conventionally used carbon black [37, 38]. In fact, Pt/carbon nanotubes have shown better performance and higher stability than Pt/carbon black due to the unique structure and properties of carbon nanotubes [31]. On the other hand, some metal oxides (TiO_x, NbO_x, etc.) even nanostructured crystalline organic whisker supports with appreciable electronic conductivity and electrochemical corrosion tolerance have also been developed [39-41]. Pt and Pt alloy deposited on such oxides have shown attractive performance toward ORR and methanol oxidation reaction (MOR).

3M has developed nanostructured thin film (NSTF) catalyst technology platform [41]; the NSTF catalysts are formed by high volume capable vacuum sputter-deposition of polycrystalline thin film catalyst alloys onto a supported monolayer of oriented crystalline organic-pigment whiskers. The whisker support particles are immune to corrosion and eliminate the high voltage corrosion plaguing carbon supports. To date it might be the only practical example of an extended surface area catalyst, which has been shown to eliminate or significantly reduce many of the performance, cost and durability barriers standing in the way of cathodes and anodes for H₂/air PEMFCs for vehicles.

1.3.3 Developing non-precious metal ORR catalyst

The dependence on expensive Pt-based electrocatalysts in PEMFCs remains a major obstacle for widespread deployment of this technology in spite of substantial reduction in platinum catalyst loading in the past 20 years, from approximately 2 mg cm⁻² of the MEA surface area to below 0.5 mg cm⁻² without significant impact on cell performance and lifetime. Further reductions in Pt loading in the PEMFCs cathode run the risk of lowering performance. One solution to overcome this predicament is to replace Pt catalysts with non-precious metal catalysts at the oxygen-reducing cathode. Up to now, many efforts have been made to develop the alternative cathode catalysts to Pt [42-47]. Among various non-Pt catalysts, a class is nitrogen-doped carbon nanostructures with and without metals, which could potentially replace platinum in PEMFCs cathodes [48-51]. Although the nature of the active sites remains elusive, nitrogen has been generally identified as an essential element for catalytic sites. Ozkan and co-workers have prepared the active catalysts for ORR in the different forms of nitrogen-doped carbon nanostructures, such as stacked cups, solid fibers, multiwall carbon nanotubes (MWNTs), and broken MWNTs [52]. Dodelet and co-workers developed the nitrogen coordinated iron in a carbon matrix, with optimal performance equal to a platinum-based cathode with a loading of 0.4mgcm⁻² at a cell voltage of $\geq 0.9V$ for PEMFCs [44]. Recently, Dai and co-workers reported that nitrogen-doped carbon nanotube arrays (6 at.% N) have high electrocatalytic activity for ORR in alkaline solution [53]. Furthermore, Star and co-workers demonstrated that the stacked nitrogen-doped carbon nanotube cups (2-7 at.% N) have similar catalytic ability in ORR as Pt/carbon nanotubes in alkaline solution [54]. Particularly, this kind of catalyst

has the more important progress. Zelenay et al. developed an approach using polyaniline as a precursor to a carbon-nitrogen template for high-temperature synthesis of catalysts incorporating iron and cobalt [55]. The researchers found that fuel cells containing the carbon-iron-cobalt catalyst not only generated comparable currents with the output of precious-metal-catalyst fuel cells, but held up favorably when cycled on and off---a condition that can damage inferior catalysts relatively quickly. Another important contribution is the development of non-precious

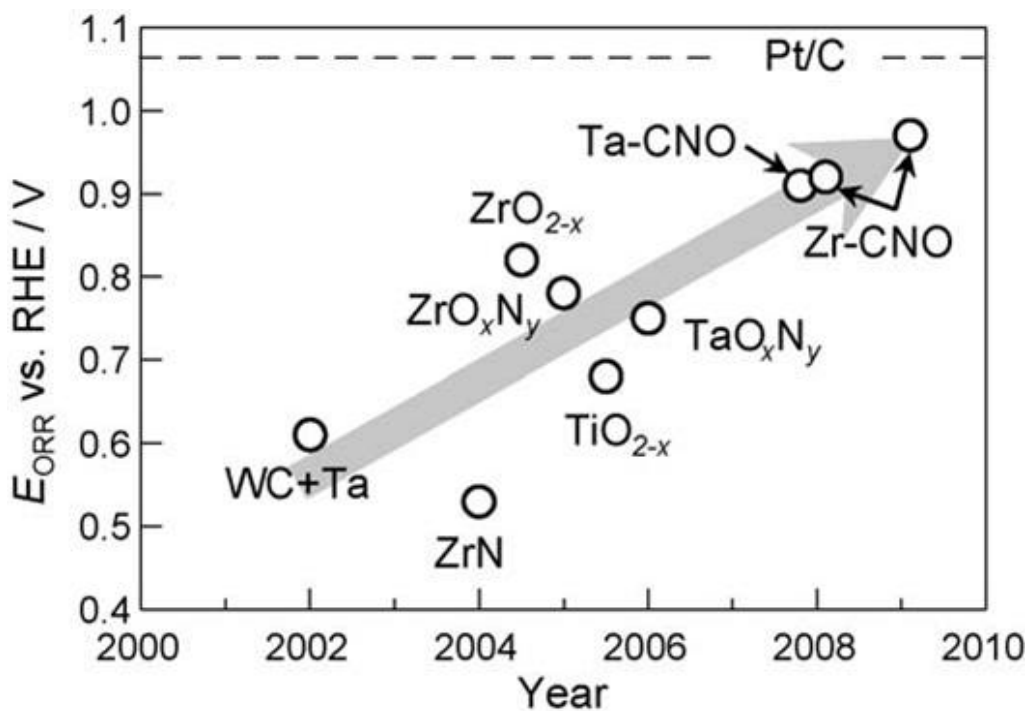


Figure 1-6 Summary of the progress over recent years with respect to transition metal oxide, carbide and nitride based materials as ORR electrocatalysts [56].

metal carbides, oxides, oxynitrides and carbonitrides, which have been considered promising inexpensive electrocatalyst alternatives for fuel cell applications in recent years [56]. From figure 1-6, one can know clearly Ta-CNO and Zr-CNO are having the close activity to Pt/C.

1.4 Objectives of thesis

Based on the above review, it is obvious that catalyst design is a key factor for enhancing the performance and realizing the commercialization of fuel cells. Surrounding the development of fuel cell catalysts, we will focus on the state-of-art mentioned above to develop new synthesis technology for 1D Pt, nitrogen doped carbon nanotubes, and 2D graphene-based materials, and investigate their electrochemical activity and durability. Figure 1-7 illustrates the separate research areas of this thesis. For Pt main catalyst, our

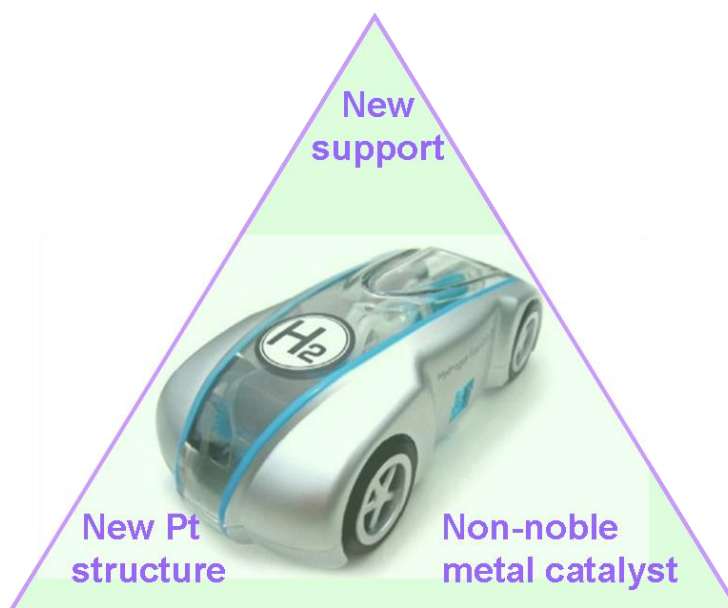


Figure 1-7 Research topic of PEM fuel cell catalyst.

group has proved that 1D Pt nanowires exhibited the higher ORR activity and durability than commercial Pt/C. But current methods for synthesis of Pt nanowires are either cumbersome or very difficult to scale up. The relative simple method to produce Pt nanowire at the large scale is always expected. In terms of support, the ideal support should have the following structure and properties: (i) high specific surface area, which is necessary for improving Pt dispersion, (ii) high electrical conductivity, (iii) low combustive reactivity under both dry and humid air conditions at low temperatures (150 °C or less), and (iv) high electrochemical stability under fuel cell operating conditions [37, 57]. Graphene, a new-type and two-dimensional (one-atom-thickness) allotrope of carbon with a planar honeycomb lattice, has attracted great interests for both fundamental

science and applied research due to its various remarkable properties including the ultra-high surface area (calculated value, $2,630 \text{ m}^2\text{g}^{-1}$), high conductivity (resistivity: $10^{-6} \Omega \text{ cm}$, less than the resistivity of silver, the lowest resistivity substance known at room temperature) and high chemical stability [58]. It is regarded as the basic building-block of carbon nanotubes and large fullerenes. All of the aforementioned properties combined with its unique graphitized basal plane structure and potential low manufacturing cost make it a promising candidate for catalyst support materials in PEMFCs. Recent work has shown that graphene used as Pt support has higher performance and higher Pt utilization over carbon black [34, 59] and higher stability [35]. However, Pt dispersion and size distribution have not been well controlled due to inert nature of graphene surface. Further investigation such as surface modification and doping other elements on graphene is desperately needed. As far as non-precious metal catalysts are concerned, we think that doping carbon materials should be good candidate. In general, chemical doping with N or B, P, S is considered an effective method to intrinsically modify the properties of carbon materials. Especially nitrogen doping plays a critical role in regulating the electronic and chemical properties of carbon materials due to its comparable atomic size and five valence electrons available to form strong valence bonds with carbon atoms. Theoretical study has shown that nitrogen doping results in the higher positive charge on a carbon atom adjacent to the nitrogen atoms [53], and a positive shift of Fermi energy at the apex of the Brillouin zone of graphene [60]. In our work, the promoting effect of nitrogen on the ORR activity was studied in detail by nitrogen doped carbon nanotubes (CN_x) with the various nitrogen contents firstly. Also the aforementioned unique properties of nitrogen-doped carbon materials and graphene promoted us to investigate the ORR activity of nitrogen-doped graphene, even boron, phosphor, and sulfur doped graphene.

1.5 Thesis structure

This thesis consists of nine chapters and fulfills the requirements on “Integrated-Article” form as outlined in the Thesis Regulation Guide by the School of Graduate and Postdoctoral Studies (SGPS) of The University of Western Ontario. It is built up with the following arrangement.

Chapter 1 gives an introduction to proton exchange membrane fuel cell, and the challenge of cathode materials, as well as the state-of-art solutions for the catalyst development. Importantly, the thesis objective and organization are also stated clearly.

Chapter 2 presents the detailed experimental process for synthesis, characterization, and performance test of nanomaterials, and provides all materials, apparatus, instruments used in the research.

Chapter 3 (Non-Noble Metal Oxygen Reduction Electrocatalysts Based on Carbon Nanotubes with Controlled Nitrogen Contents) reports the synthesis of nitrogen doped carbon nanotubes with the various nitrogen contents. The relationship between structures of CN_x and ORR activity is investigated in detail. The active site involving nitrogen, iron, carbon is further identified by the study. Most importantly, our best CN_x electrocatalyst has the similar ORR activity with a platinum-based catalyst with a loading of 1.94 microgram of platinum per square centimeter at the electrochemical window tested in alkaline solution, showing that CN_x has the potential to replace the costly Pt/C catalyst in alkaline fuel cells.

Chapter 4 (Nitrogen Doping Effects on the Structure of Graphene) gives a systematical investigation on the effects of N-doping on the structure of graphene by many characterization techniques especially XANES. Some interesting results have been obtained, such as more defects are present on nitrogen doped graphene, and N doping decreases the surface oxygen-containing groups.

Chapter 5 (High Oxygen-Reduction Activity and Durability of Nitrogen-doped Graphene) makes the contribution on the development of platinum-free catalysts. We present here that nitrogen doped graphene (the new and 2-dimensional carbon material) can be synthesized easily at a large scale and it has the comparable or better activity and stability than the commercial Pt/C (loading: $4.85 \mu\text{g}_{\text{Pt}} \text{cm}^{-2}$) towards oxygen reduction reaction. And we found that quaternary type nitrogen species seem to play the most important role for ORR activity.

Chapter 6 (Nitrogen doped graphene oxide nanoribbons from Nitrogen doped carbon nanotubes) makes an attempt to prepare nitrogen doped graphene with high aspect ratio. We obtained N-graphene oxide nanoribbons (NGON) using a simple solution-based oxidative process to unzip CN_x . The study opens a new door to synthesize nitrogen doped graphene at the large scale. The use of a low cost precursor and the solution-based procedure renders this method an attractive procedure to prepare NGON.

Chapter 7 (One-pot Solvothermal Synthesis of Doped Graphene with the Designed Nitrogen Type Used as a Pt Support for Fuel Cells) reports a large-scale preparation of nitrogen doped graphene by a novel solvothermal method featuring a lower synthesis temperature than previously reported. By the method, for the first time, nanoflower-like nitrogen doped graphene was obtained with pure sp^2 hybridized carbon and we realized the controllable synthesis of designed nitrogen types. More importantly, the synthesized materials exhibit much higher durability as Pt support for fuel cells than commercial carbon powder. The synthesis concept we proposed should pave new ways for design of the doped graphene materials with the controllable doping, which is especially important for future research and development of carbon materials for fuel cells.

Chapter 8 (A universal method to synthesize urchin-shaped Pt nanostructures) reports a simple and versatile strategy for synthesizing flower-like Pt nanostructures made of 1D Pt nanowires. Compared with those reported methods previously, our method has the following main advantages: i) It can be conducted very efficiently, even at room temperature. ii) Without any surfactant or template, the products can be purified and collected easily. iii) The process is environmentally friendly. iv) The amount of product can easily be scaled up. Our work reveals that the simplest, natural method, often overlooked, may indeed yield exciting results in scientific research again.

Chapter 9 summarizes the results and contributions of the thesis work. In addition, the author gives some personal opinions and suggestions for future work.

References

- [1] H.A. Gasteiger, S.S. Kocha, B. Sompalli, F.T. Wagner, Activity benchmarks and requirements for Pt, Pt-alloy, and non-Pt oxygen reduction catalysts for PEMFCs, *Appl Catal B-Environ*, 56 (2005) 9-35.
- [2] R. O'Hayre, S.W. Cha, W. Colella, F.B. Prinz, *Fuel cell Fundamentals*, John Wiley & Sons, New York, 2006.
- [3] J. Larminie, A. Dicks, *Fuel Cell Systems Explained* (second edition), John Wiley & Sons Ltd., West Sussex, England, 2003.
- [4] R. Borup, J. Meyers, B. Pivovar, Y.S. Kim, R. Mukundan, N. Garland, D. Myers, M. Wilson, F. Garzon, D. Wood, P. Zelenay, K. More, K. Stroh, T. Zawodzinski, J. Boncella, J.E. McGrath, M. Inaba, K. Miyatake, M. Hori, K. Ota, Z. Ogumi, S. Miyata, A. Nishikata, Z. Siroma, Y. Uchimoto, K. Yasuda, K.I. Kimijima, N. Iwashita, Scientific aspects of polymer electrolyte fuel cell durability and degradation, *Chem Rev*, 107 (2007) 3904-3951.
- [5] J.K. Nørskov, J. Rossmeisl, A. Logadottir, L. Lindqvist, J.R. Kitchin, T. Bligaard, H. Jo'ansson, Origin of the Overpotential for Oxygen Reduction at a Fuel-Cell Cathode, *J. Phys. Chem. B*, 108 (2004) 7.
- [6] E.J. Carlson, P. Kopf, J. Sinha, S. Sriramulu, Y. Yang, Cost Analysis of PEM Fuel Cell Systems for Transportation Subcontract Report NREL/SR-560-39104, (2005).
- [7] <http://www.platinum.matthey.com/cgi-bin/dynamic.pl?template=historical>.
- [8] F. Hasché, Activity, stability, and degradation mechanisms of platinum and platinum alloy nanoparticle PEM fuel cell electrocatalysts, Ph.D. Dissertation, Technische Universität Berlin, 2012.
- [9] Y.Y. Shao, G.P. Yin, Y.Z. Gao, Understanding and approaches for the durability issues of Pt-based catalysts for PEM fuel cell, *J Power Sources*, 171 (2007) 558-566.

- [10] X.W. Yu, S.Y. Ye, Recent advances in activity and durability enhancement of Pt/C catalytic cathode in PEMFC - Part II: Degradation mechanism and durability enhancement of carbon supported platinum catalyst, *J Power Sources*, 172 (2007) 145-154.
- [11] Y. Shao-Horn, W.C. Sheng, S. Chen, P.J. Ferreira, E.F. Holby, D. Morgan, Instability of supported platinum nanoparticles in low-temperature fuel cells, *Top Catal*, 46 (2007) 285-305.
- [12] M.K. Debe, Electrocatalyst approaches and challenges for automotive fuel cells, *Nature*, 486 (2012) 43-51.
- [13] F.J. Nores-Pondal, I.M.J. Vilella, H. Troiani, M. Granada, S.R. de Miguel, O.A. Scelza, H.R. Corti, Catalytic activity vs. size correlation in platinum catalysts of PEM fuel cells prepared on carbon black by different methods, *Int J Hydrogen Energ*, 34 (2009) 8193-8203.
- [14] J. Buttet, Geometrical Structure of Metal-Clusters, *Z Phys D Atom Mol Cl*, 3 (1986) 155-157.
- [15] Y.N. Xia, Y.J. Xiong, B. Lim, S.E. Skrabalak, Shape-Controlled Synthesis of Metal Nanocrystals: Simple Chemistry Meets Complex Physics?, *Angew Chem Int Edit*, 48 (2009) 60-103.
- [16] J. Solla-Gullon, J. Vidal-Iglesias, J.M. feliu, Shape dependent electrocatalysis, *Annu. Rep. Prog. Chem., Sect. C: Phys. Chem.*, 107 (2011) 263-297.
- [17] N. Tian, Z.Y. Zhou, S.G. Sun, Y. Ding, Z.L. Wang, Synthesis of tetrahedral platinum nanocrystals with high-index facets and high electro-oxidation activity, *Science*, 316 (2007) 732-735.
- [18] S.H. Sun, F. Jaouen, J.P. Dodelet, Controlled Growth of Pt Nanowires on Carbon Nanospheres and Their Enhanced Performance as Electrocatalysts in PEM Fuel Cells, *Adv Mater*, 20 (2008) 3900-3904.

- [19] Z.W. Chen, M. Waje, W.Z. Li, Y.S. Yan, Supportless Pt and PtPd nanotubes as electrocatalysts for oxygen-reduction reactions, *Angew Chem Int Edit*, 46 (2007) 4060-4063.
- [20] S.H. Sun, G.X. Zhang, D.S. Geng, Y.G. Chen, R.Y. Li, M. Cai, X.L. Sun, A Highly Durable Platinum Nanocatalyst for Proton Exchange Membrane Fuel Cells: Multiarmed Starlike Nanowire Single Crystal, *Angew Chem Int Edit*, 50 (2011) 422-426.
- [21] C.J. Zhong, J. Luo, B. Fang, B.N. Wanjala, P.N. Njoki, R. Loukrakpam, J. Yin, Nanostructured catalysts in fuel cells, *Nanotechnology*, 21 (2010) 062001.
- [22] V.R. Stamenkovic, B. Fowler, B.S. Mun, G.F. Wang, P.N. Ross, C.A. Lucas, N.M. Markovic, Improved oxygen reduction activity on Pt₃Ni(111) via increased surface site availability, *Science*, 315 (2007) 493-497.
- [23] B. Lim, M.J. Jiang, P.H.C. Camargo, E.C. Cho, J. Tao, X.M. Lu, Y.M. Zhu, Y.N. Xia, Pd-Pt Bimetallic Nanodendrites with High Activity for Oxygen Reduction, *Science*, 324 (2009) 1302-1305.
- [24] Y.H. Bing, H.S. Liu, L. Zhang, D. Ghosh, J.J. Zhang, Nanostructured Pt-alloy electrocatalysts for PEM fuel cell oxygen reduction reaction, *Chem Soc Rev*, 39 (2010) 2184-2202.
- [25] J. Greeley, I.E.L. Stephens, A.S. Bondarenko, T.P. Johansson, H.A. Hansen, T.F. Jaramillo, J. Rossmeisl, I. Chorkendorff, J.K. Nørskov, Alloys of platinum and early transition metals as oxygen reduction electrocatalysts, *Nat Chem*, 1 (2009) 552-556.
- [26] P. Strasser, S. Koh, T. Anniyev, J. Greeley, K. More, C.F. Yu, Z.C. Liu, S. Kaya, D. Nordlund, H. Ogasawara, M.F. Toney, A. Nilsson, Lattice-strain control of the activity in dealloyed core-shell fuel cell catalysts, *Nat Chem*, 2 (2010) 454-460.
- [27] J. Zhang, K. Sasaki, E. Sutter, R.R. Adzic, Stabilization of platinum oxygen-reduction electrocatalysts using gold clusters, *Science*, 315 (2007) 220-222.

- [28] J.G. Liu, Z.H. Zhou, X.X. Zhao, Q. Xin, G.Q. Sun, B.L. Yi, Studies on performance degradation of a direct methanol fuel cell (DMFC) in life test, *Phys Chem Chem Phys*, 6 (2004) 134-137.
- [29] Y.Y. Shao, J. Liu, Y. Wang, Y.H. Lin, Novel catalyst support materials for PEM fuel cells: current status and future prospects, *J Mater Chem*, 19 (2009) 46-59.
- [30] G. Girishkumar, K. Vinodgopal, P.V. Kamat, Carbon nanostructures in portable fuel cells: Single-walled carbon nanotube electrodes for methanol oxidation and oxygen reduction, *J Phys Chem B*, 108 (2004) 19960-19966.
- [31] C. Wang, M. Waje, X. Wang, J.M. Tang, R.C. Haddon, Y.S. Yan, Proton exchange membrane fuel cells with carbon nanotube based electrodes, *Nano Lett*, 4 (2004) 345-348.
- [32] C. Kim, Y.J. Kim, Y.A. Kim, T. Yanagisawa, K.C. Park, M. Endo, M.S. Dresselhaus, High performance of cup-stacked-type carbon nanotubes as a Pt-Ru catalyst support for fuel cell applications, *J Appl Phys*, 96 (2004) 5903-5905.
- [33] H. Tang, J.H. Chen, L.H. Nie, D.Y. Liu, W. Deng, Y.F. Kuang, S.Z. Yao, High dispersion and electrocatalytic properties of platinum nanoparticles on graphitic carbon nanofibers (GCNFs), *J Colloid Interf Sci*, 269 (2004) 26-31.
- [34] B. Seger, P.V. Kamat, Electrocatalytically Active Graphene-Platinum Nanocomposites. Role of 2-D Carbon Support in PEM Fuel Cells, *J Phys Chem C*, 113 (2009) 7990-7995.
- [35] Y.Y. Shao, S. Zhang, C.M. Wang, Z.M. Nie, J. Liu, Y. Wang, Y.H. Lin, Highly durable graphene nanoplatelets supported Pt nanocatalysts for oxygen reduction, *J Power Sources*, 195 (2010) 4600-4605.
- [36] H. Chang, S.H. Joo, C. Pak, Synthesis and characterization of mesoporous carbon for fuel cell applications, *J Mater Chem*, 17 (2007) 3078-3088.

- [37] D.A. Stevens, M.T. Hicks, G.M. Haugen, J.R. Dahn, Ex situ and in situ stability studies of PEMFC catalysts, *J Electrochem Soc*, 152 (2005) A2309-A2315.
- [38] J.J. Wang, G.P. Yin, Y.Y. Shao, Z.B. Wang, Y.Z. Gao, Investigation of further improvement of platinum catalyst durability with highly graphitized carbon nanotubes support, *J Phys Chem C*, 112 (2008) 5784-5789.
- [39] G.R. Dieckmann, S.H. Langer, Comparisons of Ebonex (R) and graphite supports for platinum and nickel electrocatalysts, *Electrochim Acta*, 44 (1998) 437-444.
- [40] K. Sasaki, L. Zhang, R.R. Adzic, Niobium oxide-supported platinum ultra-low amount electrocatalysts for oxygen reduction, *Phys Chem Chem Phys*, 10 (2008) 159-167.
- [41] M.K. Debe, Novel catalysts, catalysts support and catalysts coated membrane methods, in: *Handbook of Fuel Cells*, 2010.
- [42] R. Bashyam, P. Zelenay, A class of non-precious metal composite catalysts for fuel cells, *Nature*, 443 (2006) 63-66.
- [43] N.A. Vante, H. Tributsch, Energy-Conversion Catalysis Using Semiconducting Transition-Metal Cluster Compounds, *Nature*, 323 (1986) 431-432.
- [44] M. Lefevre, E. Proietti, F. Jaouen, J.P. Dodelet, Iron-Based Catalysts with Improved Oxygen Reduction Activity in Polymer Electrolyte Fuel Cells, *Science*, 324 (2009) 71-74.
- [45] Y.J. Feng, N. Alonso-Vante, Nonprecious metal catalysts for the molecular oxygen-reduction reaction, *Phys Status Solidi B*, 245 (2008) 1792-1806.
- [46] B. Wang, Recent development of non-platinum catalysts for oxygen reduction reaction, *J Power Sources*, 152 (2005) 1-15.

- [47] F. Jaouen, E. Proietti, M. Lefevre, R. Chenitz, J.P. Dodelet, G. Wu, H.T. Chung, C.M. Johnston, P. Zelenay, Recent advances in non-precious metal catalysis for oxygen-reduction reaction in polymer electrolyte fuel cells, *Energ Environ Sci*, 4 (2011) 114-130.
- [48] R.Z. Yang, K. Stevens, J.R. Dahn, Investigation of activity of sputtered transition-metal (TM)-C-N (TM = V, Cr, Mn, Co, Ni) catalysts for oxygen reduction reaction, *J Electrochem Soc*, 155 (2008) B79-B91.
- [49] Y.Y. Shao, J.H. Sui, G.P. Yin, Y.Z. Gao, Nitrogen-doped carbon nanostructures and their composites as catalytic materials for proton exchange membrane fuel cell, *Appl Catal B-Environ*, 79 (2008) 89-99.
- [50] F. Jaouen, S. Marcotte, J.P. Dodelet, G. Lindbergh, Oxygen reduction catalysts for polymer electrolyte fuel cells from the pyrolysis of iron acetate adsorbed on various carbon supports, *J Phys Chem B*, 107 (2003) 1376-1386.
- [51] P.H. Matter, E. Wang, M. Arias, E.J. Biddinger, U.S. Ozkan, Oxygen reduction reaction activity and surface properties of nanostructured nitrogen-containing carbon, *J Mol Catal a-Chem*, 264 (2007) 73-81.
- [52] P.H. Matter, E. Wang, U.S. Ozkan, Preparation of nanostructured nitrogen-containing carbon catalysts for the oxygen reduction reaction from SiO₂- and MgO-supported metal particles, *J Catal*, 243 (2006) 395-403.
- [53] K.P. Gong, F. Du, Z.H. Xia, M. Durstock, L.M. Dai, Nitrogen-Doped Carbon Nanotube Arrays with High Electrocatalytic Activity for Oxygen Reduction, *Science*, 323 (2009) 760-764.
- [54] Y.F. Tang, B.L. Allen, D.R. Kauffman, A. Star, Electrocatalytic Activity of Nitrogen-Doped Carbon Nanotube Cups, *J Am Chem Soc*, 131 (2009) 13200-13201.
- [55] G. Wu, K.L. More, C.M. Johnston, P. Zelenay, High-Performance Electrocatalysts for Oxygen Reduction Derived from Polyaniline, Iron, and Cobalt, *Science*, 332 (2011) 443-447.

- [56] A. Ishihara, Y. Ohgi, K. Matsuzawa, S. Mitsushima, K. Ota, Progress in non-precious metal oxide-based cathode for polymer electrolyte fuel cells, *Electrochim Acta*, 55 (2010) 8005-8012.
- [57] T.R. Ralph, M.P. Hogarth, Catalysis for Low Temperature Fuel Cells PART I: THE CATHODE CHALLENGES, *Platin Met Rev*, 46 (2002) 3-14.
- [58] A.K. Geim, Graphene: Status and Prospects, *Science*, 324 (2009) 1530-1534.
- [59] Y.C. Si, E.T. Samulski, Exfoliated Graphene Separated by Platinum Nanoparticles, *Chem Mater*, 20 (2008) 6792-6797.
- [60] S.U. Lee, R.V. Belosludov, H. Mizuseki, Y. Kawazoe, Designing Nanogadetry for Nanoelectronic Devices with Nitrogen-Doped Capped Carbon Nanotubes, *Small*, 5 (2009) 1769-1775.

Chapter 2

2 Experimental and characterization techniques

2.1 Experimental

2.1.1 Synthesis of carbon nanotubes with the controlled nitrogen contents via a floating catalyst chemical vapour deposition method

The floating catalyst chemical vapour deposition method (CVD) was applied to synthesize CN_x [1]. Typically, ferrocene ($Fe(C_5H_5)_2$) (100 mg, 98%, Aldrich) was placed at the entrance of the furnace in the quartz tube. Different amount of melamine (50, 200, 400, 800, and 2000 mg, 99+%, Aldrich) was placed beneath ferrocene as the nitrogen additive. A small piece of silicon wafer (1cm×3cm) with a 30 nm-thick aluminum buffer layer was located in the center of the oven. After the system was heated to 850 °C under Ar gas with a rate of 60 °C min⁻¹, ethylene gas was introduced (Fig. 2-1). After 5 min, the furnace was heated to 950 °C. The melamine vapour was brought into the reaction chamber by the gas flow and it was pyrolyzed in the middle of the reaction chamber as the nitrogen additive. After 15 min, the ethylene gas was turned off and the system was cooled down to room temperature in the flowing Ar gas. The synthesized catalysts were marked as CN_x (0%), CN_x (1.4%), CN_x (3.0%), CN_x (5.1%), CN_x (7.7%) based on the different nitrogen contents, respectively.

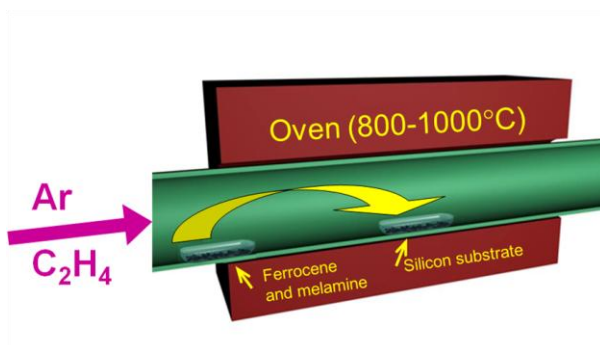


Figure 2-1 The schematic drawing of our synthesis stratagem of nitrogen doped carbon nanotubes.

2.1.2 Synthesis of graphene by modified Hummers' method

Graphite powder was used as the starting material. Graphene was first prepared by the oxidation of graphite powder using the modified Hummers' method [2, 3]. Typically, graphite powder (1 g) and sodium nitrate (0.75 g) were first stirred in concentrated sulphuric acid (37.5 mL) while being cooled in an ice water bath. Then potassium permanganate (4.5 g) was gradually added to form a new mixture. After 2 h in an ice water bath, the mixture was allowed to stand for five days at room temperature with gentle stirring. Thereafter, 100 mL of 5 wt% H_2SO_4 aqueous solution was added into the above mixture over 1 h with stirring. Then, 3 g of H_2O_2 (30 wt% aqueous solution) was also added to the above liquid and the mixture was stirred for 2 h. After that, the suspension was filtered and washed until the pH value of the filtrate was neutral. The as-received slurry is the so-called graphite oxide. Finally, the dried graphite oxide was heated at $1050\text{ }^\circ\text{C}$ for 30 s under Ar to get graphene [4]. The schematic synthesis process is shown in Figure 2-2.

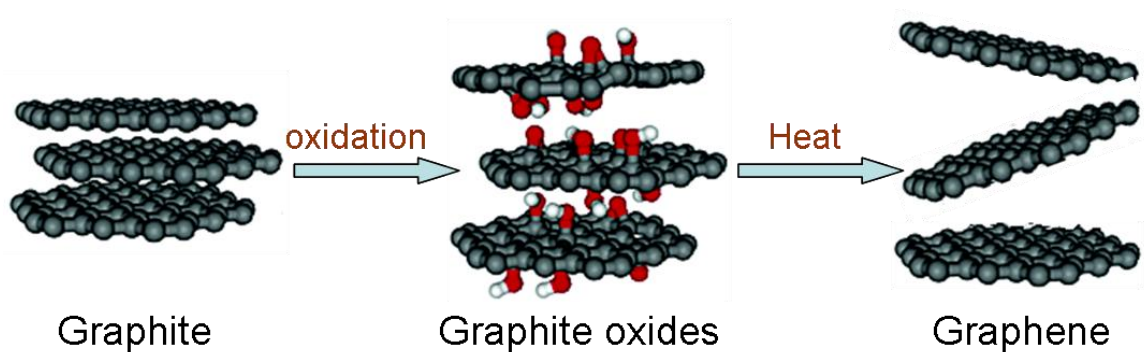


Figure 2-2 The schematic process for graphene synthesis.

2.1.3 Synthesis of nitrogen doped graphene

2.1.3.1 Ammonia treated method

Nitrogen doped graphene was further obtained by heating the graphene under high purity ammonia mixed with Ar at 800, 900, 1000 $^\circ\text{C}$ for the different time (Figure 2-3) [5].

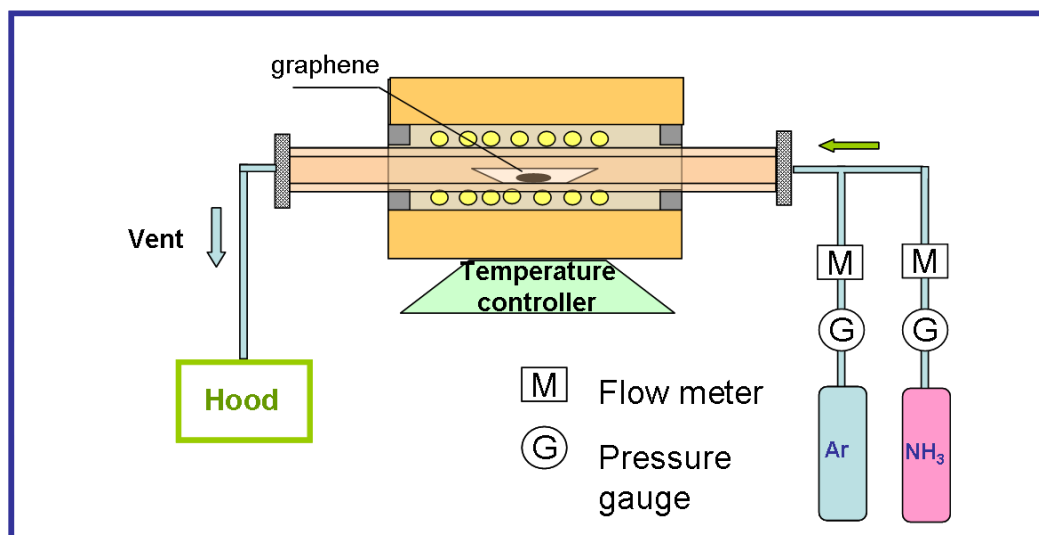


Figure 2-3 Schematic of CVD synthesis of N-graphene.

2.1.3.2 Solvothermal method

A solvothermal route was employed in the synthesis as described below. Typically, 200 mg of pentachloropyridine was placed in a 25 mL Teflon-lined autoclave. Then appropriate amount of metallic potassium was cut into flakes and rapidly added to the autoclave in the glove box. The autoclave was sealed and heated to the desired temperature, where it was maintained for 10 h before it was cooled to room temperature naturally. The products, dark precipitates, were filtered out and washed with acetone, absolute ethanol and water in sequence, and were then dried in a vacuum at 80 °C for 4 h.

2.1.3.3 From nitrogen doped carbon nanotubes to N-graphene

Commercial carbon nanotubes from Aldrich Company were used as the precursor to form graphene oxide nanoribbon (GON). CN_x (5.1% at. N) (home-made) was selected as the precursor to produce N-graphene oxide nanoribbon (NGON). They were first prepared by the oxidation of precursors using the modified Hummers' method [2, 3]. Typically, precursor (50 mg) and sodium nitrate (37.5 mg) were first stirred in concentrated sulphuric acid (3 mL) while being cooled in an ice water bath. Then potassium permanganate (225 mg) was gradually added to form a new mixture. After two hours in an ice water bath, the mixture was allowed to stand for one day at room temperature with gentle stirring. Thereafter, 30 mL of 5 wt% H₂SO₄ aqueous solution was added into the

above mixture over 1h with stirring. Then, 1 mL of H₂O₂ (30 wt% aqueous solution) was also added to the above liquid and the mixture was stirred for 2h. After that, the suspension was filtered and washed until the pH value of the filtrate was neutral. The as-received slurry is then sonicated to get the so-called GON and NGON.

2.1.4 Synthesis of S, P doped graphene

For sulphur-doped graphene, graphene was dispersed to acetone with toluenesulfonic acid (TSA) [6]. Regarding phosphor-doped graphene, graphene was dispersed to ethanol with triphenylphosphine (TPP) [7]. The slurries were stirred at room temperature until totally evaporating the solvent. Then the resulting products were dried at 100 °C and finally which were calcined at 900 °C with Ar protection for 1 hour. Thus, the S or P-containing graphene was obtained.

2.1.5 Synthesis of dendritic Pt nanostructures via a universal chemical method

The synthesis of dendritic Pt nanostructures made of Pt nanowires was conducted in aqueous solution, by the chemical reduction of Pt precursor with the reductive agents containing –OH, –CHO, or –COOH groups at lower temperatures (less than 80 °C) [8]. There will be not additional stabilizing agent used. Many reductive agents have been tried to the synthesis of novel Pt nanostructures, such as methanol, ethanol, *iso*-propanol, ethylene glycol, formaldehyde, formic acid, glucose, ascorbic acid, etc. Typically, for the synthesis of dendritic Pt nanostructures, 0.015 g potassium tetrachloroplatinate (K₂PtCl₄, 99.9 %, Sigma-Aldrich) and 1 mL formaldehyde (HCHO, 37 wt.% solution in water, Sigma-Aldrich) were dissolved in 10 mL H₂O and stored at room temperature for 72 h. The solution turned from light-pink to grey and then to dark brown. We have tried various experimental parameters, such as different reaction temperatures, different pH values, different concentrations, etc. The current conditions used in this thesis are the optimized parameters.

2.2 Characterization techniques

2.2.1 Physical characterization (SEM, TEM, XPS, XRD, BET, and Raman spectra)

To fully understand physical and chemical properties of the samples, a variety of analytical techniques have been used in this thesis.

The morphologies of the samples were characterized by Hitachi S-4800 field-emission scanning electron microscopy (SEM) operated at 5.0 kV, Philips CM10 (transmission electron microscopy) TEM operated at 80 kV. The instruments are shown in figure 2-4, 2-5, respectively. High-resolution transmission electron microscopy (HRTEM) and selected area electron diffraction (SAED) were characterized by a JEOL 2010 FEG microscope operated at 200 kV.



Figure 2-4 A photo of our SEM (Hitachi S-4800).

BET is used to determine the specific surface area, pore size, and pore volume of samples by Folio Micromeritics TriStar II 3020 surface area and porosity analyzer. Also the detailed structures for our samples have been characterized by X-ray diffraction (XRD),



Figure 2-5 A photo of our TEM (Philips CM10).

Raman spectra, Fourier transform-infrared (FT-IR) spectra. The XRD patterns were recorded on a Bruker D8 Advance diffractometer equipped with a Cu K α radiation source. FT-IR measurements were carried out by the KBr method using a Nicolet 6700 FT-IR spectrometer. FT-IR spectra were recorded in the transmittance mode over the range of 400-4000 cm^{-1} by averaging 16 scans at a resolution of 4 cm^{-1} . Raman scattering spectra were collected on a HORIBA Scientific LabRAM HR Raman spectrometer system equipped with a 532 nm laser. A laser energy filter value of 2 was applied, which prevents decomposition of the samples. The spectra were taken between 100 and 1000 cm^{-1} in a backscattering configuration at room temperature. The nitrogen contents for N-graphene and S or P contents were determined by Kratos Axis Ultra Al (alpha) X-ray photoelectron spectroscopy (XPS) operated at 14 kV. The XPS data was collected with a dual anode X-ray source using Mg K irradiation with the energy of 1253.6 eV. Binding energies were measured using a hemispherical energy analyzer with fixed pass energy of 50 eV that gave an energy resolution of approximately 1.1 eV. The data was analyzed using an XPS data analysis software, Advantage, version 3.99 developed by Thermo VG Scientific. Fittings of the peaks were performed using Gaussian-Lorentzian product

function and Shirley background algorithm. The sensitivity factors were also taken into account when we did the quantitative analysis. Furthermore, the synchrotron-based X-ray Absorption Near Edge Structure (XANES) spectroscopy measurements were performed at the Canadian Light Source (CLS) on the High Resolution Spherical Grating Monochromator (SGM) beamline for the CK-, NK-, and OK-edge spectra. This beamline uses a 45 mm planar undulator and three gratings to cover a photon energy region from 250 to 2000 eV. It offers an energy resolution greater than 5000 E/ Δ E at energy below 1500 eV [9]. The beamline is capable of providing 10^{12} photons per second at 250 eV and exceeds 10^{11} photons per second up to 1900 eV at 100 mA. Spectra were recorded in the fluorescence yield mode (FLY) using a microchannel-plate detector and the total electron yield (TEY) mode measuring the sample current. All spectra were normalized to the intensity of the incident beam (I_0), measured simultaneously as the current emitted from a gold mesh located after the last optical elements of the beamline.

2.2.2 Electrochemical characterization

The electrochemical characterizations of the catalysts were conducted in a standard three-compartment electrochemical cell using a glassy carbon (GC) rotating ring disk electrode (RRDE: $d=5\text{mm}$, Au ring (6.5mm i.d., 7.5mm o.d.)) setup on an Autolab potentiostat/galvanostat (Model, PGSTAT-30, Ecochemie, Brinkman Instruments) with rotation control (MSR, Pine Instruments) (as shown in Figure 2-6, 2-7). Usually, a Pt wire was used as the counter electrode and an Ag/AgCl (3 M NaCl) or Hg/HgSO₄ (saturated K₂SO₄) was used as the reference electrode. For convenience, all potentials in this thesis are referenced to the standard hydrogen electrode (SHE). For carbon materials, a typical catalyst film was produced at the disk electrode according to the following procedure: 5 mg of CN_x, or N-graphene was suspended in the solution (1080 μL ethanol and 180 μL of 5 wt% Nafion) and ultrasonically blended for 30 min. 10 μL of this suspension was dropped on the disk electrode. For Pt/C or Pt/N-graphene catalyst, the ink was prepared by dispersing 5 mg of the electrocatalysts in 2.5 mL of ethanol and was subject to ultrasonification for 30 min. Then 20 μL of the catalyst powder dispersion was dropped onto the surface of disk electrode. After drying the droplet at 60 °C, 20 μL of a

0.05 wt % Nafion alcoholic solution was further dropped on the electrode surface and heated again at 60°C to stabilize the electrocatalysts [10].

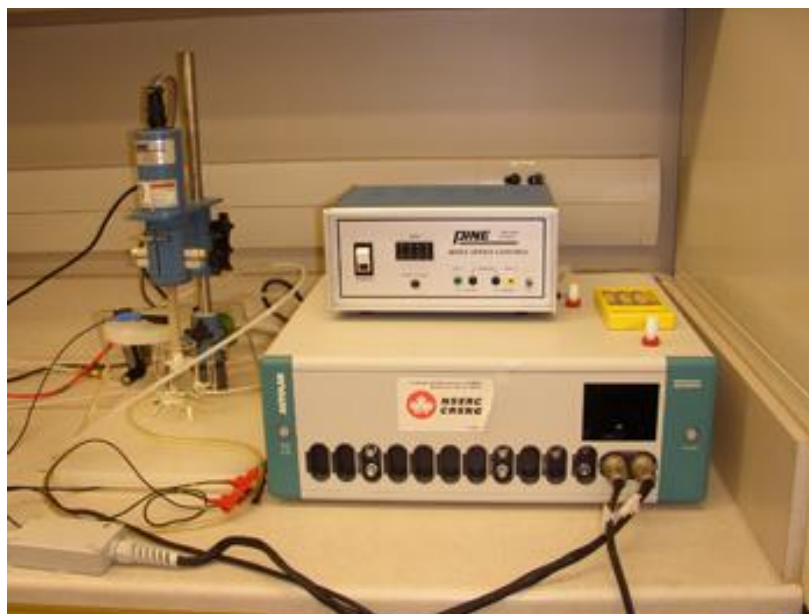


Figure 2-6 Autolab potentiostat/galvanostat (Model, PGSTAT-30, Ecochemie, Brinkman Instruments) with rotation control (MSR, Pine Instruments).

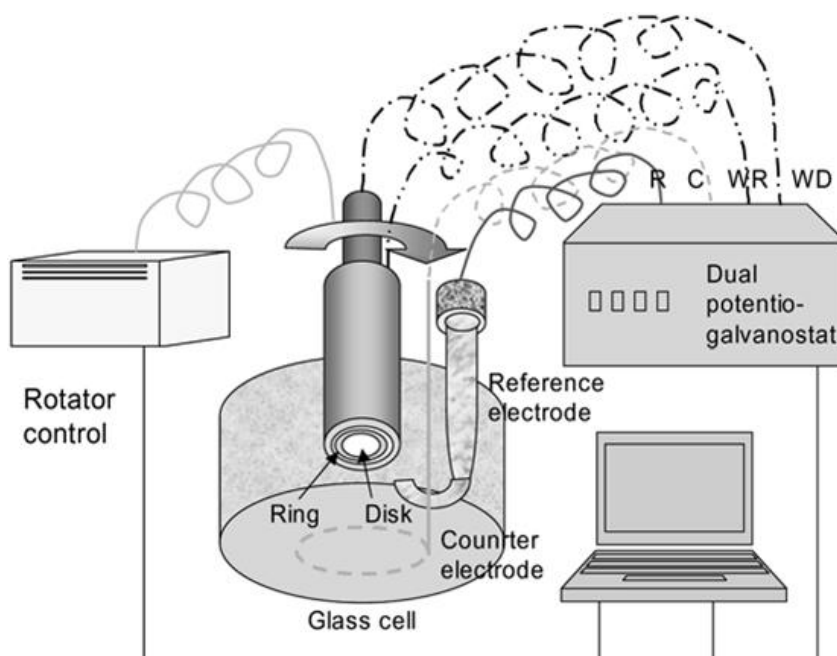


Figure 2-7 Sketch of a rotating ring-disk electrode apparatus [11].

2.2.2.1 Cyclic voltammetry

The electrodes were first pretreated to remove surface contamination by cycling the electrode potential between 0.05 and 1.2 V vs SHE at 50 mV s^{-1} for 50 cycles in nitrogen saturated electrolyte. 50 cycles should be enough to assure quasi-steady-state voltammograms. Then, the cyclic voltammetry measurements were conducted by cycling the potential between 0.05 and 1.2 V, with sweep rate of 50 mV s^{-1} . For each sample, at least three tests were run under the same condition for obtaining its repeatability.

2.2.2.2 ORR using rotation ring-disk electrode

Cyclic voltammograms (CVs) were recorded by scanning the disk potential from 1.20 to 0.05 V (0.5 M H_2SO_4 solution) and from 0.4 to -1.0V (0.1M KOH solution) vs SHE at a scan rate of 5mVs^{-1} . And the ring potential was maintained at 1.2 and 0.7 V vs SHE,

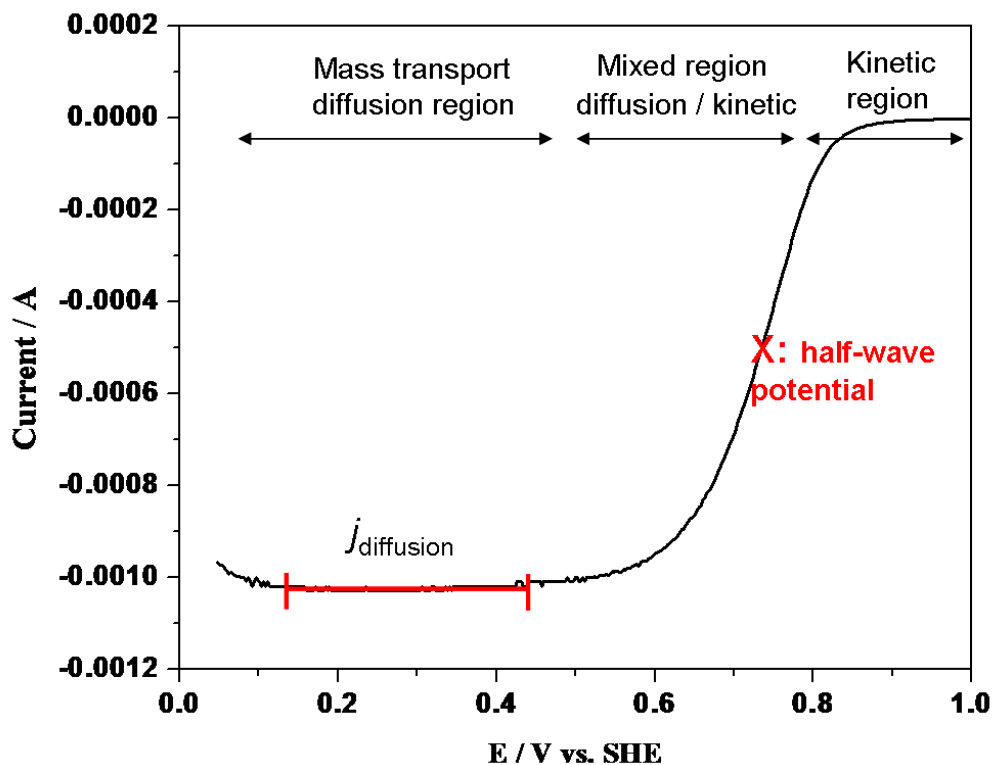


Figure 2-8 Analysis of a linear sweep voltammogram (Pt/C, 0.05 – 1.20 V vs. SHE, 5 mV s^{-1} , 1600 rpm, saturated O_2 , 0.5 M H_2SO_4 , room temperature).

respectively, for acid and alkaline solutions in order to oxidize any hydrogen peroxide produced. First, CVs were recorded at 5 mVs^{-1} using nitrogen atmosphere to obtain the background capacitive currents. Next, CVs were recorded using the oxygen-saturated electrolyte. The electrolyte solution was purged with oxygen for 30 min before commencing oxygen reduction on the disk electrode. All ORR test were performed with a rotating speed of 1600 rpm (rounds per minute). Figure 2-8 gives a typical analysis for linear sweep voltammogram of ORR. Usually, the ORR activity is evaluated by comparing the half-wave potential. The higher the half-wave potential, the higher the activity of the catalyst is [12, 13].

2.2.2.3 Accelerated durability test (ADT)

The accelerated durability test [14] was conducted with a thin film electrode. For Pt-based catalysts, the electrode was cycled between 0.6 and 1.2 V for 4,000 cycles in an O_2 -saturated H_2SO_4 solution (0.5 M) at room temperature, with scan rate of 50 mV s^{-1} . Meanwhile, full-scale voltammograms between 0.05 and 1.2 V in N_2 saturated 0.5 M H_2SO_4 were recorded to track the degradation of the Pt catalysts. The scan rate was kept at 50 mV s^{-1} constantly [15, 16]. The platinum electrochemical active surface area (ECSA) was calculated using the mean integral charge of the hydrogen adsorption/desorption area with double layer current corrected at 0.4 V vs. SHE and with $210 \mu\text{C cm}_{\text{Pt}}^{-2}$, assuming one hydrogen atom observed to one platinum atom (see Figure 2-9). The durability was evaluated by comparing the change of ECSA. For non-noble metal ORR catalysts, the durability was evaluated by tracking the change of the current density for the ORR at 0.05 V with the potential cycles from the cyclic voltammograms.

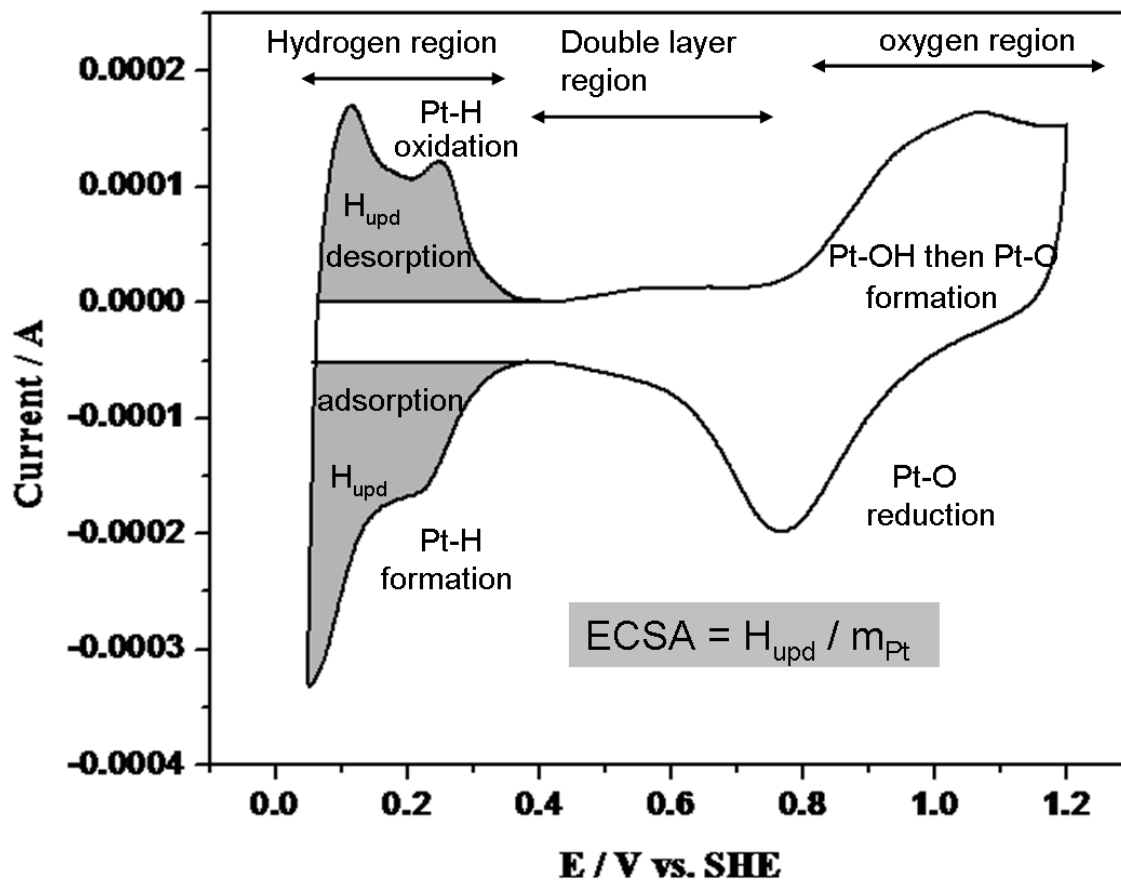


Figure 2-9 Analysis of cyclic voltammogram (Pt/C, 0.05 – 1.20 V vs. SHE, 50 mV s⁻¹, saturated N₂, 0.5 M H₂SO₄, room temperature).

References

- [1] H. Liu, Y. Zhang, R.Y. Li, X.L. Sun, S. Desilets, H. Abou-Rachid, M. Jaidann, L.S. Lussier, Structural and morphological control of aligned nitrogen-doped carbon nanotubes, *Carbon*, 48 (2010) 1498-1507.
- [2] W.S. Hummers, R.E. Offeman, Preparation of Graphitic Oxide, *J Am Chem Soc*, 80 (1958) 1339-1339.
- [3] M. Hirata, T. Gotou, S. Horiuchi, M. Fujiwara, M. Ohba, Thin-film particles of graphite oxide 1: High-yield synthesis and flexibility of the particles, *Carbon*, 42 (2004) 2929-2937.

- [4] H.C. Schniepp, J.L. Li, M.J. McAllister, H. Sai, M. Herrera-Alonso, D.H. Adamson, R.K. Prud'homme, R. Car, D.A. Saville, I.A. Aksay, Functionalized single graphene sheets derived from splitting graphite oxide, *J Phys Chem B*, 110 (2006) 8535-8539.
- [5] H.B. Wang, T. Maiyalagan, X. Wang, Review on Recent Progress in Nitrogen-Doped Graphene: Synthesis, Characterization, and Its Potential Applications, *Acs Catal*, 2 (2012) 781-794.
- [6] K. Kwon, S.A. Jin, C. Pak, H. Chang, S.H. Joo, H.I. Lee, J.H. Kim, J.M. Kim, Enhancement of electrochemical stability and catalytic activity of Pt nanoparticles via strong metal-support interaction with sulfur-containing ordered mesoporous carbon, *Catal Today*, 164 (2011) 186-189.
- [7] J. Liu, H. Liu, Y. Zhang, R.Y. Li, G.X. Liang, M. Gauthier, X.L. Sun, Synthesis and characterization of phosphorus-nitrogen doped multiwalled carbon nanotubes, *Carbon*, 49 (2011) 5014-5021.
- [8] L. Wang, Y. Yamauchi, Synthesis of Mesoporous Pt Nanoparticles with Uniform Particle Size from Aqueous Surfactant Solutions toward Highly Active Electrocatalysts, *Chem-Eur J*, 17 (2011) 8810-8815.
- [9] <http://exshare.lightsource.ca/sgm/Pages/Beamline.aspx>.
- [10] D.S. Geng, D. Matsuki, J.J. Wang, T. Kawaguchi, W. Sugimoto, Y. Takasu, Activity and Durability of Ternary PtRuIr/C for Methanol Electro-oxidation, *J Electrochem Soc*, 156 (2009) B397-B402.
- [11] T. Okada, M. Kaneko, Electrochemical Methods for Catalyst Evaluation in Fuel Cells and Solar Cells, in: T. Okada, M. Kaneko (Eds.) *Molecular Catalysts for Energy Conversion*, Springer, 2009.
- [12] J. Snyder, T. Fujita, M.W. Chen, J. Erlebacher, Oxygen reduction in nanoporous metal-ionic liquid composite electrocatalysts, *Nat Mater*, 9 (2010) 904-907.

- [13] Y. Takasu, N. Yoshinaga, W. Sugimoto, Oxygen reduction behavior of RuO₂/Ti, IrO₂/Ti and IrM (M : Ru, Mo, W, V) O-x/Ti binary oxide electrodes in a sulfuric acid solution, *Electrochem Commun*, 10 (2008) 668-672.
- [14] J. Zhang, K. Sasaki, E. Sutter, R.R. Adzic, Stabilization of platinum oxygen-reduction electrocatalysts using gold clusters, *Science*, 315 (2007) 220-222.
- [15] U.S. Department of Energy, The Department of Energy Hydrogen and Fuel Cells Program Plan, 2011.
- [16] Y.G. Chen, J.J. Wang, H. Liu, R.Y. Li, X.L. Sun, S.Y. Ye, S. Knights, Enhanced stability of Pt electrocatalysts by nitrogen doping in CNTs for PEM fuel cells, *Electrochem Commun*, 11 (2009) 2071-2076.

Chapter 3

3 Non-Noble Metal Oxygen Reduction Electrocatalysts Based on Carbon Nanotubes with Controlled Nitrogen Contents

Dongsheng Geng^a, Hao Liu^a, Yougui Chen^a, Ruying Li^a, Xueliang Sun^{a,*},

Siyu Ye^b, Shanna Knights^b

^a*Department of Mechanical and Materials Engineering, University of Western Ontario,
1151 Richmond Street N., London, Ontario, Canada N6A 5B9*

^b*Ballard Power Systems Inc., 9000 Glenlyon Parkway, Burnaby, BC, Canada V5J 5J8*

**To whom correspondence should be addressed. E-mail: xsun@eng.uwo.ca*

Tel: +1-519-6612111, Ext. 87759, Fax: +1-519-6613020

A version of this chapter has been published in *Journal of Power sources*, 2011, **196**, 1795-1801.

Proton exchange membrane fuel cells (PEMFCs) are being considered as a potential alternative energy conversion device for stationary and automotive applications, which use platinum supported on carbon black as electrocatalysts in both the anode and the cathode. Pt is a highly expensive material and has a geopolitical and availability shortcoming. Most importantly, Pt is still not an ideal material for use in a PEMFCs cathode for oxygen reduction reaction (ORR) because of poor performance. The search for cheap and more active electrocatalysts for ORR is thus of great importance. Among the current non-noble metal catalyts, the nitrogen-doped carbon nanotubes (CN_x) show

promising results; however, the promoting effect of nitrogen on the ORR activity has not been studied in detail with various nitrogen contents.

In this work, we conducted a systematic study on CN_x system by preparing a series of catalysts via a floating catalyst chemical vapor deposition method using precursors consisting of ferrocene and melamine to control the nitrogen content. The emphasis was mainly placed on study of the correlation between surface structure and the ORR activity in acid and alkaline solutions. Structure, morphology and composition of all CN_x catalysts were characterized by SEM, TEM, and XPS. These results indicated that the surface nitrogen content (up to 7.7 at%) increases with the increase of melamine used. Electrochemical data indicated that the higher the nitrogen content is, the higher the oxygen reduction activity. Especially, the results demonstrated that CN_x (7.7%) has similar ORR activity and selectivity with commercial Pt/C in alkaline solution. Therefore, nitrogen-doped carbon nanotubes may have the potential to replace the costly Pt/C catalyst in fuel cells in an alkaline solution.

Keywords: *Oxygen reduction reaction, Nitrogen-doped carbon nanotubes, Proton exchange membrane fuel cells, Rotating ring disk electrode.*

3.1 Introduction

Proton exchange membrane fuel cells (PEMFCs) are being considered as a potential alternative energy conversion device for stationary and automotive applications, which use platinum supported on carbon black as electrocatalysts in both the anode and the cathode [1]. Pt is a highly expensive material and has a geopolitical and availability shortcoming. Most importantly, Pt is still not an ideal material for use in a PEMFCs cathode because of poor performance compared to what may theoretically be attainable. Therefore, many efforts have been made to develop the alternative cathode catalysts to Pt [2-11]. Among various non-Pt catalysts, a class is nitrogen-doped carbon nanostructures with and without metals, which could potentially replace platinum in PEMFCs cathodes [12-24]. Although the nature of the active sites remains elusive, nitrogen has been generally identified as an essential element for catalytic sites. Ozkan et al. have prepared the active catalysts for ORR in the different forms of nitrogen-doped carbon nanostructures, such as stacked cups, solid fibers, multi-wall carbon nanotubes (MWNTs), and broken MWNTs [25]. Dodelet et al. developed the nitrogen coordinated iron in a carbon matrix, with optimal performance equal to a platinum-based cathode with a loading of 0.4 mg cm^{-2} at a cell voltage of $\geq 0.9 \text{ V}$ for PEMFCs [22]. Recently, Dai and co-workers reported that nitrogen-doped carbon nanotube arrays (6 at% N) have high electrocatalytic activity for ORR in alkaline solution [23]. Furthermore, Star et al. demonstrated that the stacked nitrogen-doped carbon nanotube cups (2-7 at% N) have similar catalytic ability in ORR as Pt/carbon nanotubes in alkaline solution [24]. Among the above catalysts, the nitrogen-doped carbon nanotubes show promising results; however, the promoting effect of nitrogen on the ORR activity has not been studied in detail with various nitrogen contents [26, 27].

In this work, we conducted a systematic study on CN_x system by preparing a series of catalysts with various nitrogen contents and studied their ORR activity in not only acid solution but also alkaline solution. In addition, the activities were compared with that of the commercial Pt/C catalyst. We will show here that CN_x (7.7%) has the similar ORR activity and selectivity with commercial Pt/C in alkaline solution.

3.2 Experimental

3.2.1 Preparation of CN_x

The floating catalyst chemical vapor deposition method was applied to synthesize CN_x [28]. Typically, ferrocene ($Fe(C_5H_5)_2$) (100 mg, 98%, Aldrich) was placed at the entrance of the furnace in the quartz tube. Different amount of melamine (50, 200, 400, 800, and 2000 mg, 99+%, Aldrich) was placed beneath ferrocene as the nitrogen additive. A small piece of silicon wafer (1 cm \times 3 cm) with 30 nm-thick aluminum buffer layer was located in the center of the oven. After the system was heated to 850 °C under Ar gas with a rate of 60 °C/min, ethylene gas was introduced. After 5 minutes, the furnace was heated to 950 °C. The melamine vapor was brought into the reaction chamber by the gas flow and it was pyrolyzed in the middle of the reaction chamber as the nitrogen additive. After 15 minutes, the ethylene gas was turned off and the system was cooled down to room temperature in the flowing Ar gas. The synthesized catalysts were marked as CN_x (0%), CN_x (1.4%), CN_x (3.0%), CN_x (5.1%), CN_x (7.7%) based on the different nitrogen contents, respectively.

3.2.2 Physical characterizations

The samples were characterized by Hitachi S-4800 field-emission scanning electron microscopy (SEM) operated at 5.0 kV, Philips CM10 transmission electron microscopy (TEM) operated at 80 kV. Furthermore, a JEOL 2010 FEG TEM at 200 kV was used to obtain the high resolution imaging. The nitrogen contents on the surface of all catalysts were also determined by Kratos Axis Ultra Al (alpha) X-ray photoelectron spectroscopy (XPS) operated at 14 kV.

3.2.3 Electrochemical characterization

Autolab potentiostat/galvanostat (model PGSTAT-30 Ecochemie Brinkman Instruments) and a three-compartment cell were employed for the electrochemical measurement. The electrocatalytic activity of CN_x was studied using the rotating ring disk electrode (RRDE) technique. Briefly, a rotating ring disk electrode from Pine Instruments employing a glassy carbon (GC) disk (d = 5 mm) and Au ring (6.5 mm i.d., 7.5 mm o.d.) was used as

the working electrode. Platinum wire and Ag/AgCl electrode were used as the counter and the reference electrode, respectively. The potentials presented in this study are referred with respect to standard hydrogen electrode (SHE). A typical catalytic film was produced at the disk electrode according to the following procedure: 5 mg of CN_x was suspended in the solution (1080 μ L ethanol and 180 μ L of 5 wt % Nafion) and ultrasonically blended for 30 min. 10 μ L of this suspension was dropped on the disk electrode. Cyclic voltammograms (CVs) were recorded by scanning the disk potential from 1.20 to 0.05 V (0.5 M H_2SO_4 solution) and from 0.4 to -1.0 V (0.1 M KOH solution) vs SHE at a scan rate of 5 $mV s^{-1}$. And the ring potential was maintained at 1.2 and 0.7 V vs SHE, respectively for acid and alkaline solutions in order to oxidize any hydrogen peroxide produced. First, CVs were recorded at 5 $mV s^{-1}$ using nitrogen atmosphere to obtain the background capacitive currents. Next, CVs were recorded using the oxygen-saturated electrolyte. The electrolyte solution was purged with oxygen for 30 min before commencing oxygen reduction on the disk electrode.

3.3 Results and discussion

3.3.1 SEM, TEM and XPS analysis

The morphology and structure of CN_x are presented in Figure 3-1. Figure 3-1 shows the representative SEM image of the CN_x (1.4%). It can be seen that CN_x with high density were formed and totally covered the silicon wafer.

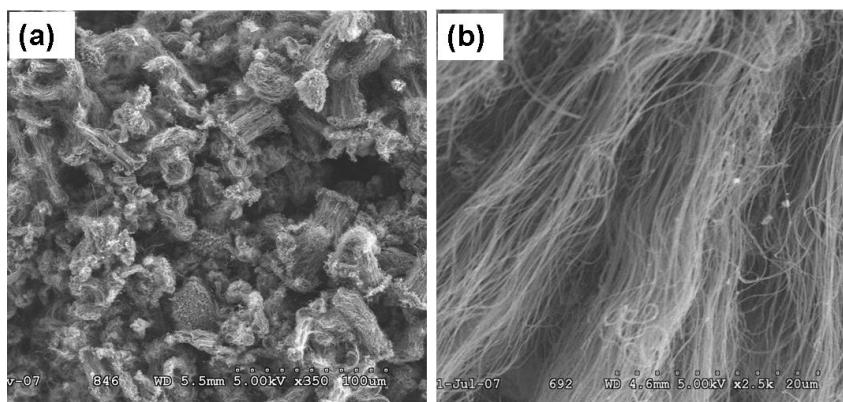


Figure 3-1 (a) SEM image of CN_x prepared with 200 mg of melamine; (b) the magnified images.

Typical TEM images of the catalysts (CN_x (1.4%), CN_x (3.0%), CN_x (5.1%), and CN_x (7.7%) are also presented in Fig. 3-2a, b, c, and d. From these figures, it can be seen that with the increase of melamine used, inner structure of the CN_x displays a regular morphology transition from a straight and smooth wall (melamine of 50 mg) to cone-stacked shaped or bamboo-like structure (melamine of 200 mg), then to corrugated structure (melamine of 400 mg and above). To characterize the surface composition of

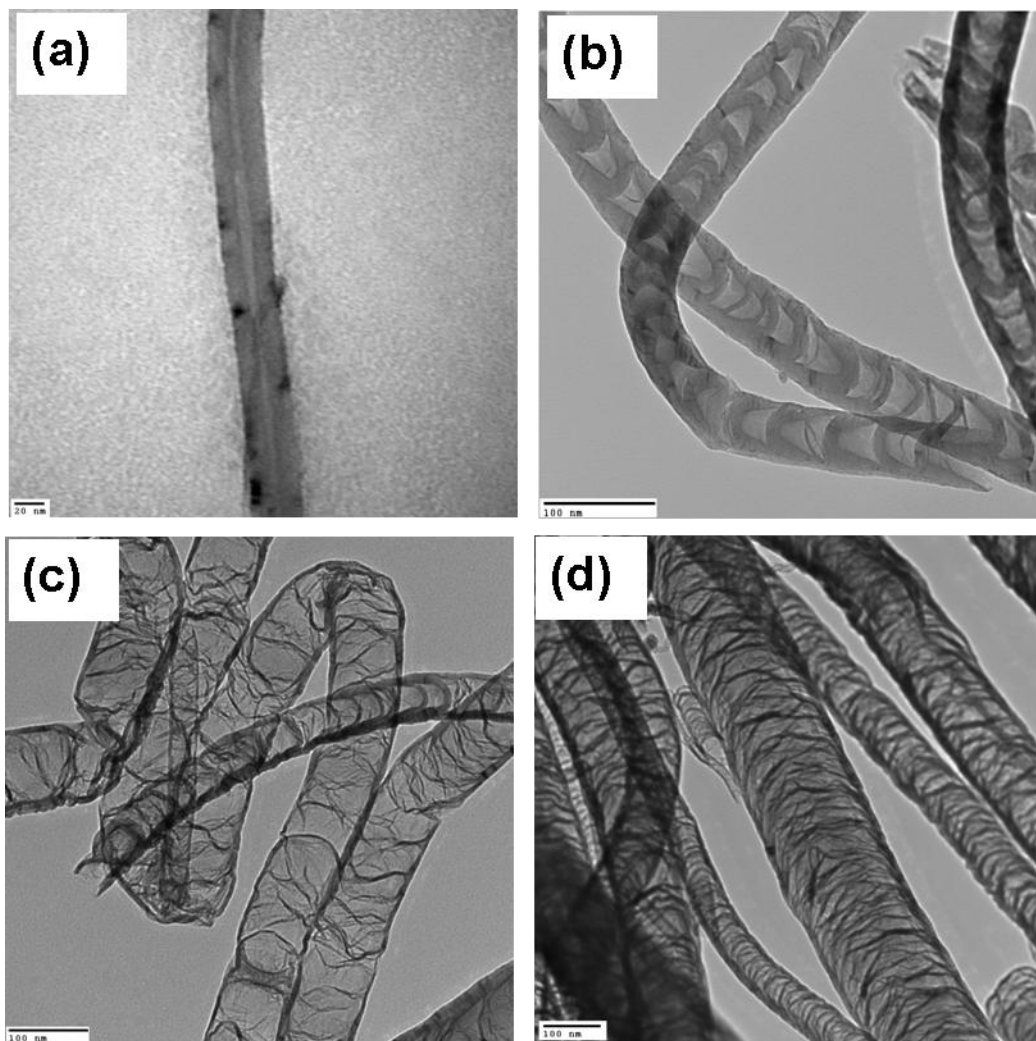


Figure 3-2 TEM images of CN_x prepared with various amount of melamine: (a) 50 mg, (b) 200 mg, (c) 400 mg, (d) 2000 mg.

the samples, all of CN_x catalysts prepared were analyzed by XPS. Table 3-1 shows the results of XPS analysis. An important trend is apparent in these results. The surface

nitrogen content increases with increasing melamine amount used for preparing CN_x . But the nitrogen content can only be 7.7 % at most by the method. The limitation might come from the nitrogen precursor and catalyst used. The more detailed structure analysis has been reported in our previous work [28].

Table 3-1 Surface composition (at. %) determined with XPS experiments.

Sample	C	N	O	Fe
CN_x (0%)	99.6	/	0.4	/
CN_x (1.4%)	96.3	1.4	1.8	0.4
CN_x (3.0%)	96.5	3.0	0.3	0.2
CN_x (5.1%)	93.8	5.1	0.7	0.4
CN_x (7.7%)	91.6	7.7	0.5	0.2

/ — below detection limit

3.3.2 ORR activities of CN_x in acid solution

Fig. 3-3a shows the cyclic voltammograms of CN_x (7.7%) catalyst in N_2 -saturated 0.5 M H_2SO_4 (black lines) and in O_2 -saturated 0.5 M H_2SO_4 (red lines). During both anodic and cathodic potential sweeps, an enhanced cathodic current was observed for the CV with the O_2 -saturated solution than for the N_2 -saturated solution. The enhanced cathodic current is due to the ORR on CN_x . To study the influence of various nitrogen contents in CN_x on the ORR activity, the polarization curves at a rotation speed of 900 rpm were recorded (Fig. 3-3b). We can see that the curves did not reach any diffusion limited current plateau within the whole potential range. The onset potential (E_{ORR}), a key factor for evaluating the catalyst activity, is defined as the potential where the enhanced cathodic current begins to be observed on the CV. For all CN_x , the values are quite different, spanning a potential range of about 300 mV. It indicates a large variation in the

electrocatalytic activity among these materials. The positive shift of E_{ORR} with increasing

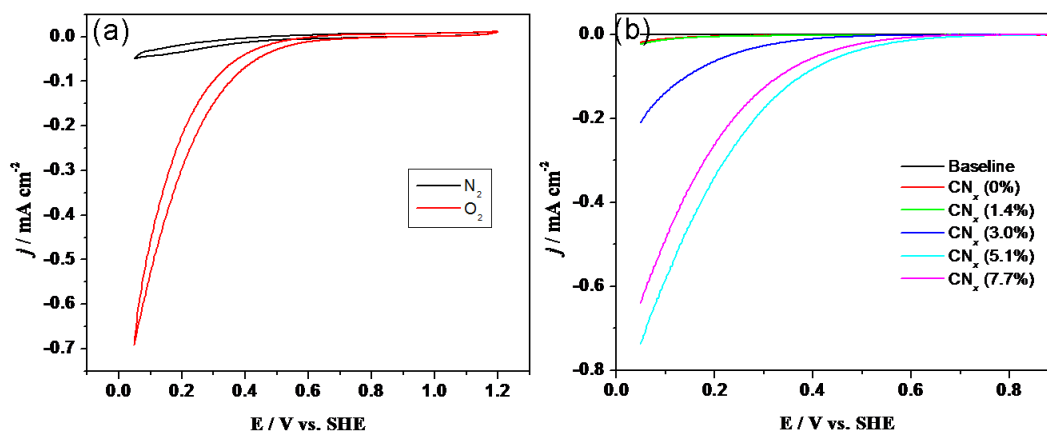


Figure 3-3 (a) Typical CV curves of CN_x (7.7%) in 0.5 M H_2SO_4 . Scan rate: 5 mVs^{-1} ; rotation speed: 900 rpm. (b) ORR polarization curves at a rotation speed of 900 rpm for the different CN_x with the loading of $160 \mu\text{g cm}^{-2}$.

nitrogen content in CN_x implies an improved catalytically active (kinetically more facile) for O_2 reduction. In an attempt to correlate the iron, nitrogen surface concentration and the onset potential, some interesting phenomena are obtained. There is no clear correlation of the onset potential with the iron content. Many researchers consider that graphene-coordinated FeN_4 or FeN_2 moieties are active sites [16, 22, 29]. However, the role of iron has been doubted recently. Ozkan et al. stated that iron acts as a catalysts for building the active site but is not a part of it itself [30]. Nevertheless, iron and nitrogen are very important to achieve electrocatalytic activity. Actually all catalysts containing Fe and nitrogen (CN_x (1.4%), CN_x (3.0%), CN_x (5.1%), CN_x (7.7%)) are more active than the catalyst without Fe and nitrogen (CN_x (0%)), as shown in Table 3-1. Furthermore, a dependence of ORR activity on nitrogen content in CN_x was obtained. Obviously, we can see that the onset potential of ORR increases with the increase of nitrogen content from Table 3-2. We can thus believe that the N-content should play a dominant role. The enhanced activity of the CN_x catalysts toward oxygen reduction is a direct result of nitrogen doping. Some special C-N structure of CN_x catalysts may be responsible for the enhancement of ORR activity. Ozkan et al. think that the higher activity of N-doped

Table 3-2 The onset electrode potentials for the ORR on various CN_x electrodes.

	CN _x (0%)	CN _x (1.4%)	CN _x (3.0%)	CN _x (5.1%)	CN _x (7.7%)
E _{ORR} / V(vs SHE) in 0.5 M H ₂ SO ₄	0.410	0.480	0.600	0.631	0.705
E _{ORR} / V(vs SHE) in 0.1 M KOH	-0.013	0.040	0.107	0.170	0.167

carbon fibers should be related to edge plane exposure, and not necessarily to the presence of metal residues [15]. In addition, an experimental and theoretical study of oxygen reduction on nitrogen-doped graphite has been presented by Anderson's group [20]. Their results showed that substitutional nitrogen atoms that are far from graphite sheet edges will be active, and those that are close to the edge will be less active.

In view of the higher catalytic activity of CN_x (7.7%), the kinetic behavior of ORR on CN_x (7.7%) electrode was further investigated using RRDE (Figures 3-4 and 3-5) [31, 32]. The voltammograms of CN_x (7.7%) (Figure 3-4) show a large current increase when the disk electrode rotates at 400 and 900 rpm. The large cathodic current results from an increase of the surface oxygen concentration available at the electrode surface due to the rotation. However, there is no well-defined limiting current plateau at any rotation rate. With the increase of rotation rate from 0 to 400 and 900 rpm, the line is more inclined. All these demonstrated that the reaction is under mixed kinetic control [17]. Simultaneously, these results also indicated that CN_x is still a poorer electrocatalyst than Pt/C catalyst in acidic solution. Some of the electrocatalytic active sites inside the electrode might be in contact with O₂ even at high overpotentials [33]. In addition, Anson et al. have proposed a model explaining that the distribution of electrocatalytic sites on the electrode surface is responsible for such behavior [34]. When distribution of active sites is less uniform and reaction is slower, the plateau is more inclined. Based on this model, the distribution of active sites in CN_x catalysts should not be uniform.

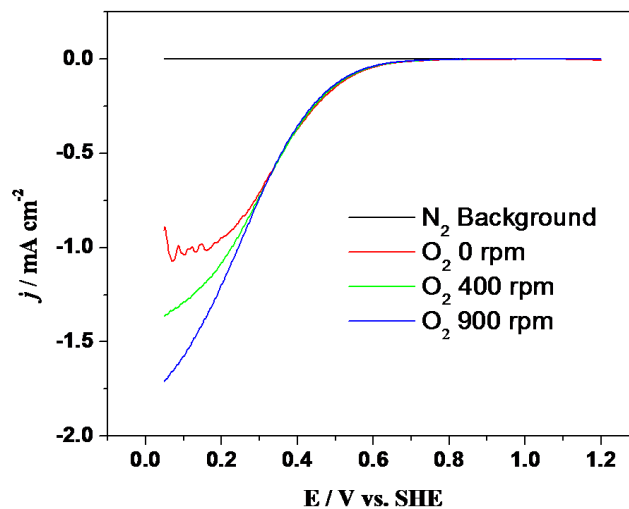


Figure 3-4 Oxygen reduction currents for CN_x (7.7%) in 0.5 M H_2SO_4 with saturated O_2 . Scan rate: 5 mV s^{-1} .

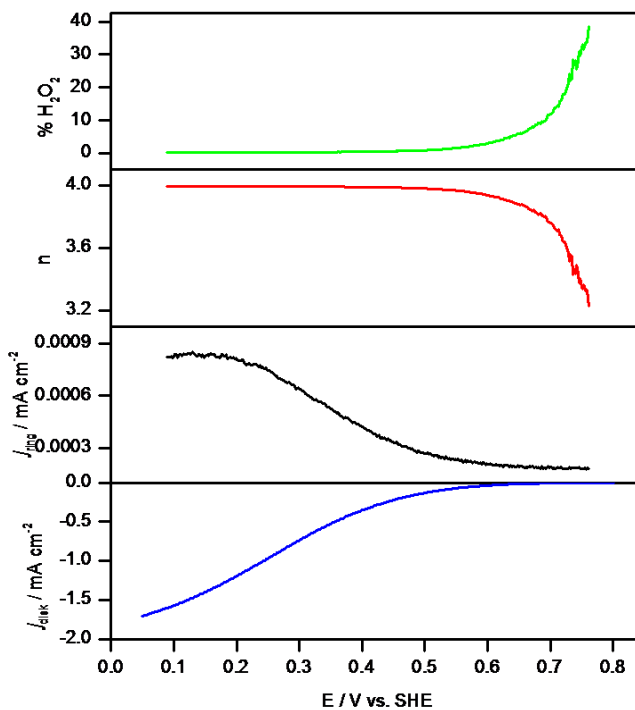


Figure 3-5 I_{Disk} , I_{Ring} , n (the apparent number of electrons transferred during ORR), and $\% \text{H}_2\text{O}_2$ measured by RRDE in O_2 saturated H_2SO_4 at room temperature for CN_x (7.7%).

To obtain selectivity data, both ring and disc currents at 900 rpm were recorded by RRDE measurements. For CN_x (7.7%) catalyst, Fig. 3-5 presented the reduction currents on the disk and the oxidation current on the ring, versus the potential applied on the disk. The apparent number of electrons transferred during ORR, n , and the percentage of H_2O_2 released during ORR, $\% \text{H}_2\text{O}_2$ were shown there as well as. The following equations are used to calculate n and $\% \text{H}_2\text{O}_2$ [32]:

$$n = 4 I_D / (I_D + (I_R / N)) \quad (1)$$

$$\% \text{H}_2\text{O}_2 = 100 (4 - n) / 2 \quad (2)$$

Where I_D is the Faradic current on the disk, I_R is the Faradic current on the ring and N is the ring collection efficiency (reported by the manufacturer to be 0.37). It can be seen that both I_R and I_D onset at about the same potential; and I_R increases with increasing I_D . The maximum of the ring current is not reached at the potential window applied. However, very little peroxide was formed on the CN_x (7.7%) sample, demonstrating its ability to completely reduce oxygen to water. Also from this figure, we can see that the apparent numbers of electrons transferred during ORR are close to 4 at the potentials lower than 0.5 V for CN_x (7.7%) (while $n = 3.4$ for CN_x (5.1%), and $n < 1$ for CN_x (3.0, 1.4, 0%) at 0.5 V), which further demonstrated its selectivity is high. Although CN_x catalysts have the lower activity than Pt/C catalyst for ORR mentioned above, the CN_x with high nitrogen content has high selectivity. Apparently, there is a loose correlation between activity and selectivity for the ORR, which has been reported by Ozkan and co-workers [15].

3.3.3 ORR activities of CN_x in alkaline solution

The CN_x towards ORR was also studied in alkaline solution. The effect of the electrode rotating rate on the ORR current over CN_x (7.7%) catalyst is shown in Figure 3-6a. The recorded ORR currents increase with increasing the electrode rotating rate. This is consistent with the general understanding that the ORR is under mixed kinetic-diffusion control. Figure 3-6b shows the disk current densities for CN_x (7.7%) catalyst measured at different loadings. The data for bare GC disk electrode (no catalyst applied) is also

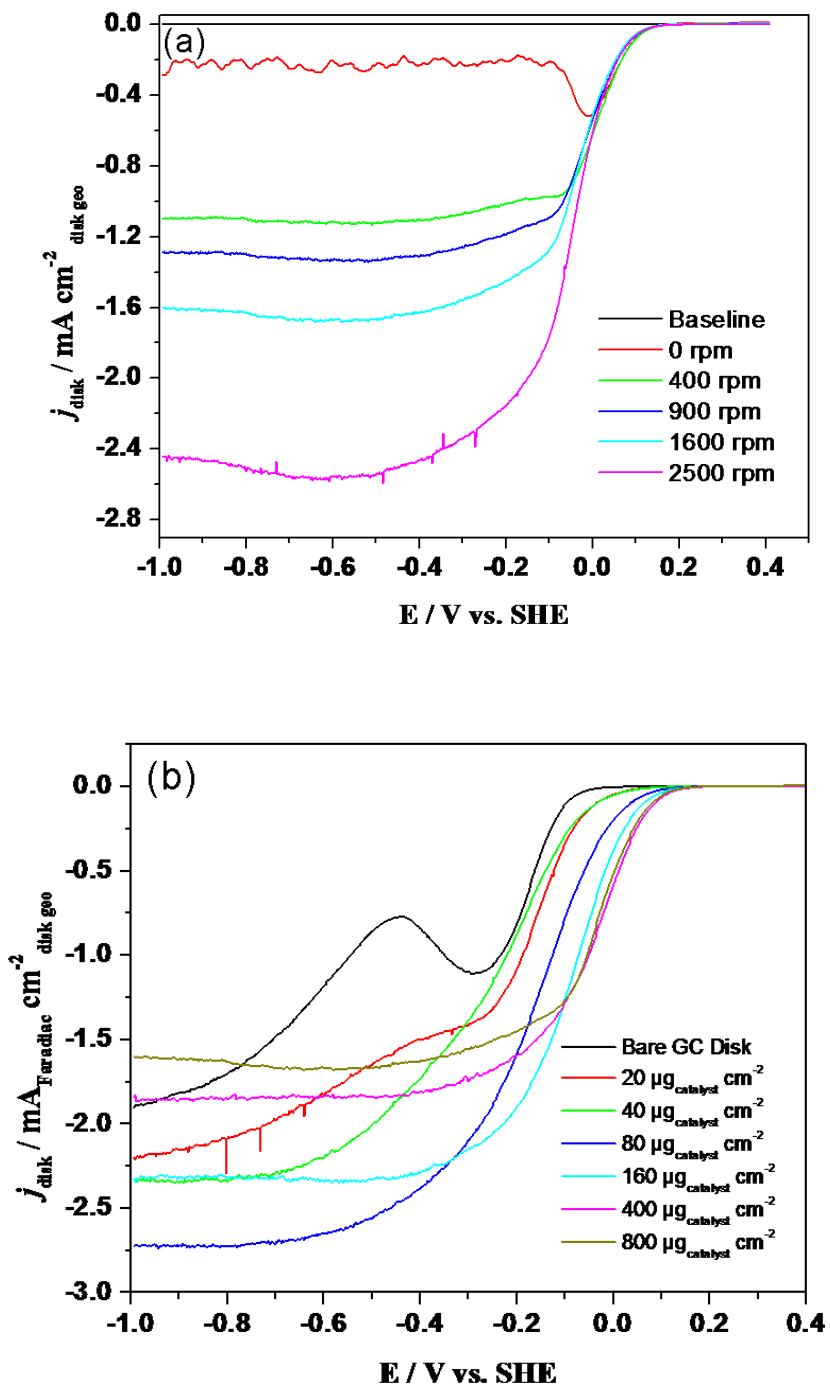


Figure 3-6 Measured ORR currents of CN_x (7.7%) catalyst at different electrode rotation speed (a) and different catalyst loading (b). Scan rate: 5 mV s^{-1} , electrolyte: 0.1 M KOH .

included in this figure to show that the GC-itself is negligible. At lower loading ($\leq 20 \mu\text{g cm}^{-2}$) no limiting current plateau is observed here. At the loading from 40 to $800 \mu\text{g cm}^{-2}$, not only can be the limiting current plateau obtained, but the limiting currents first increase and then have a decrease. It is suggested that besides the external diffusion limitation of oxygen from the bulk electrolyte to the electrode surface, a second mass transfer limitation within the catalyst layer is involved. As for the mass transfer within the catalyst layer, its hindrance effect is higher with the increase of catalyst loading, that is, with increasing thickness of the catalyst layer. In addition, one can find that E_{ORR} and the half-wave potentials (E_{hw}) of oxygen reduction increase with the increase of catalyst loading. All these activity data are summarized in Table 3-3. By combined analysis of E_{ORR} , E_{hw} , and current density ($j_{\text{disk Faradiac}}$), the loading of $160 \mu\text{g cm}^{-2}$ was considered to be the optimized loading. The importance of the catalyst loading to study the ORR activity is well recognized [35].

Table 3-3 The catalytic activity data for GC and CN_x (7.7%) with different loading. Data were obtained from Fig. 3-6b.

Catalyst	GC	CN_x (7.7%)					
		$20 \mu\text{g cm}^{-2}$	$40 \mu\text{g cm}^{-2}$	$80 \mu\text{g cm}^{-2}$	$160 \mu\text{g cm}^{-2}$	$400 \mu\text{g cm}^{-2}$	$800 \mu\text{g cm}^{-2}$
$E_{\text{ORR}} / \text{V}(\text{vs SHE})$	0.014	0.118	0.132	0.155	0.162	0.186	0.181
$E_{\text{hw}} / \text{V}(\text{vs SHE})$	-	-	-0.251	-0.171	-0.087	-0.041	-0.033
$j_{\text{disk Faradiac}}@-0.150\text{V}$	0.403	0.712	0.558	1.202	1.649	1.478	1.379
$j_{\text{disk Faradiac}}@-0.992\text{V}$	1.903	2.202	2.336	2.730	2.327	1.841	1.602

The polarization curves of oxygen reduction on CN_x catalysts with different nitrogen contents are shown in Figure 3-7. The perfect limiting current plateau can only be observed on the catalysts with high nitrogen content (5.1 and 7.7%). Also, there is no clear dependence of current density on the nitrogen content. However, it was observed that the E_{ORR} shifts positively with increasing the nitrogen content. These values are also given at Table 3-2.

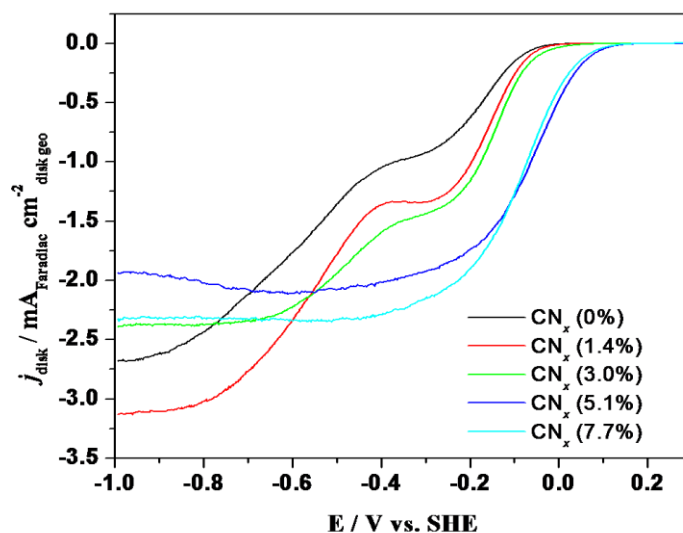


Figure 3-7 The polarization curves of oxygen reduction on CN_x catalysts with different nitrogen content. Electrolyte: 0.1 M KOH, scan rate: 5 mV s^{-1} , and rotation speed: 1600 rpm.

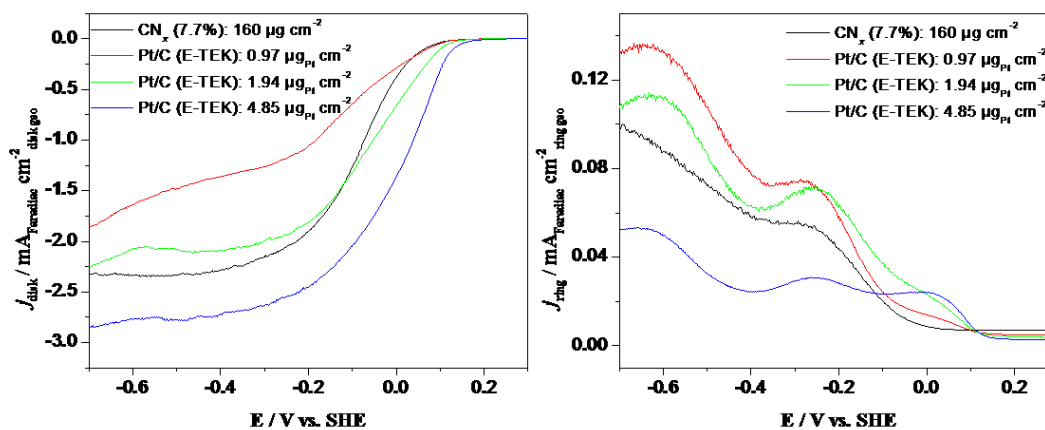


Figure 3-8 RRDE voltammograms of CN_x (7.7%) and Pt/C with different loading in 0.1 M KOH solution saturated with O_2 . The ring-disk electrode rotation rate was 1600 rpm, and the Au ring electrode was held at 0.7 V.

Based on the above results, CN_x (7.7%) with the loading of $160 \mu\text{g cm}^{-2}$ was selected as a control sample. Its ORR activity was compared with that of commercial Pt/C catalyst. RRDE voltammograms for CN_x (7.7%) and Pt/C with different loading are depicted in

Figure 3-8. For Pt/C catalysts, the value of the limiting disk current decreases with decreasing loading; and the ring current is low at high loading because the fraction of H₂O₂ released is low. The detailed catalytic activity data are given in Table 3-4. Herein the transport-corrected kinetic current (i_{kinetic}) is obtained using the well-known Levich-Koutecky expression:

$$1/i_{\text{measured}} = 1/i_{\text{kinetic}} + 1/i_{\text{diffusion}} \quad (3)$$

From these catalytic activity data, one can believe that CN_x (7.7%, loading: 160 μg cm⁻²) have similar catalytic ability towards ORR, in comparison to the commercial Pt/C catalyst (loading: 1.94 μg_{Pt} cm⁻²). Further, we calculated their apparent number of electrons (n) transferred during ORR according to the disk and ring current to compare the selectivity. The result indicated that they have comparable n values, which is 3.8 and 3.7 for CN_x (7.7%, loading: 160 μg cm⁻²) and Pt/C (loading: 1.94 μg_{Pt} cm⁻²) at -0.20 V, respectively.

Table 3-4 The catalytic activity data for CN_x (7.7%) with the loading of 160 μg cm⁻² and Pt/C (E-TEK) with different loading. Data were obtained from Fig. 3-8.

Catalyst and kinetic data	Loading / μg cm ⁻²	E _{ORR} / V	E _{hw} / V	Kinetic current density	Kinetic current density
			at 1600 rpm	at 0 V / mA cm ⁻²	at -0.05 V / mA cm ⁻²
CN _x (7.7%)	160	0.162	-0.087	-0.460	-1.204
Pt/C (E-TEK)	0.97	0.161	-0.166	-0.340	-0.592
Pt/C (E-TEK)	1.94	0.185	-0.070	-0.940	-1.759
Pt/C (E-TEK)	4.85	0.213	-0.006	-2.643	-4.567

As discussed above, the detailed structure of the active site of CN_x is not clear at present. It might be a Fe/N/C-type structure similar to those described in the literature proposed by Dodelet et al. [22]. They believe that four factors are responsible to the ORR activity

on Fe/N/C: (i) disordered carbon content in the catalyst precursor, (ii) iron, (iii) surface nitrogen, and (iv) micropores in the catalyst. Using quantum mechanics calculations, Dai et al. [23] suggested that the strong electronic affinity of the nitrogen atoms and the substantially high positive charge density on the adjacent carbon atoms should contribute to the catalytic activity. We do not yet clearly understand why CN_x have the comparable ORR activity with the Pt/C in alkaline solution, but much lower than that of Pt/C in acid solution. It may be due to quinone systems being capable of reducing oxygen catalytically only in a strong base [36]. The detailed mechanism needs further investigation.

3.4 Conclusions

CN_x catalysts for ORR have been prepared. TEM and XPS results showed the nitrogen surface content and morphology of CN_x can be controlled by adjusting the content of melamine used. In this work, the emphasis was mainly placed on the study of structure-activity relationship. It has been showed that the ORR activity increased with the increase of surface nitrogen content in both acid and alkaline solutions according to the E_{ORR} values. There was not apparent correlation between the current density and the nitrogen surface content. However, the catalyst loading has an obvious impact on the ORR current density. Most importantly, the onset potential and current density of CN_x (7.7%) electrocatalyst reported in this work is equal to a platinum-based catalyst with a loading of 1.94 microgram of platinum per square centimeter at the electrochemical window tested in alkaline solution, showing that CN_x has the potential to replace the costly Pt/C catalyst in alkaline fuel cells.

Acknowledgments

This research was supported by Natural Sciences and Engineering Research Council of Canada (NSERC), Ballard Power System Inc., Canada Research Chair (CRC) Program, Canada Foundation for Innovation (CFI), Ontario Research Fund (ORF), Ontario Early Researcher Award (ERA) and the University of Western Ontario.

References

- [1] J. Zhang, PEM Fuel Cell Electrocatalysts and Catalyst Layers: Fundamentals and Applications, in, Springer, 2008.
- [2] R. Bashyam, P. Zelenay, A class of non-precious metal composite catalysts for fuel cells, *Nature*, 443 (2006) 63-66.
- [3] N.A. Vante, H. Tributsch, Energy-Conversion Catalysis Using Semiconducting Transition-Metal Cluster Compounds, *Nature*, 323 (1986) 431-432.
- [4] B. Viswanathan, C.V. Rao, U.V. Varadaraju, On the Search for Non-Noble Metal Based Electrodes for Oxygen Reduction Reaction, *Photo/Electrochem. & Photobiol. Environ, Energy Fuel*, (2006) 43-101.
- [5] B. Wang, Recent development of non-platinum catalysts for oxygen reduction reaction, *J Power Sources*, 152 (2005) 1-15.
- [6] P.H. Matter, E.J. Biddinger, U.S. Ozkan, Non-precious metal oxygen reduction catalysts for PEM fuel cells, *Catalysis*, 20 (2007) 338-366.
- [7] J.H. Zagal, F. Bedioui, J.-P. Dodelet, N4-Macrocyclic Metal Complexes, Springer Science + Business Media, Inc., New York, 2006.
- [8] C.W.B. Bezerra, L. Zhang, H.S. Liu, K.C. Lee, A.L.B. Marques, E.P. Marques, H.J. Wang, J.J. Zhang, A review of heat-treatment effects on activity and stability of PEM fuel cell catalysts for oxygen reduction reaction, *J Power Sources*, 173 (2007) 891-908.
- [9] V.I. Zaikovskii, K.S. Nagabhushana, V.V. Kriventsov, K.N. Loponov, S.V. Cherepanova, R.I. Kvon, H. Bonnemann, D.I. Kochubey, E.R. Savinova, Synthesis and structural characterization of Se-modified carbon-supported Ru nanoparticles for the oxygen reduction reaction, *J Phys Chem B*, 110 (2006) 6881-6890.

- [10] K.C. Lee, A. Ishihara, S. Mitsushima, N. Kamiya, K.I. Ota, Stability and electrocatalytic activity for oxygen reduction in WC plus Ta catalyst, *Electrochim Acta*, 49 (2004) 3479-3485.
- [11] Y. Takasu, N. Yoshinaga, W. Sugimoto, Oxygen reduction behavior of RuO₂/Ti, IrO₂/Ti and IrM (M : Ru, Mo, W, V) O-x/Ti binary oxide electrodes in a sulfuric acid solution, *Electrochem Commun*, 10 (2008) 668-672.
- [12] R.Z. Yang, K. Stevens, J.R. Dahn, Investigation of activity of sputtered transition-metal (TM)-C-N (TM = V, Cr, Mn, Co, Ni) catalysts for oxygen reduction reaction, *J Electrochem Soc*, 155 (2008) B79-B91.
- [13] Y.Y. Shao, J.H. Sui, G.P. Yin, Y.Z. Gao, Nitrogen-doped carbon nanostructures and their composites as catalytic materials for proton exchange membrane fuel cell, *Appl Catal B-Environ*, 79 (2008) 89-99.
- [14] F. Jaouen, S. Marcotte, J.P. Dodelet, G. Lindbergh, Oxygen reduction catalysts for polymer electrolyte fuel cells from the pyrolysis of iron acetate adsorbed on various carbon supports, *J Phys Chem B*, 107 (2003) 1376-1386.
- [15] P.H. Matter, E. Wang, M. Arias, E.J. Biddinger, U.S. Ozkan, Oxygen reduction reaction activity and surface properties of nanostructured nitrogen-containing carbon, *J Mol Catal a-Chem*, 264 (2007) 73-81.
- [16] A.L. Bouwkamp-Wijnoltz, W. Visscher, J.A.R. van Veen, E. Boellaard, A.M. van der Kraan, S.C. Tang, On active-site heterogeneity in pyrolyzed carbon-supported iron porphyrin catalysts for the electrochemical reduction of oxygen: An in situ Mossbauer study, *J Phys Chem B*, 106 (2002) 12993-13001.
- [17] S.L. Gojkovic, S. Gupta, R.F. Savinell, Heat-treated iron(III) tetramethoxyphenyl porphyrin chloride supported on high-area carbon as an electrocatalyst for oxygen reduction - Part II. Kinetics of oxygen reduction, *J Electroanal Chem*, 462 (1999) 63-72.
- [18] S. Maldonado, K.J. Stevenson, Influence of nitrogen doping on oxygen reduction electrocatalysis at carbon nanofiber electrodes, *J Phys Chem B*, 109 (2005) 4707-4716.

- [19] J. Ozaki, N. Kimura, T. Anahara, A. Oya, Preparation and oxygen reduction activity of BN-doped carbons, *Carbon*, 45 (2007) 1847-1853.
- [20] R.A. Sidik, A.B. Anderson, N.P. Subramanian, S.P. Kumaraguru, B.N. Popov, O₂ reduction on graphite and nitrogen-doped graphite: Experiment and theory, *J Phys Chem B*, 110 (2006) 1787-1793.
- [21] S. Biniak, M. Walczyk, G.S. Szymanski, Modified porous carbon materials as catalytic support for cathodic reduction of dioxygen, *Fuel Process Technol*, 79 (2002) 251-257.
- [22] M. Lefevre, E. Proietti, F. Jaouen, J.P. Dodelet, Iron-Based Catalysts with Improved Oxygen Reduction Activity in Polymer Electrolyte Fuel Cells, *Science*, 324 (2009) 71-74.
- [23] K.P. Gong, F. Du, Z.H. Xia, M. Durstock, L.M. Dai, Nitrogen-Doped Carbon Nanotube Arrays with High Electrocatalytic Activity for Oxygen Reduction, *Science*, 323 (2009) 760-764.
- [24] Y.F. Tang, B.L. Allen, D.R. Kauffman, A. Star, Electrocatalytic Activity of Nitrogen-Doped Carbon Nanotube Cups, *J Am Chem Soc*, 131 (2009) 13200-13201.
- [25] P.H. Matter, E. Wang, U.S. Ozkan, Preparation of nanostructured nitrogen-containing carbon catalysts for the oxygen reduction reaction from SiO₂- and MgO-supported metal particles, *J Catal*, 243 (2006) 395-403.
- [26] K. Prehn, A. Warburg, T. Schilling, M. Bron, K. Schulte, Towards nitrogen-containing CNTs for fuel cell electrodes, *Compos Sci Technol*, 69 (2009) 1570-1579.
- [27] Y. Okamoto, First-principles molecular dynamics simulation of O₂ reduction on nitrogen-doped carbon, *Appl Surf Sci*, 256 (2009) 335-341.
- [28] H. Liu, Y. Zhang, R.Y. Li, X.L. Sun, S. Desilets, H. Abou-Rachid, M. Jaidann, L.S. Lussier, Structural and morphological control of aligned nitrogen-doped carbon nanotubes, *Carbon*, 48 (2010) 1498-1507.

- [29] U.I. Koslowski, I. Abs-Wurmbach, S. Fiechter, P. Bogdanoff, Nature of the catalytic centers of porphyrin-based electrocatalysts for the ORR: A correlation of kinetic current density with the site density of Fe-N₄ Centers, *J Phys Chem C*, 112 (2008) 15356-15366.
- [30] P.H. Matter, E. Wang, J.M.M. Millet, U.S. Ozkan, Characterization of the iron phase in CN_x-based oxygen reduction reaction catalysts, *J Phys Chem C*, 111 (2007) 1444-1450.
- [31] S.L. Gojkovic, S.K. Zecevic, R.F. Savinell, O₂ reduction on an ink-type rotating disk electrode using Pt supported on high-area carbons, *J Electrochem Soc*, 145 (1998) 3713-3720.
- [32] U.A. Paulus, T.J. Schmidt, H.A. Gasteiger, R.J. Behm, Oxygen reduction on a high-surface area Pt/Vulcan carbon catalyst: a thin-film rotating ring-disk electrode study, *J Electroanal Chem*, 495 (2001) 134-145.
- [33] S.Y. Ye, A.K. Vijh, Non-noble metal-carbonized aerogel composites as electrocatalysts for the oxygen reduction reaction, *Electrochem Commun*, 5 (2003) 272-275.
- [34] R.Z. Jiang, F.C. Anson, The Origin of Inclined Plateau Currents in Steady-State Voltammograms for Electrode Processes Involving Electrocatalysis, *J Electroanal Chem*, 305 (1991) 171-184.
- [35] A. Bonakdarpour, M. Lefevre, R.Z. Yang, F. Jaouen, T. Dahn, J.P. Dodelet, J.R. Dahn, Impact of loading in RRDE experiments on Fe-N-C catalysts: Two- or four-electron oxygen reduction?, *Electrochem Solid St*, 11 (2008) B105-B108.
- [36] J.R.T.J. Wass, E. Ahlberg, I. Panas, D.J. Schiffrin, Quantum chemical modelling of the rate determining step for oxygen reduction on quinones, *Phys Chem Chem Phys*, 8 (2006) 4189-4199.

Chapter 4

4 Nitrogen doping effects on the structure of graphene

Dongsheng Geng^a, Songlan Yang^{a,b}, Yong Zhang^a, Jinli Yang^a, Jian Liu^a,

Ruying Li^a, Tsun-Kong Sham^b, Xueliang Sun^{a,*}, Siyu Ye^c, Shanna Knights^c

^a*Department of Mechanical and Materials Engineering, University of Western Ontario, 1151
Richmond Street N., London, Ontario, Canada N6A 5B9*

^b*Department of Chemistry, University of Western Ontario, 1151 Richmond Street N., London,
Ontario, Canada N6A 5B9*

^c*Ballard Power Systems Inc., 9000 Glenlyon Parkway, Burnaby, BC, Canada V5J 5J8*

**To whom correspondence should be addressed. E-mail: xsun@eng.uwo.ca*

Tel: +1-519-6612111, Ext. 87759, Fax: +1-519-6613020

A version of this chapter has been published in *Applied Surface Science*, 2011, **257**,
9193-9198.

In Chapter 3, we demonstrated that nitrogen doping can improve the electrocatalytic activity of carbon nanotubes for ORR. To further design and improve this kind of non-noble metal ORR catalyst, a central question to be answered is how nitrogen doping

affects the structure of carbon materials? In this chapter, we will elucidate the question by an example of the new carbon materials: graphene and N-graphene.

Graphene, the two-dimensional (2D) monolayer of carbon atoms arranged in a honeycomb lattice, has unique physical and chemical properties, such as high surface area, high chemical stability, excellent conductivity, which lead graphene as an ideal base for applications in many fields. Since material properties are always related to the structure of the material, many attempts have been made to modify the electrical properties of graphene by controlling its structure. Chemical doping with foreign atom is considered an effective method to intrinsically modify the properties of carbon materials. Especially nitrogen doping plays a critical role in regulating the electronic and chemical properties of carbon materials due to its comparable atomic size and five valence electrons available to form strong valence bonds with carbon atoms.

Therefore, for us it is of fundamental interest to investigate how nitrogen doping affects the structure of graphene and in turn the chemical properties can be adjusted accordingly. The question is then: what is the difference between the structure of graphene and N-graphene? In this chapter, we systematically investigated the effects of N-doping on the structure of graphene by many characterization techniques especially XANES. Some interesting results have been obtained, such as more defects are present on nitrogen doped graphene, and N doping decreases the surface oxygen-containing groups.

Key words: *Graphene, Nitrogen doping, Defects, Structure*

4.1 Introduction

Graphene, the two-dimensional (2D) monolayer of carbon atoms arranged in a honeycomb lattice, has recently attracted great interests for both fundamental and applied research since its discovery by Novoselov, Geim and their co-workers at the University of Manchester using the deceptively simple Scotch tape method [1]. Graphene has unique physical and chemical properties, such as high surface area (theoretical value: $\sim 2630 \text{ m}^2 \text{ g}^{-1}$), high chemical stability, excellent conductivity ($10^6 \text{ S}\cdot\text{cm}^{-1}$, higher than the conductivity of silver, the highest conductive substance known at room temperature), unique graphitic basal plane structure, and the easiness of functionalization and production. These unique physical and chemical properties lead graphene as an ideal base for applications in electric device [2], biosensors [3], field effect transistors [4], supercapacitors [5], lithium secondary batteries [6], and fuel cells [7-10]. Since material properties are always related to the structure of the material, many attempts have been made to modify the electrical properties of graphene by controlling its structure, which includes preparing carbon sheets with different layers and graphene with and without defects by new synthesis methods [11, 12], chemical functionalization of graphene [13-15], and chemical doping with foreign atoms [16-18]. In general, chemical doping with N or B is considered an effective method to intrinsically modify the properties of carbon materials. Especially nitrogen doping plays a critical role in regulating the electronic and chemical properties of carbon materials due to its comparable atomic size and five valence electrons available to form strong valence bonds with carbon atoms. Theoretical study has shown that nitrogen doping results in the higher positive charge on a carbon atom adjacent to the nitrogen atoms [19], and a positive shift of Fermi energy at the apex of the Brillouin zone of graphene [20]. Some recent experimental results also proved that nitrogen doped graphene (N-graphene) has higher electrocatalytic activity for the reduction of hydrogen peroxide and oxygen than graphene [19, 21]. Also, N-graphene has shown better performance in Li ion battery applications [22]. Furthermore, N-graphene as Pt support exhibited the higher electrocatalytic activity for methanol oxidation than graphene [23]. Therefore, it is of fundamental interest to investigate how nitrogen doping affects the structure of graphene and in turn the chemical properties can

be adjusted accordingly. The question is then: what is the difference between the structure of graphene and N-graphene? To date, however, only limited works have been done to investigate the structural difference between graphene and N-graphene [16, 24, 25]. Here, we report the results from a series of experiments designed and various advanced characterization techniques to address this question.

In this work, we prepared the N-graphene (2.8 % N content) by the heat treatment of graphene under ammonia, and studied the effect of nitrogen doping on the structure of graphene systematically by various characterization techniques - BET (Brunauer, Emmett, and Teller) isotherm, scanning electron microscopy (SEM), transmission electron microscopy (TEM), X-ray diffraction (XRD), Raman spectra, FT-IR spectra, X-ray photoelectron spectroscopy (XPS), and X-ray absorption near-edge structure (XANES) spectroscopy.

4.2 Experimental

4.2.1 Preparation of graphene and N-graphene

Graphite powder was used as the starting material. Graphene was first prepared by the oxidation of graphite powder using the modified Hummers' method [26, 27]. Typically, graphite powder (1 g) and sodium nitrate (0.75 g) were first stirred in concentrated sulphuric acid (37.5 mL) while being cooled in an ice water bath. Then potassium permanganate (4.5 g) was gradually added to form a new mixture. After two hours in an ice water bath, the mixture was allowed to stand for five days at room temperature with gentle stirring. Thereafter, 100 mL of 5 wt% H_2SO_4 aqueous solution was added into the above mixture over 1h with stirring. Then, 3 g of H_2O_2 (30 wt% aqueous solution) was also added to the above liquid and the mixture was stirred for 2h. After that, the suspension was filtered and washed until the pH value of the filtrate was neutral. The as-received slurry is the so-called graphite oxide. Finally, the dried graphite oxide was heated at 1050 °C for 30 s under Ar to get graphene [28]. Nitrogen-doped graphene was further obtained by heating the graphene under high purity ammonia mixed with Ar at 900 °C [29].

4.2.2 Physical characterizations

The morphologies of the samples were characterized by Hitachi S-4800 field-emission SEM operated at 5.0 kV, Philips CM10 TEM operated at 80 kV. BET is used to determine the specific surface area, pore size, and pore volume. Also the detailed structures have been characterized by XRD, Raman spectra, FT-IR spectra. The nitrogen contents for N-graphene was determined by Kratos Axis Ultra Al (alpha) XPS. The synchrotron-based XANES spectroscopy measurements were performed at the Canadian Light Source (CLS) on the High Resolution Spherical Grating Monochromator (SGM) beamline for the C K-, N K-, and O K-edge spectra. This beamline uses a 45 mm planar undulator and three gratings to cover a photon energy region from 250 to 2000 eV. It offers an energy resolution greater than 5,000 E/ Δ E at energy below 1500 eV [30]. The beamline is capable of providing 10^{12} photons per second at 250 eV and exceeds 10^{11} photons per second up to 1900 eV at 100 mA. Spectra were recorded in the fluorescence yield mode (FLY) using a microchannel-plate detector and the total electron yield (TEY) mode measuring the sample current. All spectra were normalized to the intensity of the incident beam (I_0), measured simultaneously as the current emitted from a gold mesh located after the last optical elements of the beamline.

4.3 Results and discussion

Figure 4-1 shows the typical SEM and TEM images of graphene and N-graphene. It can be seen that the material is transparent with the voile-like structure. These materials consist of randomly crumpled sheets closely associated with each other and forming a disordered solid. The graphene planar sheets are clearly observed in N-doped graphene, indicating that the features of high surface/volume ratio and the two-dimensional structure of graphene morphology are well maintained. However, it is hard to distinguish the difference between graphene and N-graphene from the general SEM and TEM observations.

Table 4-1 shows the detailed BET data for the two samples. It has been recently shown that graphene and N-graphene can be used as the catalysts or catalyst supports in fuel cells and batteries [10, 23, 31]. High specific surface area is thus usually required for the

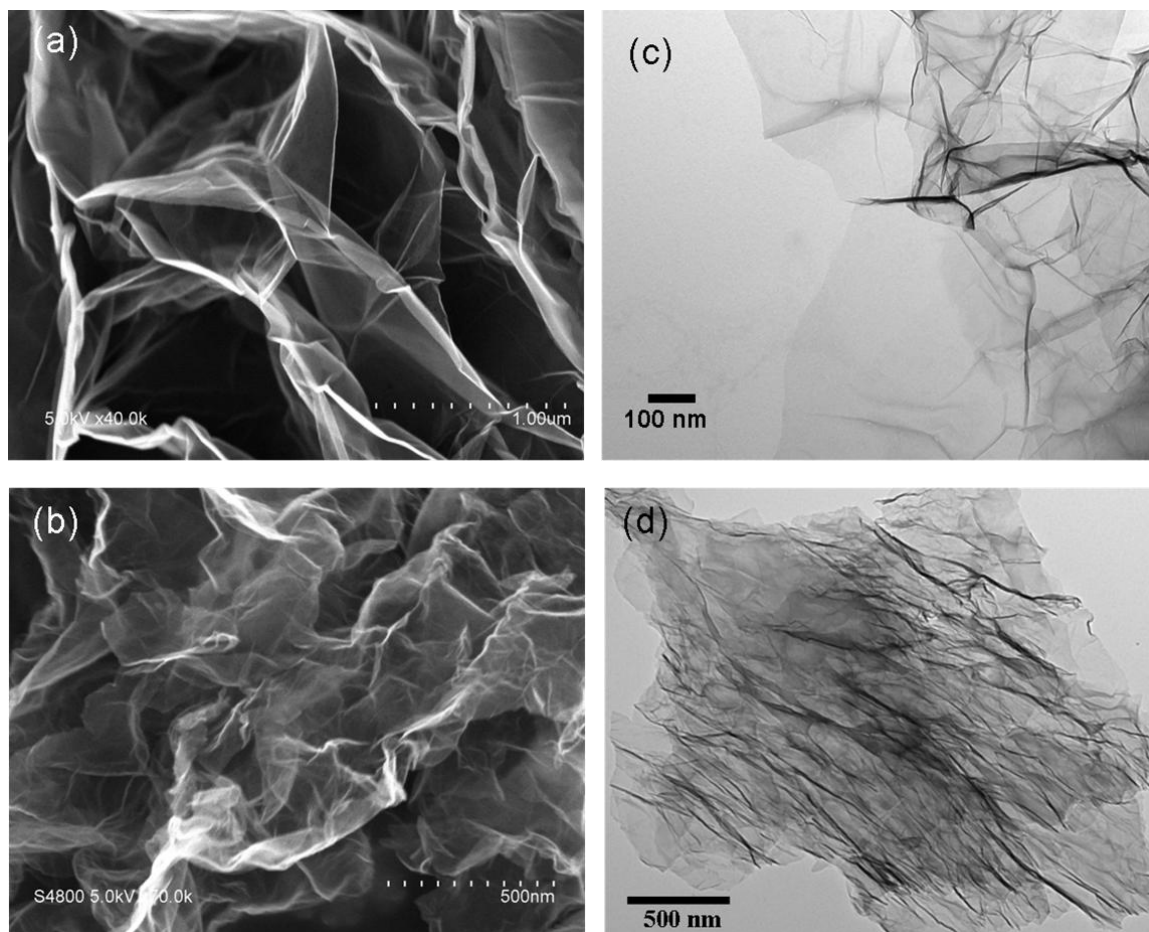


Figure 4-1 SEM and TEM images of graphene (a, c) and N-graphene samples (b, d).

Table 4-3 Specific surface area of graphene and N-graphene determined by BET method.

Sample	Specific surface area ($\text{m}^2 \text{g}^{-1}$)	Pore volume ($\text{cm}^3 \text{g}^{-1}$)	Pore size (\AA)
Graphene	455.6	1.34	118.1
N-graphene	595.6	1.82	122.0

deposition of metals or metal oxides uniformly on these materials to enhance the electrochemical activity. As one expects, the specific surface area increases from 455.6 to 595.6 $\text{m}^2 \text{g}^{-1}$ for graphene and N-graphene, respectively. The high specific surface area is an indication of a higher degree of graphite exfoliation in the latter. However, it is still lower than the theoretical specific surface area for completely exfoliated and isolated graphene sheets, due to incomplete exfoliation and the agglomeration of graphene upon rapid heating. Also, one can notice that the pore volume and pore size increase slightly after nitrogen doping. During the preparation process of N-graphene, not only nitrogen atoms can substitute some carbon atoms that most likely located on the reactive edge [18], but ammonia also reacts with graphene to form hydrogen cyanide and hydrogen ($\text{C} + \text{NH}_3 = \text{HCN} + \text{H}_2$). This process consumed some carbon and may make the material more porous, which in turn resulted in the higher specific surface area, pore volume, and pore size.

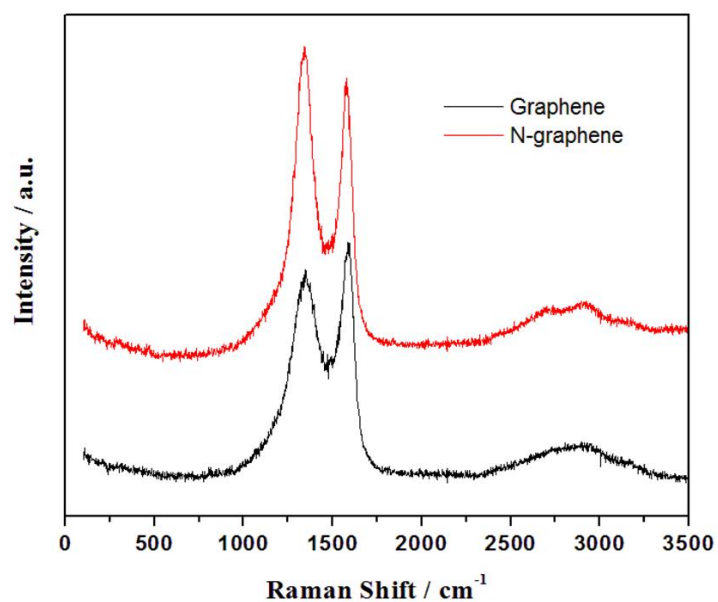


Figure 4-2 Raman spectra of graphene and N-graphene samples.

In order to evaluate the degree of structural deformations of the graphene and N-graphene samples, Raman spectroscopy was carried out (Fig. 4-2). Two distinct peaks were

observed. The D band, at approximately 1340 cm^{-1} for our samples, is disorder induced, attributable to structural defects and other disordered structures on the graphitic plane. The G band, at approximately 1570 cm^{-1} , is commonly observed for all graphitic structures and can be attributed to the E_{2g} vibrational mode present in the sp^2 bonded graphitic carbons. The intensity ratio of D band to G band, namely the I_D/I_G ratio, provides the gauge for the amount of structural defects and a quantitative measure of edge plane exposure. N-graphene was found to have a I_D/I_G ratio of 1.12, obviously larger than 0.87 observed for graphene. The larger I_D/I_G ratio for N-graphene is a result of the structural defects and edge plane exposure caused by heterogeneous nitrogen atom incorporation into the graphene layers. The result is also consistent with our previous study about carbon nanotube and N-doped carbon nanotubes [32].

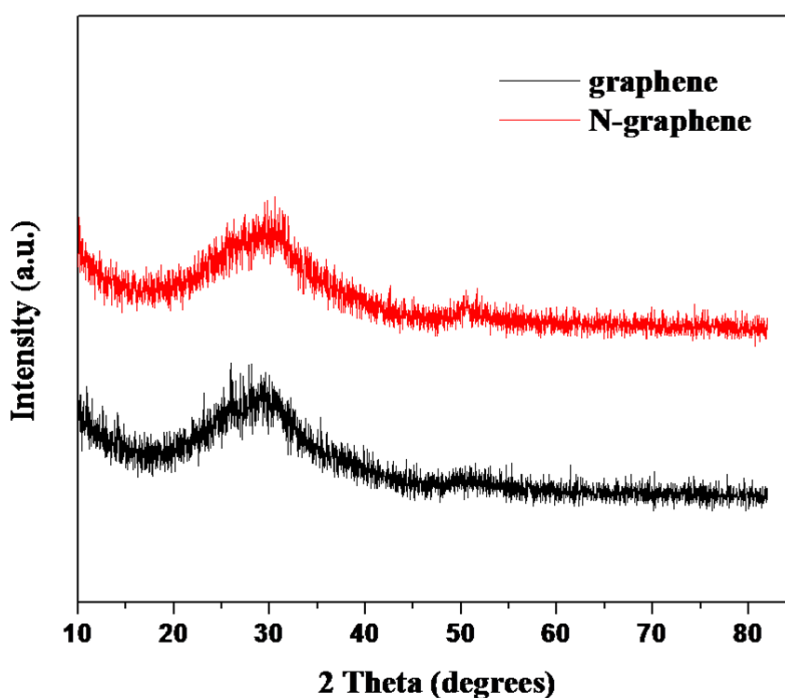


Figure 4-3 XRD patterns of graphene and N-graphene samples.

Fig. 4-3 shows the XRD patterns for graphene and N-graphene. The pronounced (002) peaks at about 29.0 degree were seen for both samples, which is also assigned to the layer-to-layer distance (d -spacing: $d = \lambda / 2 \sin\theta$). The average stacking number of a graphene layer was calculated [33] by using the d -spacing and size of the crystallite,

which was evaluated from the width of the diffraction peak using the Scherrer equation ($\tau = K \lambda / \beta \cos\theta$, where K is the shape factor, λ is the X-ray wavelength, β is the line broadening at half the maximum intensity (FWHM) in radians, and θ is the Bragg angle; τ is the mean size of the crystalline domains). The detailed X-ray crystalline parameters are shown in Table 4-2. From these data, it can be seen that the interlayer spacing of graphene and N-graphene are larger than that of graphite (3.35 Å); and the size of crystallite for N-graphene has slightly decreased compared with graphene, maybe due to ammonia corrosion and defects resulted from nitrogen doping. However, ammonia treatment process can not affect the layers of graphene.

Table 4-4 X-ray structural parameters of graphene and N-graphene from plane (002).

Sample	θ , Plane (002)	Value of d (Å)	Value of τ (Å)	No. of layers
Graphene	29.2	3.55	0.832	3.3
N-graphene	29.9	3.46	0.799	3.3

Furthermore, FT-IR spectra were used to investigate the bonding difference between graphene and N-graphene. From Fig. 4-4, it can be seen that although graphite oxide was reduced by rapid heating, the FT-IR spectrum of graphene still shows some characteristic bands of surface oxidized groups, at 3450 cm^{-1} (O-H stretching vibrations), at 1384 cm^{-1} (C-O-H stretching vibrations), and at 1100 cm^{-1} (C-O stretching vibrations) [34]. The peak located at 1635 cm^{-1} could be ascribed to the skeletal vibration of graphitic domains. For N-graphene, in addition to the above-mentioned peaks, C-N stretching vibrations were observed at 1257 and 1326 cm^{-1} and N-H bend vibration at 1550 cm^{-1} was also obtained. Due to the overlap of peaks for C=C and C=N, and the relative low ratio of nitrogen to carbon atoms, it is difficult to prove the existence of C=N by FT-IR.

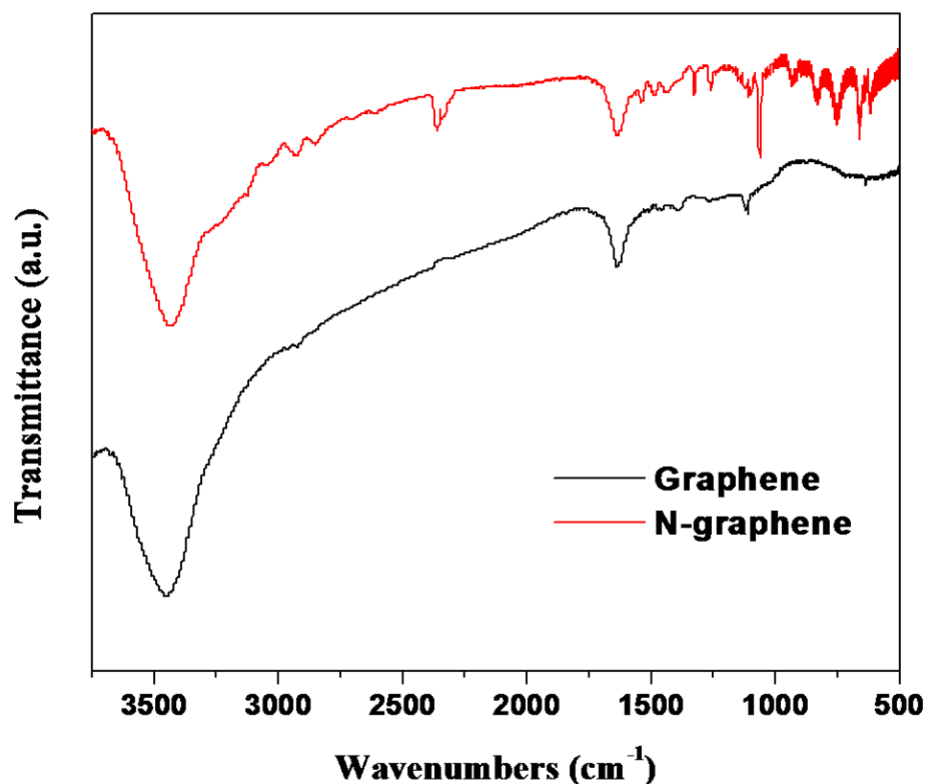


Figure 4-4 Infrared spectra of graphene and N-graphene samples.

XPS, a powerful tool to identify the elements' states in bulk material, was thus used to prove the existence of C=N and other existing forms of nitrogen. XPS characterization (Fig. 4-5) indicated that about 2.8 at.% nitrogen was introduced to the graphene sheet by ammonia treatment under 900 °C. Based on the detailed analysis of N1s (insert, Fig. 4-5), the different proportion of pyridine-like N (398.1 eV), pyrrole-like N (399.9 eV), and quaternary N (401.3 eV) were observed. In addition, it was found that ammonia annealing temperature has the effect on N doping content and the existence forms of nitrogen. The N content is 2.8 and 2.0 at.% for N-graphene under 800 and 1000 °C annealing temperature, respectively. N-graphene under treatment temperature of 900 °C has the highest content of quaternary N, which is considered as the real doping [35]. Thus, it is clear that nitrogen was doped into the graphene structure.

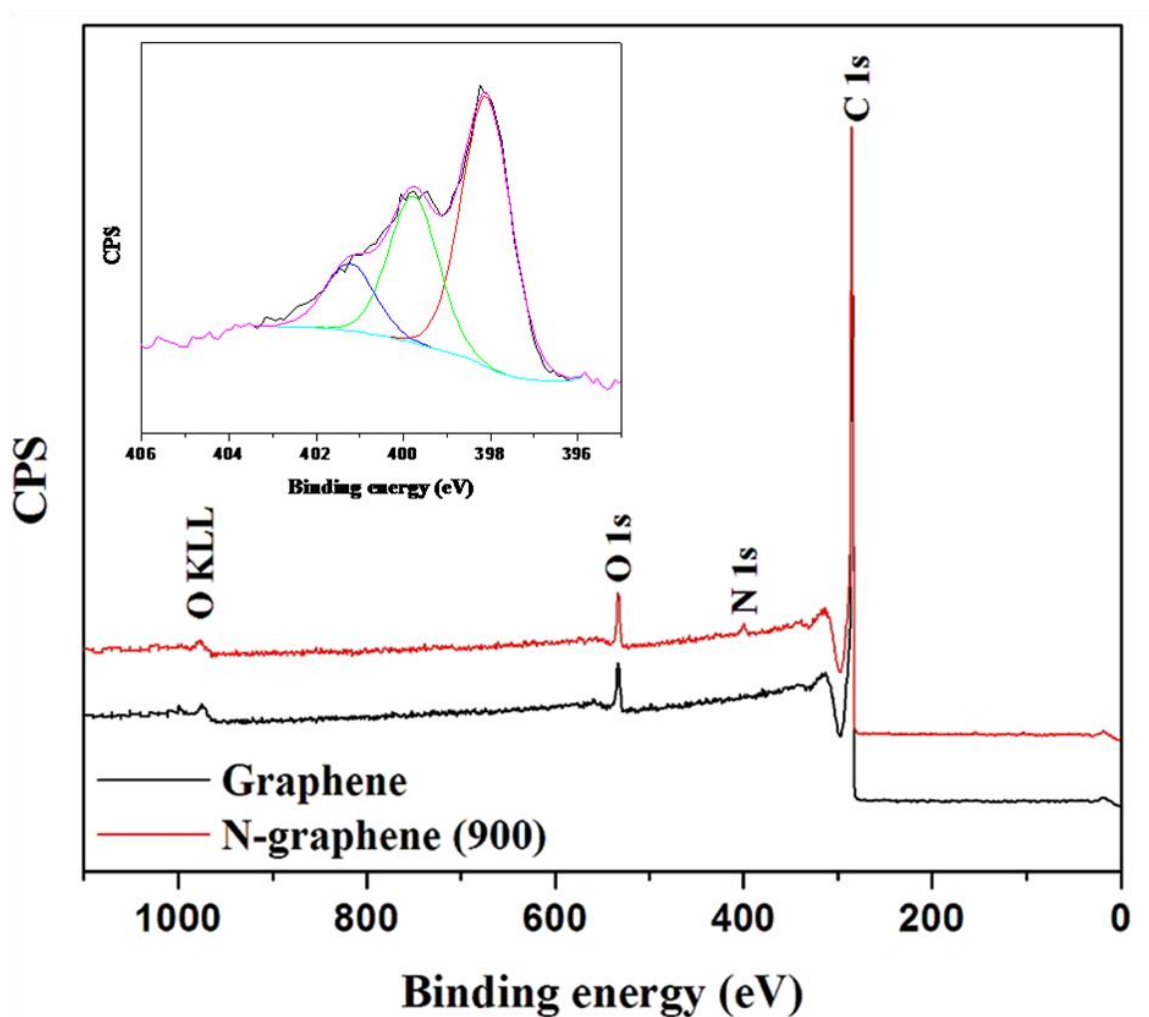


Figure 4-5 XPS spectra of graphene and N-graphene samples. The inset: the high resolution N1s spectra of N-graphene sample: The pink and black lines are the raw and fitted spectra. The red, green, and blue lines correspond to pyridine-like N (398.1 eV), pyrrole-like N (399.9 eV), and quaternary N (401.3 eV), respectively.

XANES measurements were carried out to investigate the nitrogen doping effect in detail. C K-edge XANES spectra of graphene and N doped graphene are compared in Fig. 4-6(a). XANES spectroscopy is element specific and it concerns with the measurement and interpretation of the absorption coefficient above an absorption edge of an element in a chemical environment. At the C and N K-edge, the area under the resonance in the vicinity of the threshold in XANES (also called white line) is

proportional to the unoccupied density of state (DOS) when tunable X-rays are used to excite the 1s electron into previously unoccupied electronic states of p character (dipole selection rules). In graphite, the C K-edge will clearly exhibit a π^* (~ 285 eV) and a σ^* (~ 291 eV) resonance [36]. In high purity graphene, similar resonance patterns have been observed together with a well-defined peak at ~ 283.6 eV [37]. The region between the π^* and σ^* resonance is usually flat or monotonic if the samples are without impurity. For surface functionalized graphite, graphene, carbon nanotubes, resonance structures characteristic of oxygen or nitrogen functionalized surface groups will appear. For better comparison, the C K-edge spectra of graphene and N-graphene are normalized to the edge jump (where the absorption coefficient reaches a flat region above the edge) of unity. At a first glance of Fig. 4-6(a), both spectra show two main features, the π^* transition at around 285.5 eV and the σ^* transition at around 291.7 eV, which is the signature of the graphitic structure. It should be noted that the relative intensity of the π^* vs. σ^* transition depends on the relative orientation of the graphitic plane with respect to the polarization of the incident photon, which is linearly polarized in the plane of the electron orbit of the synchrotron. At normal incidence, the σ^* dominates and at grazing incidence, the π^* dominates. In the present case, the angle of incidence was at 45° , and the sample is not perfectly flat, both resonances are noticeable. In-between these two main features, a weak peak at 288.3 eV can also be detected in the undoped graphene, the intensity of which decreased obviously after N doping. This feature has been previously characterized as the resonance from the π^* of the C=O bond of the carboxylic COOH group [38]. It is worth reiterating that no spectral feature in the region between the π^* and σ^* can be observed for high purity graphite, carbon nanotube and graphene with little defects. Another pre-edge feature centered at around 283.6 eV can also be detected in both cases. This feature is due to the surface defects, for example, dangling bonds [39] and amorphous carbon. The intensity for this pre-edge feature increased with N doping. Therefore, with N doping, more defect sites have been created in the graphene. Even though, those features from N related functional groups in between 287-288 eV cannot be easily discerned, the intensity for both π^* transition and σ^* transition increased a little after N doping. This is a powerful evidence that after the N doping the unoccupied DOS

increased by the charge transfer from carbon to the more electronegative nitrogen, which is beneficial for the electric conductivity of the material.

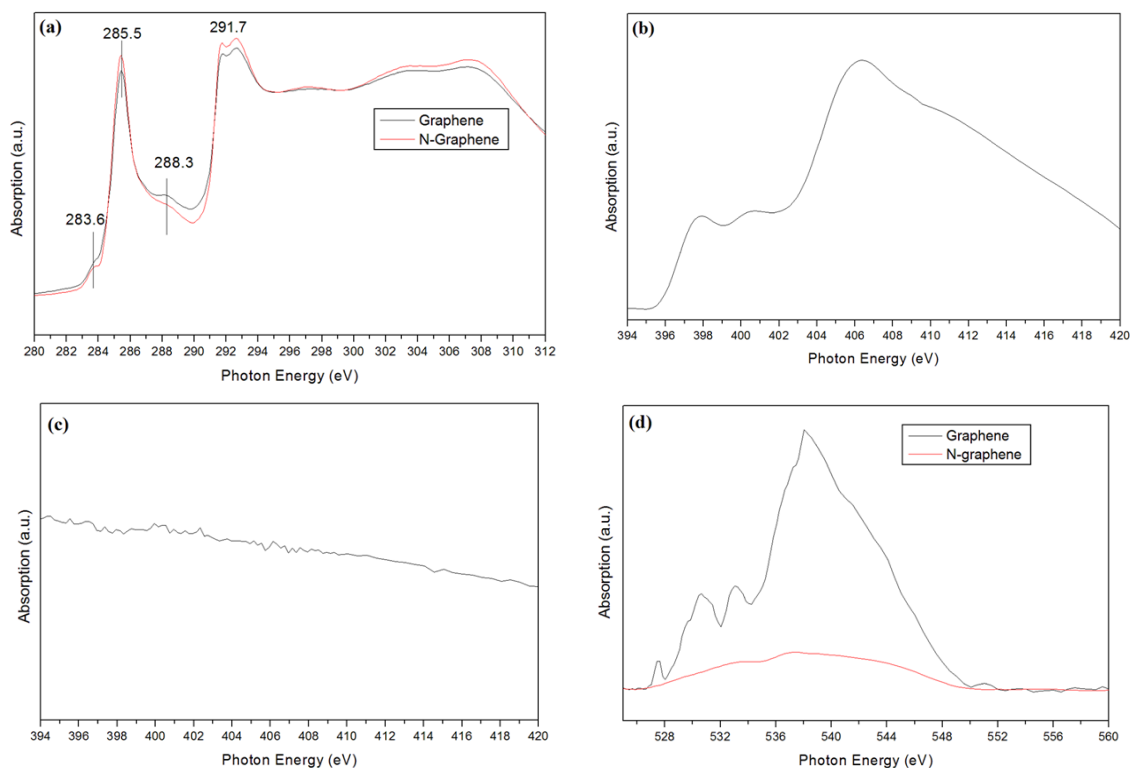


Figure 4-6 (a) and (b) TEY of the C K-edge and N K-edge XANES spectra of graphene and N-doped graphene, (c) FLY of the XANES spectra of the N-doped graphene, and (d) TEY of the O K-edge XANES spectra of graphene and N-doped graphene.

The existence of N in the N-graphene can be confirmed by the corresponding TEY of the N K-edge XANES spectra as shown in Fig. 4-6(b). Three main peaks can be detected as centered at 397.9 eV, 400.7 eV and 406.3 eV. The first two features arise from transitions from the K shell (N 1s) to unoccupied π^* orbital containing N character and the last is due to the transition into σ^* orbital [40]. They are undoubtedly a direct support of successful doping into the graphene matrix, forming unsaturated C-N bonds. The π^* resonance at 397.9 eV is attributable to the pyridine-like bonding in nitrogenated carbon materials, and the other broad peak from 399.3 to 401.7 eV may come from pyrrole- and graphite-like bonding. No signal from the N K-edge can be found through the bulk

sensitive FLY, as shown in Fig. 4-6(c), therefore, the doping predominately occurred in the surface of graphene specimen under investigation.

The effect of N doping on the content of oxygen-containing groups in graphene can be confirmed by the comparison of O K-edge as shown in Fig. 4-6(d). Several features corresponding to different oxygen-containing groups are visible from the graphene (the black line). The peak at 530.6 eV is from the π^* state of C=O, the one at 533.3 eV is related from to the π^* state of C(sp²)-O, and that at 536.3 eV belongs to the σ^* state of the C-O [41]. After N doping, the peak intensity diminishes and the presence of those oxygen-containing groups once exist on the surface of un-doped graphene is no longer evident.

4.4 Conclusions

Nitrogen doped graphene has been prepared by the heat-treatment of graphene using ammonia. XPS results indicated that about 2.8 at.% nitrogen was introduced into the graphene layer. The effects of N-doping on graphene have been systematically investigated by a number of techniques for microstructure and bonding studies. The results show that after nitrogen doping, the graphene basically maintains the initial morphology based on the SEM and TEM images. Most importantly, XANES confirms the incorporation of N into the graphene lattice. Several observations must be noted. First, these results show that there are several nitrogen species such as pyridine-like, pyrrole-like, pyridine-like, and quaternary N contents on the N-graphene. Second, after N doping, XANES results reveal that the unoccupied DOS increases, suggesting charge transfer from carbon to the more electronegative nitrogen, which is beneficial for the electric conductivity of the material. Finally, the N-doping decreases the surface oxygen-containing groups, which may provide a new way to control the surface oxygen contents, and improve the corrosion resistance of graphene. In addition, BET analysis reveals that N-graphene has the increased specific surface area compared with graphene, indicating that more defects exist on the surface, which is supported by the observation of decreased size and higher I_D/I_G ratio after doping from XRD and Raman results, respectively. The resulting surface defects due to nitrogen doping is expected to enhance Li⁺ storage for Li

ion battery applications and the anchoring of Pt nanoparticles on N-graphene for fuel cell electrocatalyst applications.

Acknowledgments

This research was supported by Natural Sciences and Engineering Research Council of Canada (NSERC), Ballard Power Systems Inc., Canada Research Chair (CRC) Program, Canada Foundation for Innovation (CFI), Ontario Research Fund (ORF), Ontario Early Researcher Award (ERA) and the University of Western Ontario. CLS is supported by CFI, NRC, NSERC, CIHR and the University of Saskatchewan.

References

- [1] K.S. Novoselov, A.K. Geim, S.V. Morozov, D. Jiang, Y. Zhang, S.V. Dubonos, I.V. Grigorieva, A.A. Firsov, Electric field effect in atomically thin carbon films, *Science*, 306 (2004) 666-669.
- [2] N. Levy, S.A. Burke, K.L. Meaker, M. Panlasigui, A. Zettl, F. Guinea, A.H.C. Neto, M.F. Crommie, Strain-Induced Pseudo-Magnetic Fields Greater Than 300 Tesla in Graphene Nanobubbles, *Science*, 329 (2010) 544-547.
- [3] Y.Y. Shao, J. Wang, H. Wu, J. Liu, I.A. Aksay, Y.H. Lin, Graphene Based Electrochemical Sensors and Biosensors: A Review, *Electroanal*, 22 (2010) 1027-1036.
- [4] F.N. Xia, D.B. Farmer, Y.M. Lin, P. Avouris, Graphene Field-Effect Transistors with High On/Off Current Ratio and Large Transport Band Gap at Room Temperature, *Nano Lett*, 10 (2010) 715-718.
- [5] L.L. Zhang, R. Zhou, X.S. Zhao, Graphene-based materials as supercapacitor electrodes, *J Mater Chem*, 20 (2010) 5983-5992.
- [6] E. Yoo, J. Kim, E. Hosono, H. Zhou, T. Kudo, I. Honma, Large reversible Li storage of graphene nanosheet families for use in rechargeable lithium ion batteries, *Nano Lett*, 8 (2008) 2277-2282.

- [7] D.R. Kauffman, A. Star, Graphene versus carbon nanotubes for chemical sensor and fuel cell applications, *Analyst*, 135 (2010) 2790-2797.
- [8] B. Seger, P.V. Kamat, Electrocatalytically Active Graphene-Platinum Nanocomposites. Role of 2-D Carbon Support in PEM Fuel Cells, *J Phys Chem C*, 113 (2009) 7990-7995.
- [9] L.T. Qu, Y. Liu, J.B. Baek, L.M. Dai, Nitrogen-Doped Graphene as Efficient Metal-Free Electrocatalyst for Oxygen Reduction in Fuel Cells, *Acs Nano*, 4 (2010) 1321-1326.
- [10] Y.Y. Shao, S. Zhang, C.M. Wang, Z.M. Nie, J. Liu, Y. Wang, Y.H. Lin, Highly durable graphene nanoplatelets supported Pt nanocatalysts for oxygen reduction, *J Power Sources*, 195 (2010) 4600-4605.
- [11] A. Gupta, G. Chen, P. Joshi, S. Tadigadapa, P.C. Eklund, Raman scattering from high-frequency phonons in supported n-graphene layer films, *Nano Lett*, 6 (2006) 2667-2673.
- [12] O.C. Compton, S.T. Nguyen, Graphene Oxide, Highly Reduced Graphene Oxide, and Graphene: Versatile Building Blocks for Carbon-Based Materials, *Small*, 6 (2010) 711-723.
- [13] K.P. Loh, Q.L. Bao, P.K. Ang, J.X. Yang, The chemistry of graphene, *J Mater Chem*, 20 (2010) 2277-2289.
- [14] D.W. Boukhvalov, M.I. Katsnelson, Chemical Functionalization of Graphene with Defects, *Nano Lett*, 8 (2008) 4373-4379.
- [15] Y. Zhu, A.L. Higginbotham, J.M. Tour, Covalent Functionalization of Surfactant-Wrapped Graphene Nanoribbons, *Chem Mater*, 21 (2009) 5284-5291.
- [16] L.S. Panchokarla, K.S. Subrahmanyam, S.K. Saha, A. Govindaraj, H.R. Krishnamurthy, U.V. Waghmare, C.N.R. Rao, Synthesis, Structure, and Properties of Boron- and Nitrogen-Doped Graphene, *Adv Mater*, 21 (2009) 4726-4730.

- [17] J. Meyer, S. Kurasch, H.-J. Park, V. Skakalova, D. Künzel, A. Groß, A. Chuvilin, S. Roth, U. Kaiser, Bonding Effects in Nitrogen Doped Graphene and Hexagonal Boron Nitride, *Microscopy and Microanalysis*, 16 (2010) 542-543.
- [18] X.R. Wang, X.L. Li, L. Zhang, Y. Yoon, P.K. Weber, H.L. Wang, J. Guo, H.J. Dai, N-Doping of Graphene Through Electrothermal Reactions with Ammonia, *Science*, 324 (2009) 768-771.
- [19] K.P. Gong, F. Du, Z.H. Xia, M. Durstock, L.M. Dai, Nitrogen-Doped Carbon Nanotube Arrays with High Electrocatalytic Activity for Oxygen Reduction, *Science*, 323 (2009) 760-764.
- [20] S.U. Lee, R.V. Belosludov, H. Mizuseki, Y. Kawazoe, Designing Nanogadgets for Nanoelectronic Devices with Nitrogen-Doped Capped Carbon Nanotubes, *Small*, 5 (2009) 1769-1775.
- [21] Y. Wang, Y.Y. Shao, D.W. Matson, J.H. Li, Y.H. Lin, Nitrogen-Doped Graphene and Its Application in Electrochemical Biosensing, *Acs Nano*, 4 (2010) 1790-1798.
- [22] A.L.M. Reddy, A. Srivastava, S.R. Gowda, H. Gullapalli, M. Dubey, P.M. Ajayan, Synthesis Of Nitrogen-Doped Graphene Films For Lithium Battery Application, *Acs Nano*, 4 (2010) 6337-6342.
- [23] L.S. Zhang, X.Q. Liang, W.G. Song, Z.Y. Wu, Identification of the nitrogen species on N-doped graphene layers and Pt/NG composite catalyst for direct methanol fuel cell, *Phys Chem Chem Phys*, 12 (2010) 12055-12059.
- [24] S.F. Huang, K. Terakura, T. Ozaki, T. Ikeda, M. Boero, M. Oshima, J. Ozaki, S. Miyata, First-principles calculation of the electronic properties of graphene clusters doped with nitrogen and boron: Analysis of catalytic activity for the oxygen reduction reaction, *Phys Rev B*, 80 (2009) 235410.
- [25] B.D. Guo, Q.A. Liu, E.D. Chen, H.W. Zhu, L.A. Fang, J.R. Gong, Controllable N-Doping of Graphene, *Nano Lett*, 10 (2010) 4975-4980.

- [26] W.S. Hummers, R.E. Offeman, Preparation of Graphitic Oxide, *J Am Chem Soc*, 80 (1958) 1339-1339.
- [27] M. Hirata, T. Gotou, S. Horiuchi, M. Fujiwara, M. Ohba, Thin-film particles of graphite oxide 1: High-yield synthesis and flexibility of the particles, *Carbon*, 42 (2004) 2929-2937.
- [28] H.C. Schniepp, J.L. Li, M.J. McAllister, H. Sai, M. Herrera-Alonso, D.H. Adamson, R.K. Prud'homme, R. Car, D.A. Saville, I.A. Aksay, Functionalized single graphene sheets derived from splitting graphite oxide, *J Phys Chem B*, 110 (2006) 8535-8539.
- [29] X.L. Li, H.L. Wang, J.T. Robinson, H. Sanchez, G. Diankov, H.J. Dai, Simultaneous Nitrogen Doping and Reduction of Graphene Oxide, *J Am Chem Soc*, 131 (2009) 15939-15944.
- [30] <http://exshare.lightsource.ca/sgm/Pages/Beamline.aspx>.
- [31] S.M. Paek, E. Yoo, I. Honma, Enhanced Cyclic Performance and Lithium Storage Capacity of SnO₂/Graphene Nanoporous Electrodes with Three-Dimensionally Delaminated Flexible Structure, *Nano Lett*, 9 (2009) 72-75.
- [32] H. Liu, Y. Zhang, R.Y. Li, X.L. Sun, S. Desilets, H. Abou-Rachid, M. Jaidann, L.S. Lussier, Structural and morphological control of aligned nitrogen-doped carbon nanotubes, *Carbon*, 48 (2010) 1498-1507.
- [33] B.K. Saikia, R.K. Boruah, P.K. Gogoi, A X-ray diffraction analysis on graphene layers of Assam coal, *J Chem Sci*, 121 (2009) 103-106.
- [34] S. Stankovich, R.D. Piner, S.T. Nguyen, R.S. Ruoff, Synthesis and exfoliation of isocyanate-treated graphene oxide nanoplatelets, *Carbon*, 44 (2006) 3342-3347.
- [35] D.S. Geng, Y. Chen, Y.G. Chen, Y.L. Li, R.Y. Li, X.L. Sun, S.Y. Ye, S. Knights, High oxygen-reduction activity and durability of nitrogen-doped graphene, *Energ Environ Sci*, 4 (2011) 760-764.

- [36] T.K. Sham, Nanoparticles and nanowires: synchrotron spectroscopy studies, *Int J Nanotechnol*, 5 (2008) 1194-1246.
- [37] D. Pacile, M. Papagno, A.F. Rodriguez, M. Grioni, L. Papagno, Near-edge x-ray absorption fine-structure investigation of graphene, *Phys Rev Lett*, 101 (2008) 066806.
- [38] A. Kuznetsova, I. Popova, J.T. Yates, M.J. Bronikowski, C.B. Huffman, J. Liu, R.E. Smalley, H.H. Hwu, J.G.G. Chen, Oxygen-containing functional groups on single-wall carbon nanotubes: NEXAFS and vibrational spectroscopic studies, *J Am Chem Soc*, 123 (2001) 10699-10704.
- [39] R. Gago, M. Vinnichenko, H.U. Jager, A.Y. Belov, I. Jimenez, N. Huang, H. Sun, M.F. Maitz, Evolution of sp(2) networks with substrate temperature in amorphous carbon films: Experiment and theory, *Phys Rev B*, 72 (2005) 014120.
- [40] R. McCann, S.S. Roy, P. Papakonstantinou, I. Ahmad, P. Maguire, J.A. McLaughlin, L. Petaccia, S. Lizzit, A. Goldoni, NEXAFS study and electrical properties of nitrogen-incorporated tetrahedral amorphous carbon films, *Diam Relat Mater*, 14 (2005) 1057-1061.
- [41] H.K. Jeong, H.J. Noh, J.Y. Kim, M.H. Jin, C.Y. Park, Y.H. Lee, X-ray absorption spectroscopy of graphite oxide, *Epl-Europhys Lett*, 82 (2008).

Supporting information

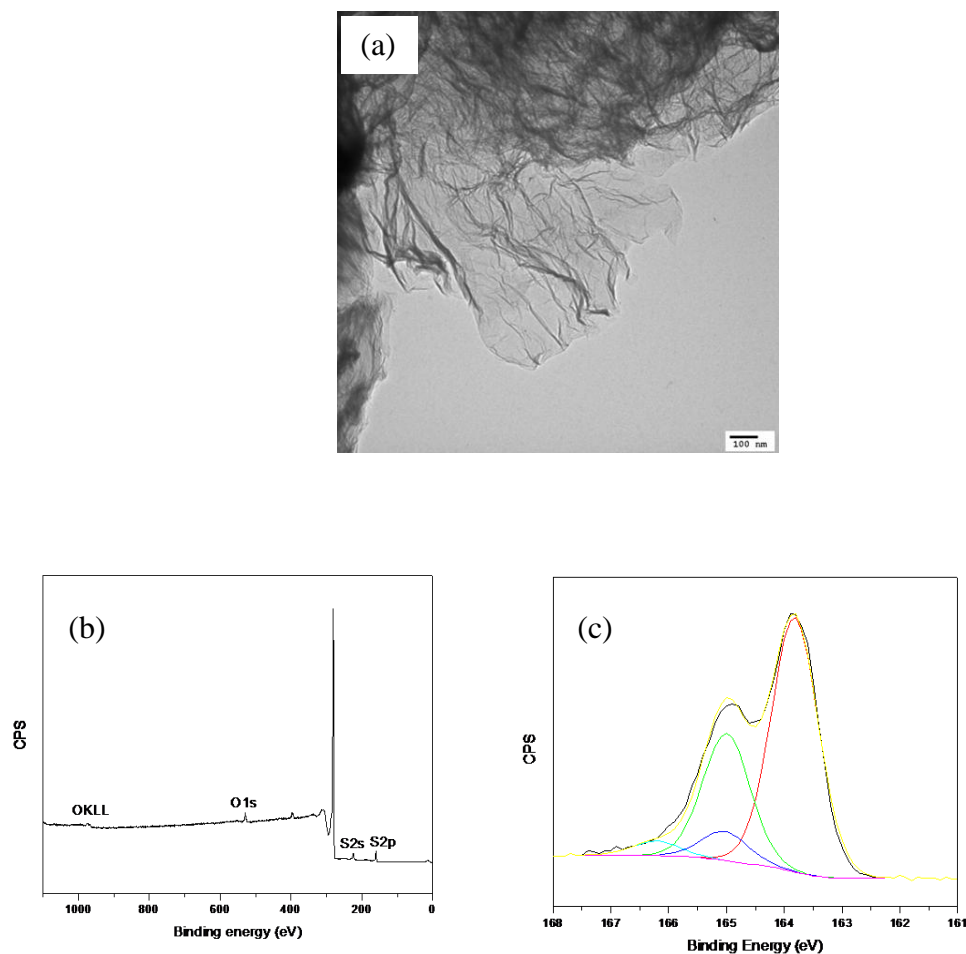


Figure 4-7 (a) Typical TEM image of S-graphene; (b) XPS survey scan spectra of S-graphene; (c) Deconvoluted XPS spectrum of the S-2p-orbital for S-graphene.

The sulphur content is about 1.9 at.% using the equation: $S / (S+C)$. Based on the detailed analysis of S2p (Fig. 4-7c), it exhibits a higher complexity. A clear assignment is difficult, especially being based on these data obtained by deconvolution. The S 2p core level line exhibits two resolved components at 163.6 and 165.0 eV that correspond to spin-orbit splitting and the features at 165.2 and 166.3 eV which are due to shake-up processes.

Chapter 5

5 High Oxygen-Reduction Activity and Durability of Nitrogen-doped Graphene

Dongsheng Geng^a, Ying Chen^a, Yougui Chen^a, Yongliang Li^a, Ruying Li^a, Xueliang Sun^{a,*}, Siyu Ye^b, Shanna Knights^b

^a*Department of Mechanical and Materials Engineering, University of Western Ontario, 1151 Richmond Street N., London, Ontario, Canada N6A 5B9*

^b*Ballard Power Systems Inc., 9000 Glenlyon Parkway, Burnaby, BC, Canada V5J 5J8*

**To whom correspondence should be addressed. E-mail: xsun@eng.uwo.ca*

Tel: +1-519-6612111, Ext. 87759, Fax: +1-519-6613020

A version of the chapter has been published in *Energy & Environmental Sciences*, 2011, **4**, 760-764.

Energy shortages and environmental pollution are serious challenges that humanity will face for the long-term. Proton Exchange Membrane Fuel cells (PEMFCs) are non-polluting and efficient energy conversion devices that are expected to play a dominant role in future energy solutions. However, the current PEMFCs system still faces significant technological roadblocks which have to be overcome before the system can become economically viable. A major impediment to the commercialization of PEMFC is the high cost and stability of Pt-based electrocatalysts. Thus, one of the important challenges is the development of platinum-free catalysts.

Nitrogen doped carbon materials as the metal-free catalysts have recently been found to exhibit high catalytic activity for oxygen reduction reaction in fuel cell (see our previous study about CN_x (chapter 3)). And in chapter 4, we investigated the effect of nitrogen

doping on the structure of carbon by taking graphene as an example. In this chapter, we will extend the study to investigate the N-graphene as non-noble metal ORR catalyst. So this article reports the synthesis of nitrogen-doped graphene as a metal-free catalyst for oxygen reduction by heat-treatment of graphene using ammonia. The ORR activity of N-graphene is strongly dependent on the heat treatment temperature. Moreover, our electrochemical measurements showed that the optimum catalysts promote the desired $4e^-$ ORR in alkaline solution. In comparison to the commercial Pt/C catalyst, the catalyst presented higher ORR onset potential (0.308 V), 43 mV more positive ORR half-wave potential. Also, it demonstrated better stability than Pt/C (loading: $4.85 \mu\text{gPt cm}^{-2}$) in the studied conditions. Therefore, N-doped graphene may have the potential to replace the costly Pt/C catalyst in fuel cells in an alkaline solution.

Keywords: *Nitrogen-doped graphene, electrocatalyst, Oxygen reduction reaction, Fuel cell*

5.1 Introduction

Both fuel cells, for power generation, and metal-air batteries, for energy storage, require an efficient electrode for oxygen reduction reaction (ORR). Such electrodes are usually carbon-supported platinum electrodes that are used to catalyze four-electron oxygen reduction to water. However, the kinetics of ORR is sluggish, even on pure Pt. Also, Pt particles dissolve and agglomerate over time, which diminishes the performance of fuel cell. Combined with the performance durability problems, the high cost of Pt, due to its low abundance in nature, hinders the commercial viability of fuel cells. The search for cheap, stable and more active electrocatalysts for ORR is thus of great importance.

Along with recent intense research efforts in reducing or replacing Pt-based catalysts in fuel cells [1-4], it has been found that nitrogen-doped carbon materials (especially, vertically aligned nitrogen-containing carbon nanotubes, nitrogen doped ordered mesoporous graphitic carbon, and silk-derived carbon (0.8% nitrogen in the carbon network)) could act as effective metal-free electrocatalysts [5-11]. Although the real active site of nitrogen-doped carbon materials remains unclear, in general, it has been believed that the doped nitrogen atoms (such as graphite-like, pyridine-like, pyrrole-like, and quaternary nitrogen atoms) play a crucial role for ORR [11-13]. Graphene, on the other hand, a new and 2-dimensional carbon material, has recently attracted great interests for both fundamental science and applied research [14-18]. It has not only high surface area, and excellent conductivity, but also unique graphitic basal plane structure that should guarantee its durability. It is well known that the greater the extent of graphitization of the carbon material, the greater the durability it has [19]. The unique properties of nitrogen-doped carbon materials and graphene promoted us to investigate the ORR activity of nitrogen-doped graphene. Although nitrogen-doped graphene has been shown very recently to have high electrocatalytic activity and long-term operation stability for the ORR [20], the exact extent of the electrocatalytic activity of this material remains unknown, perhaps due to the limitation of the chemical vapour deposition (CVD) preparation method used. The CVD method only made a graphene film on a surface of Ni-coated SiO₂/Si wafer. It is very difficult to scale up, which will inevitably limit the wide use as practical electrodes of N-graphene. And it appears impossible to fabricate

membrane electrode assembly (MEA) for fuel cells based on the method. In this work, we prepare nitrogen-doped graphene at a large scale, and provide a detailed comparison to commercial Pt/C (E-TEK) as catalysts for ORR.

5.2 Experimental

Natural flake graphite (Aldrich, +100 mesh) was used as the starting material. Graphene was first prepared by the oxidation of the natural flake graphite using the Staudemaier method followed by the heat-treatment at 1050 °C for 30 s [21]. The nitrogen-doped graphene was obtained by heating under high purity ammonia mixed with Ar at 800 °C (N-graphene (800)), 900 °C (N-graphene (900)), 1000 °C (N-graphene (1000)) [22].

The ORR activity of nitrogen-doped graphenes was evaluated in 0.1 M KOH solution with a rotating ring-disk electrode equipment (RRDE). Platinum wire and Hg/HgO (20% KOH) electrode were used as the counter and the reference electrode, respectively. The potentials presented in this study are referred to standard hydrogen electrode (SHE). The potential is 0.098 V versus SHE with respect to the electrodes Hg/HgO. The working electrode was prepared by the thin-film electrode method. Briefly, 5 mg of N-graphene was dispersed in the solution (1080 μL ethanol and 180 μL of 5 wt % Nafion) and ultrasonically blended for 30 min. 10 μL of this suspension (loading: 160 $\mu\text{g cm}^{-2}$) was dropped on the disk electrode. Cyclic voltammograms (CVs) were recorded by scanning the disk potential from 0.4 to -1.0 V vs. SHE at a scan rate of 5 mV s^{-1} . And the ring potential was maintained at 0.7 V vs. SHE in order to oxidize any hydrogen peroxide produced. First, CVs were recorded at 5 mV s^{-1} using nitrogen atmosphere to obtain the background capacitive currents. Next, the CVs were recorded using the oxygen-saturated electrolyte. The electrolyte solution was purged with oxygen for 30 min before commencing oxygen reduction on the disk electrode.

5.3 Results and discussion

Fig. 5-1 shows the linear-sweep voltammograms in O_2 -saturated 0.1 M KOH of graphene and graphene treated by ammonia at various temperatures. N-graphene (900) was shown to have a considerably higher activity toward ORR than the other materials. It has high

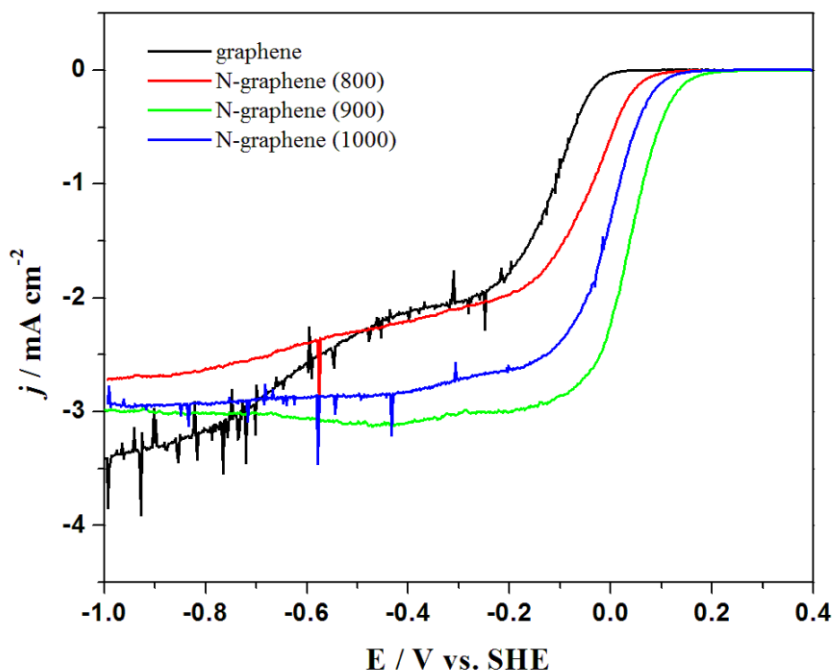


Figure 5-1 The linear-sweep voltammograms of graphene and N-graphene under different temperatures. Electrolyte: O_2 -saturated 0.1 M KOH, scan rate: 5 mV s^{-1} , and rotation speed: 1600 rpm.

onset potential for ORR (E_{ORR}), and a well-defined limiting current plateau. The values of onset potential for ORR (E_{ORR}) for graphene, N-graphene (800), N-graphene (900), N-graphene (1000) were 0.046, 0.184, 0.308, and 0.204 V, respectively. Obviously, the ORR activity of N-graphene is strongly dependent on the heat treatment temperature and the optimum temperature appears to be 900 °C. Although the catalyst roughness effect cannot be completely excluded, we don't think that it is the major effect on the ORR activity. This conclusion has been obtained in our recent work [23]. By comparing the onset potential of glassy carbon and graphene, it has been revealed that they have similar activity although graphene has the higher roughness factor than the polished glassy carbon electrode. Generally, it has been believed that the nitrogen content and N species proportion in the carbon materials play a key role for the improved activity [6, 9]. It is thus interesting to investigate the difference in nitrogen content and N species proportion

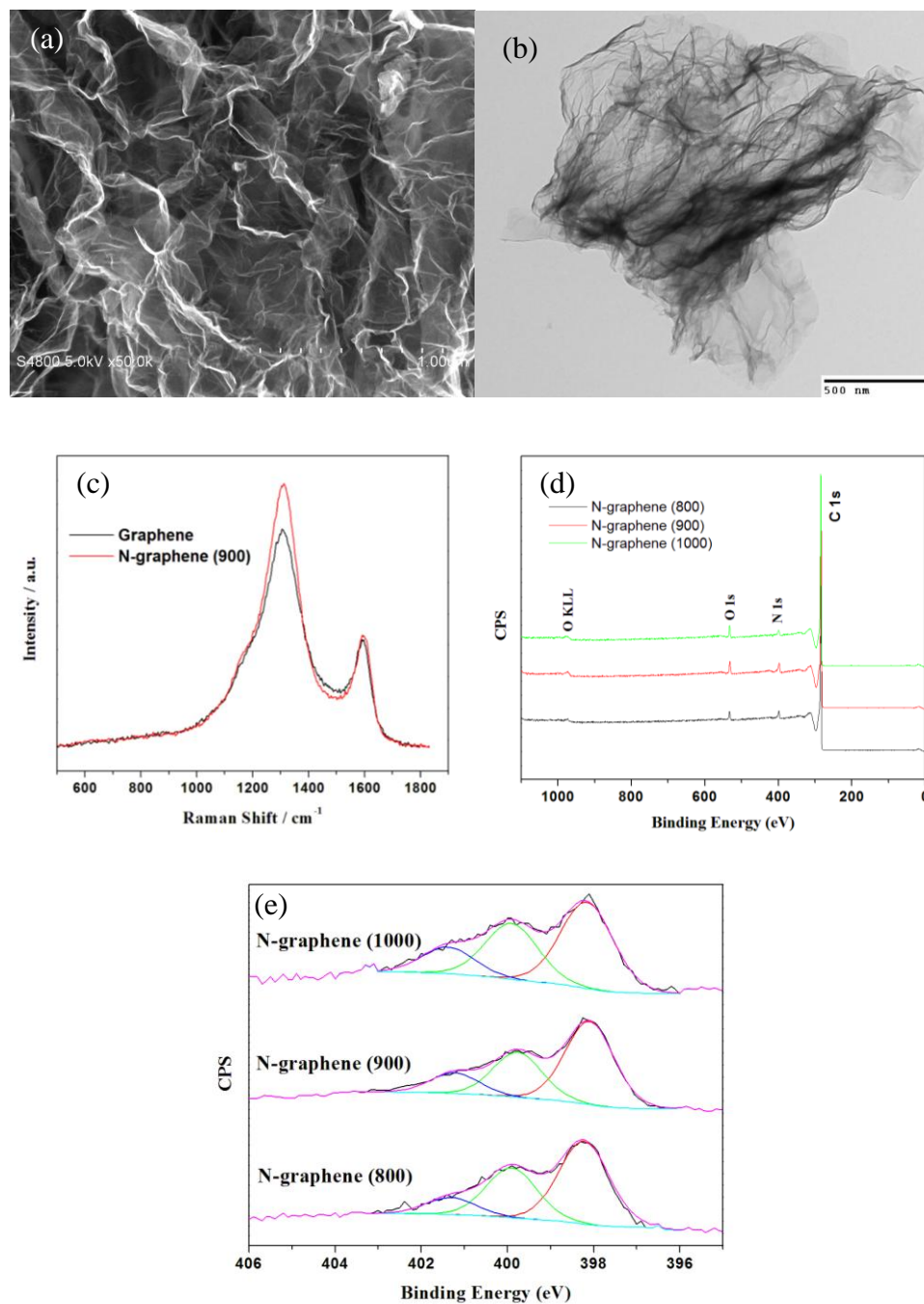


Figure 5-2 The typical SEM (a) and TEM (b) images for N-graphene (900). (c) The Raman spectrum of graphene and N-graphene (900). (d) The XPS survey for three samples; (e) the high-resolution N1s spectrum for N-graphene: the black and purple lines are the raw and fitted spectra; the red, green, and blue lines correspond to pyridine-like N (398.1 eV), pyrrole-like N (399.9 eV), and quaternary N (401.3 eV), respectively.

of these ammonia-treated graphenes as a function of heat-treatment temperature. Fig. 5-2a, b show the typical SEM, TEM images of N-graphene. It can be seen that the material is transparent with a voile-like structure. Meanwhile, from the Raman spectrum shown here (Fig.5-2c), it can be known that the D band, observed at approximately 1310 cm^{-1} , is disorder induced. It is attributed to structural defects on the graphitic plane. The G band, observed at approximately 1583 cm^{-1} , is commonly observed for all graphitic structures and attributed to the E_{2g} vibrational mode present in the sp² bonded graphitic carbons. The intensity ratio of the first peak to the second peak, namely the I_D/I_G ratio, provides the indication of the amount of structural defects and a quantitative measure of edge plane exposure. N-graphene was found to have the higher I_D/I_G ratio of 2.25, obviously larger than 1.97 observed for graphene. The larger I_D/I_G ratio observed for N-graphene is a result of the structural defects and edge plane exposure caused by heterogeneous nitrogen atom incorporation into the graphene layers. Furthermore, XPS characterization (Fig. 5-2d) indicated that about 2.8, 2.8, and 2.0% nitrogen were introduced to the graphene sheet for N-graphene (800), N-graphene (900), and N-graphene (1000), respectively. Based on the detailed analysis of N1s (Fig. 5-2e and Table 5-1), no obvious dependence of ORR activity on the content of pyridine-like and pyrrole-like N species was observed. But this investigation showed that quaternary nitrogen atoms seem to be the most important species for the ORR due to the matching relationship between activity and quaternary N contents [7, 24]. Thus any specific N species which resulted in the enhanced activity should not be selectively eliminated.

Table 5-5 Distribution of N species obtained from the de-convolution of the N1s peaks by XPS.

Sample	N content (at.%)	Pyridine-like (398.1 eV, at.%)	Pyrrole-like (399.9 eV, at.%)	Quaternary (401.3 eV, at.%)
N-graphene (800)	2.8	1.5455	0.9352	0.3192
N-graphene (900)	2.8	1.5596	0.8484	0.3892
N-graphene (1000)	2.0	1.022	0.662	0.316

The electrochemical reduction of O₂ is a multi-electron reaction that has two main possible pathways: one is the transfer of two electrons to produce H₂O₂, and the other is a direct four-electron pathway to produce water. To obtain maximum energy capacity, it is highly desirable to reduce O₂ via the 4e⁻ pathway. Although the usual reaction that occurs on carbon electrodes is far less than the four-electron reaction, there have been reports that reactions involving more electrons may take place on nitrogen-containing carbon electrodes [24-27]. Herein, the selectivity of ORR was analyzed by two methods: RDE to obtain the slope of the Koutecky-Levich (K-L) plots, and RRDE to directly measure the portion of H₂O₂ formation via ring/disk current ratio. RRDE current-potential curves for N-graphene (900) at various rotating speeds are shown in Fig. 5-3a. Rotating rate-dependent limited diffusion currents were observed here. Fig. 5-3b shows the Koutecky-Levich (K-L) plots of 1/*I*_{lim} vs. 1/*ω*^{1/2} at fixed potential (-0.5 V) on N-graphene (900) electrode derived from the data in Fig. 5-3a. The number of electrons calculated is 3.6, based on the K-L equation:

$$I_{\text{lim}} = 0.62nFD^{2/3}v^{-1/6}C_o\omega^{1/2} \quad (1)$$

where *I*_{lim} is the limiting current density, *n* is the number of electrons transferred per oxygen molecule, *F* is the Faraday constant (96485 C mol⁻¹), *D* is the O₂ diffusion coefficient (1.73 × 10⁻⁵ cm² s⁻¹) in 0.1 M KOH, *C*_o is the concentration of oxygen (1.21 × 10⁻⁶ mol cm⁻³) [28]. To further verify the ORR pathways on the N-graphene (900), the formation of H₂O₂ during the ORR process was monitored using RRDE measurement. Analyses of the ORR by the reduction currents of the ring and disk (Fig. 5-3c and d) showed that the ORR on N-graphene (900) proceeds by a 3.8-electron reaction at -0.5 V to give about 10% of hydrogen peroxide according to the two equations [29]:

$$n = 4 I_D / (I_D + (I_R / N)) \quad (2)$$

$$\%H_2O_2 = 100 (4 - n) / 2 \quad (3)$$

It is consistent with the data obtained from the slope of K-L plots. The results suggest that the ORR catalyzed on N-graphene (900) is a close 4 e⁻ reduction process leading to the formation of H₂O.

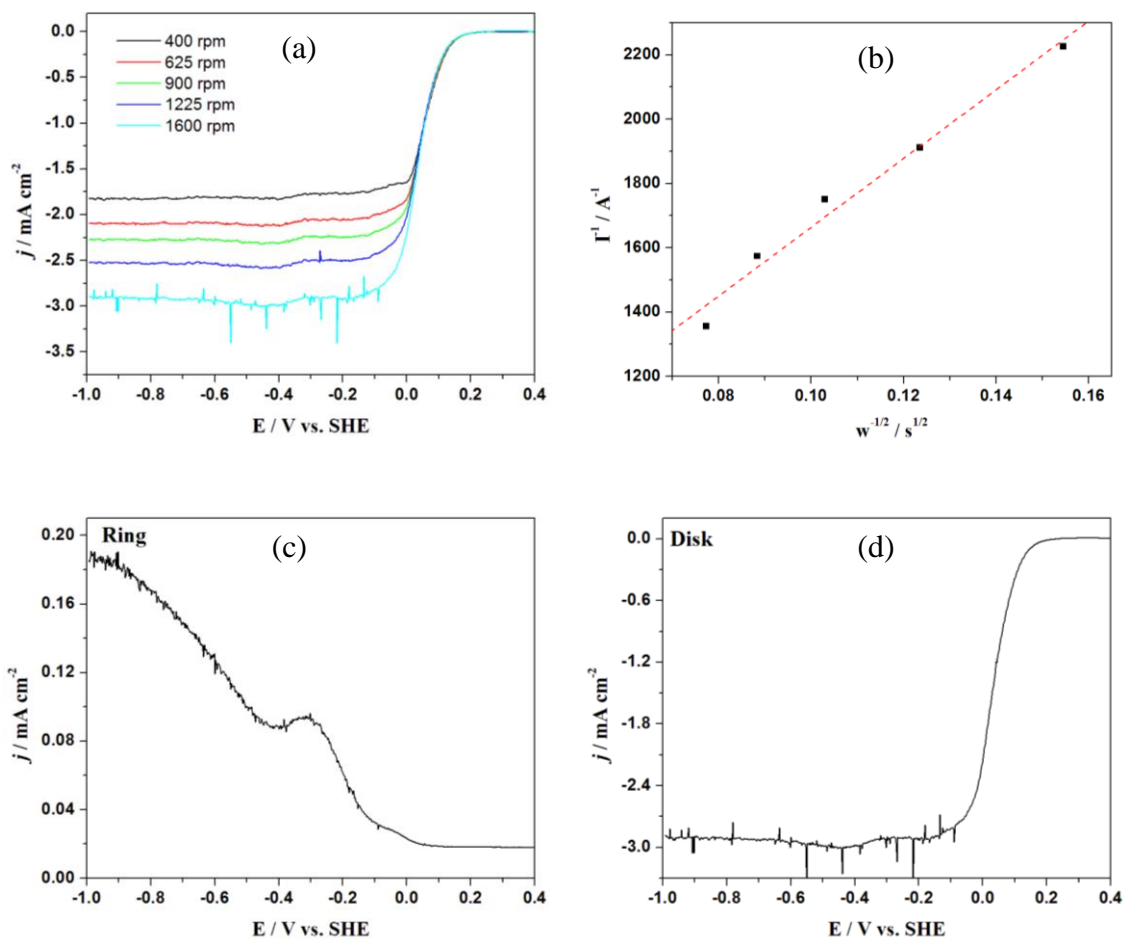


Figure 5-3 (a) Measured ORR currents of N-graphene (900) catalyst at different electrode rotation speed and (b) Koutecký-Levich plot at -0.5 V using the data obtained from (a). (c) and (d): The current density of ring and disk measured by RRDE for N-graphene (900). Scan rate: 5 mV s^{-1} , electrolyte: 0.1 M KOH .

Furthermore, the activity of N-graphene (900) for ORR was compared with commercial Pt/C electrocatalyst. From Fig. 5-4a, it can be seen that the two electrocatalysts have the same onset potentials and limited diffusion currents for oxygen reduction. In addition, one can believe that N-graphene (900) has the slightly higher ORR activity than Pt/C (loading: $4.85 \mu\text{g}_{\text{Pt}} \text{ cm}^{-2}$) based on its half-wave potential (shifted positively about 43 mV).

A durability test of N-graphene (900) was also carried out by cyclic voltammetry in O_2 -saturated 0.1 M KOH . Fig. 5-4b shows the CVs at various potential sweeps: 50, 500,

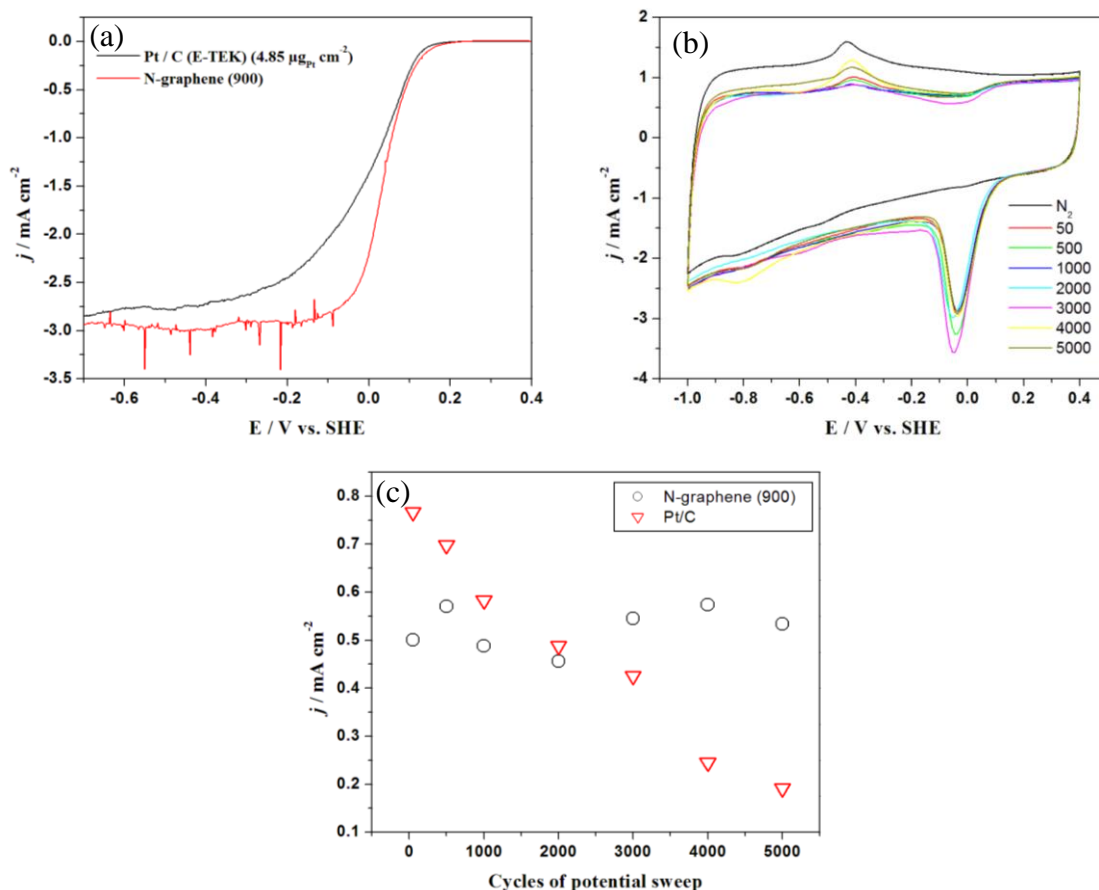


Figure 5-4 (a) The polarization curves of oxygen reduction on N-graphene (900) and Pt/C (E-TEK) catalysts. Electrolyte: 0.1 M KOH, scan rate: 5 mV s^{-1} , and rotation speed: 1600 rpm. (b) Cyclic voltammograms of N-graphene (900) in N_2 -saturated 0.1 M KOH (the black line) and O_2 -saturated 0.1 M KOH after 50, 500, 1000, 2000, 3000, 4000, and 5000 potential cycles, respectively. Potential Sweep rate: 100 mV s^{-1} . (c) Dependence of the current density for the ORR at 0.05 V on the potential cycles evaluated from the cyclic voltammograms.

1000, 2000, 3000, 4000, and 5000 cycles. The cathodic peaks relate to the reduction of oxygen. Almost no change in the voltammetric charge was found after 5000 cycles of the potential sweep. In Fig. 5-4c, the dependence of the current density for the ORR on the potential cycles is presented based on the data from the insert. Clearly, the ORR current density on N-graphene (900) electrode remains stable. In contrast, the ORR current

density on Pt/C electrode, subjected to an identical test (CV data not shown) has a rapid decline. N-graphene (900) thus demonstrated better durability than Pt/C under the studied conditions.

5.4 Conclusions

It is clearly shown here that nitrogen-doped graphene catalysts can be synthesized by the treatment of graphene by ammonia under different temperature. The highest ORR activity in alkaline solution was obtained with the catalyst treated at 900 °C. XPS indicated that only 2.8% nitrogen was introduced into the graphene for N-graphene (900). Quaternary type nitrogen species seem to play the most important role for ORR activity. Moreover, our electrochemical measurements showed that N-graphene (900) catalysts promote the desired 4e⁻ ORR in alkaline solution. In comparison to the commercial Pt/C catalyst, N-graphene (900) catalyst presented higher ORR onset potential (0.308 V), 43 mV more positive ORR half-wave potential. Also importantly, it demonstrated better stability than Pt/C (loading: 4.85 μg_{Pt} cm⁻²) in the studied conditions. Therefore, N-doped graphene may have the potential to replace the costly Pt/C catalyst in fuel cells in an alkaline solution.

Acknowledgments

This research was supported by Natural Sciences and Engineering Research Council of Canada (NSERC), Ballard Power Systems Inc., Canada Research Chair (CRC) Program, Canada Foundation for Innovation (CFI), Ontario Research Fund (ORF), Ontario Early Researcher Award (ERA) and the University of Western Ontario.

References

- [1] M. Lefevre, E. Proietti, F. Jaouen, J.P. Dodelet, Iron-Based Catalysts with Improved Oxygen Reduction Activity in Polymer Electrolyte Fuel Cells, *Science*, 324 (2009) 71-74.

- [2] B. Winther-Jensen, O. Winther-Jensen, M. Forsyth, D.R. MacFarlane, High rates of oxygen reduction over a vapor phase-polymerized PEDOT electrode, *Science*, 321 (2008) 671-674.
- [3] J. Zhang, K. Sasaki, E. Sutter, R.R. Adzic, Stabilization of platinum oxygen-reduction electrocatalysts using gold clusters, *Science*, 315 (2007) 220-222.
- [4] H.A. Gasteiger, S.S. Kocha, B. Sompalli, F.T. Wagner, Activity benchmarks and requirements for Pt, Pt-alloy, and non-Pt oxygen reduction catalysts for PEMFCs, *Appl Catal B-Environ*, 56 (2005) 9-35.
- [5] R.L. Liu, D.Q. Wu, X.L. Feng, K. Mullen, Nitrogen-Doped Ordered Mesoporous Graphitic Arrays with High Electrocatalytic Activity for Oxygen Reduction, *Angew Chem Int Edit*, 49 (2010) 2565-2569.
- [6] T.C. Nagaiah, S. Kundu, M. Bron, M. Muhler, W. Schuhmann, Nitrogen-doped carbon nanotubes as a cathode catalyst for the oxygen reduction reaction in alkaline medium, *Electrochem Commun*, 12 (2010) 338-341.
- [7] N.P. Subramanian, X.G. Li, V. Nallathambi, S.P. Kumaraguru, H. Colon-Mercado, G. Wu, J.W. Lee, B.N. Popov, Nitrogen-modified carbon-based catalysts for oxygen reduction reaction in polymer electrolyte membrane fuel cells, *J Power Sources*, 188 (2009) 38-44.
- [8] Y.F. Tang, B.L. Allen, D.R. Kauffman, A. Star, Electrocatalytic Activity of Nitrogen-Doped Carbon Nanotube Cups, *J Am Chem Soc*, 131 (2009) 13200-13201.
- [9] K. Prehn, A. Warburg, T. Schilling, M. Bron, K. Schulte, Towards nitrogen-containing CNTs for fuel cell electrodes, *Compos Sci Technol*, 69 (2009) 1570-1579.
- [10] K.P. Gong, F. Du, Z.H. Xia, M. Durstock, L.M. Dai, Nitrogen-Doped Carbon Nanotube Arrays with High Electrocatalytic Activity for Oxygen Reduction, *Science*, 323 (2009) 760-764.

- [11] T. Iwazaki, R. Obinata, W. Sugimoto, Y. Takasu, High oxygen-reduction activity of silk-derived activated carbon, *Electrochem Commun*, 11 (2009) 376-378.
- [12] M. Lefevre, J.P. Dodelet, P. Bertrand, Molecular oxygen reduction in PEM fuel cells: Evidence for the simultaneous presence of two active sites in Fe-based catalysts, *J Phys Chem B*, 106 (2002) 8705-8713.
- [13] A.L. Bouwkamp-Wijnoltz, W. Visscher, J.A.R. van Veen, E. Boellaard, A.M. van der Kraan, S.C. Tang, On active-site heterogeneity in pyrolyzed carbon-supported iron porphyrin catalysts for the electrochemical reduction of oxygen: An in situ Mossbauer study, *J Phys Chem B*, 106 (2002) 12993-13001.
- [14] M.J. Allen, V.C. Tung, R.B. Kaner, Honeycomb Carbon: A Review of Graphene, *Chem Rev*, 110 (2010) 132-145.
- [15] A.K. Geim, Graphene: Status and Prospects, *Science*, 324 (2009) 1530-1534.
- [16] K.I. Bolotin, K.J. Sikes, Z. Jiang, M. Klima, G. Fudenberg, J. Hone, P. Kim, H.L. Stormer, Ultrahigh electron mobility in suspended graphene, *Solid State Commun*, 146 (2008) 351-355.
- [17] A.K. Geim, K.S. Novoselov, The rise of graphene, *Nat Mater*, 6 (2007) 183-191.
- [18] M.D. Stoller, S.J. Park, Y.W. Zhu, J.H. An, R.S. Ruoff, Graphene-Based Ultracapacitors, *Nano Lett*, 8 (2008) 3498-3502.
- [19] D.A. Stevens, M.T. Hicks, G.M. Haugen, J.R. Dahn, Ex situ and in situ stability studies of PEMFC catalysts, *J Electrochem Soc*, 152 (2005) A2309-A2315.
- [20] L.T. Qu, Y. Liu, J.B. Baek, L.M. Dai, Nitrogen-Doped Graphene as Efficient Metal-Free Electrocatalyst for Oxygen Reduction in Fuel Cells, *Acs Nano*, 4 (2010) 1321-1326.
- [21] H.C. Schniepp, J.L. Li, M.J. McAllister, H. Sai, M. Herrera-Alonso, D.H. Adamson, R.K. Prud'homme, R. Car, D.A. Saville, I.A. Aksay, Functionalized single graphene sheets derived from splitting graphite oxide, *J Phys Chem B*, 110 (2006) 8535-8539.

- [22] X.L. Li, H.L. Wang, J.T. Robinson, H. Sanchez, G. Diankov, H.J. Dai, Simultaneous Nitrogen Doping and Reduction of Graphene Oxide, *J Am Chem Soc*, 131 (2009) 15939-15944.
- [23] D.S. Geng, H. Liu, Y.G. Chen, R.Y. Li, X.L. Sun, S.Y. Ye, S. Knights, Non-noble metal oxygen reduction electrocatalysts based on carbon nanotubes with controlled nitrogen contents, *J Power Sources*, 196 (2011) 1795-1801.
- [24] T. Iwazaki, H.S. Yang, R. Obinata, W. Sugimoto, Y. Takasu, Oxygen-reduction activity of silk-derived carbons, *J Power Sources*, 195 (2010) 5840-5847.
- [25] P.H. Matter, E. Wang, M. Arias, E.J. Biddinger, U.S. Ozkan, Oxygen reduction reaction activity and surface properties of nanostructured nitrogen-containing carbon, *J Mol Catal a-Chem*, 264 (2007) 73-81.
- [26] J. Ozaki, N. Kimura, T. Anahara, A. Oya, Preparation and oxygen reduction activity of BN-doped carbons, *Carbon*, 45 (2007) 1847-1853.
- [27] R.A. Sidik, A.B. Anderson, N.P. Subramanian, S.P. Kumaraguru, B.N. Popov, O₂ reduction on graphite and nitrogen-doped graphite: Experiment and theory, *J Phys Chem B*, 110 (2006) 1787-1793.
- [28] R.E. Davis, G.L. Horvath, C.W. Tobias, Solubility and Diffusion Coefficient of Oxygen in Potassium Hydroxide Solutions, *Electrochim Acta*, 12 (1967) 287-297.
- [29] U.A. Paulus, T.J. Schmidt, H.A. Gasteiger, R.J. Behm, Oxygen reduction on a high-surface area Pt/Vulcan carbon catalyst: a thin-film rotating ring-disk electrode study, *J Electroanal Chem*, 495 (2001) 134-145.

Chapter 6

6 Nitrogen doped graphene oxide nanoribbons from Nitrogen doped carbon nanotubes

Dongsheng Geng^a, Yuhai Hu^a, Jian Liu^a, Ruying Li^a, Xueliang Sun^{a,*},

Siyu Ye^b, Shanna Knights^b

^a*Department of Mechanical and Materials Engineering, University of Western Ontario,
1151 Richmond Street N., London, Ontario, Canada N6A 5B9*

^b*Ballard Power Systems Inc., 9000 Glenlyon Parkway, Burnaby, BC, Canada V5J 5J8*

**To whom correspondence should be addressed. E-mail: xsun@eng.uwo.ca*

Tel: +1-519-6612111, Ext. 87759, Fax: +1-519-6613020

A version of this chapter will be submitted for publishing.

In previous chapters, the authors introduced the work of nitrogen doped graphene synthesis by post-treatment of graphene using ammonia. N-graphene with the controlled nitrogen contents were obtained by treating graphene under the various temperatures.

Looking for the new methods to synthesize N-graphene is always of concern to material scientists. Previous methods usually use two steps, which involves post-treatment of graphene. In this chapter, the authors propose the new one-step method for the production of N-graphene oxide nanoribbons (NGON) via unzipping of nitrogen doped carbon nanotubes (CN_x). TEM results show that the simple solution-based oxidative process generates a nearly 100% yield of nanoribbon structures by lengthwise cutting and unravelling of the nitrogen doped carbon nanotube side walls. In addition, the nitrogen content was traced before and after oxidation process by XPS. More importantly, there is still 2.1 at.% N existing on NGON.

Keywords: *Nitrogen doped carbon nanotube, nitrogen doped graphene ribbon, unzipping*

6.1 Introduction

Graphene, the two-dimensional (2D) monolayer of carbon atoms arranged in a honeycomb lattice, has recently attracted great interests for both fundamental and applied research due to its unique physical and chemical properties [1]. Importantly, graphene nanoribbons with high aspect ratio have shown peculiar edge states: they can be metallic if their edges exhibit a zigzag morphology, whereas armchair edges can give rise to either semiconducting or metallic transport. Thus it can be noticed that the high aspect ratio of nanoribbon will result in novel properties due to the amazing edge states. That is, the shape of the edge largely determines the properties of nanoribbons [2, 3].

In addition, foreign atom doping such as N has been proved as an effective method to modify the properties of graphene. Theoretical study has shown that nitrogen doping results in the higher positive charge on a carbon atom adjacent to the nitrogen atoms [4], and a positive shift of Fermi energy at the apex of the Brillouin zone of graphene [5]. Actually, nitrogen doped graphene has exhibited the enhanced oxygen reaction reactivity as non-noble metal electrocatalysts [6, 7] and superior electrochemical performance as anodes for lithium ion batteries than graphene [8-10]. Studies relating to N-graphene synthesis have been limited to use graphene and nitrogen precursor or other carbon and nitrogen precursors [11-14]. Typically, Rao et al. prepared nitrogen doped graphene by carrying out the arc discharge in the presence of H_2 +pyridine or H_2 +ammonia. The XPS results indicated that only 0.6 and 1% nitrogen were doped into graphene [11]. Liu et al. reported that the atomic percentage of N in the sample is about 8.9 at% by chemical vapour deposition (CVD) method [12]. However, CVD can only grow N-graphene thin films on a substrate and thereby suffers from difficulties in scaling up. Recently, Deng et al. developed a novel method for one-pot direct synthesis of N-doped graphene via the reaction of tetrachloromethane with lithium nitride under mild conditions, and the nitrogen content can vary in the range of 4.5-16.4% [14]. But the operation process is cumbersome because water-sensitive lithium nitride must be treated at glove box. Also there is potential danger for the reaction proceeded under higher pressure in autoclave. Therefore a simple, efficient and low-cost process still needs to be developed.

Based on the adjustable properties of graphene nanoribbon mentioned above, one is wondering how about nitrogen doped graphene nanoribbons. To date, MWCNTs and single-wall carbon nanotubes (SWCNTs) have been unzipped to nanoribbons by wet chemical methods [15], lithium and ammonia [16], or potassium reaction [17], and the high direct pulse current sintering process [18]. However, to the best of our knowledge, up to now, nitrogen doped graphene oxide nanoribbons (NGON) have never been reported in the literature. Here we describe a simple one-step approach to prepare nitrogen doped graphene oxide nanoribbons by unzipping the nitrogen doped carbon nanotubes directly for the first time.

6.2 Experimental

Commercial carbon nanotubes from Aldrich Company were used as the precursor to form graphene oxide nanoribbon (GON). CN_x (5.1% at. N) (home-made) was selected as the precursor to produce NGON. They were first prepared by the oxidation of precursors using the modified Hummers' method [19, 20]. Typically, precursor (50 mg) and sodium nitrate (37.5 mg) were first stirred in concentrated sulphuric acid (3 mL) while being cooled in an ice water bath. Then potassium permanganate (225 mg) was gradually added to form a new mixture. After two hours in an ice water bath, the mixture was allowed to stand for one day at room temperature with gentle stirring. Thereafter, 30 mL of 5 wt% H_2SO_4 aqueous solution was added into the above mixture over 1h with stirring. Then, 1 mL of H_2O_2 (30 wt% aqueous solution) was also added to the above liquid and the mixture was stirred for 2h. After that, the suspension was filtered and washed until the pH value of the filtrate was neutral. The as-received slurry is then sonicated to get the so-called GON and NGON.

6.3 Results and discussion

The commercial MWCNTs as the control sample were unzipped to GON. Figure 6-1(a) shows the SEM picture of the initial carbon nanotubes, it can be seen that the carbon nanotubes have a length of several micrometers and tubular structure with diameter of 100 to 120 nm. After oxidation using modified Hummers' method, their tubular is change

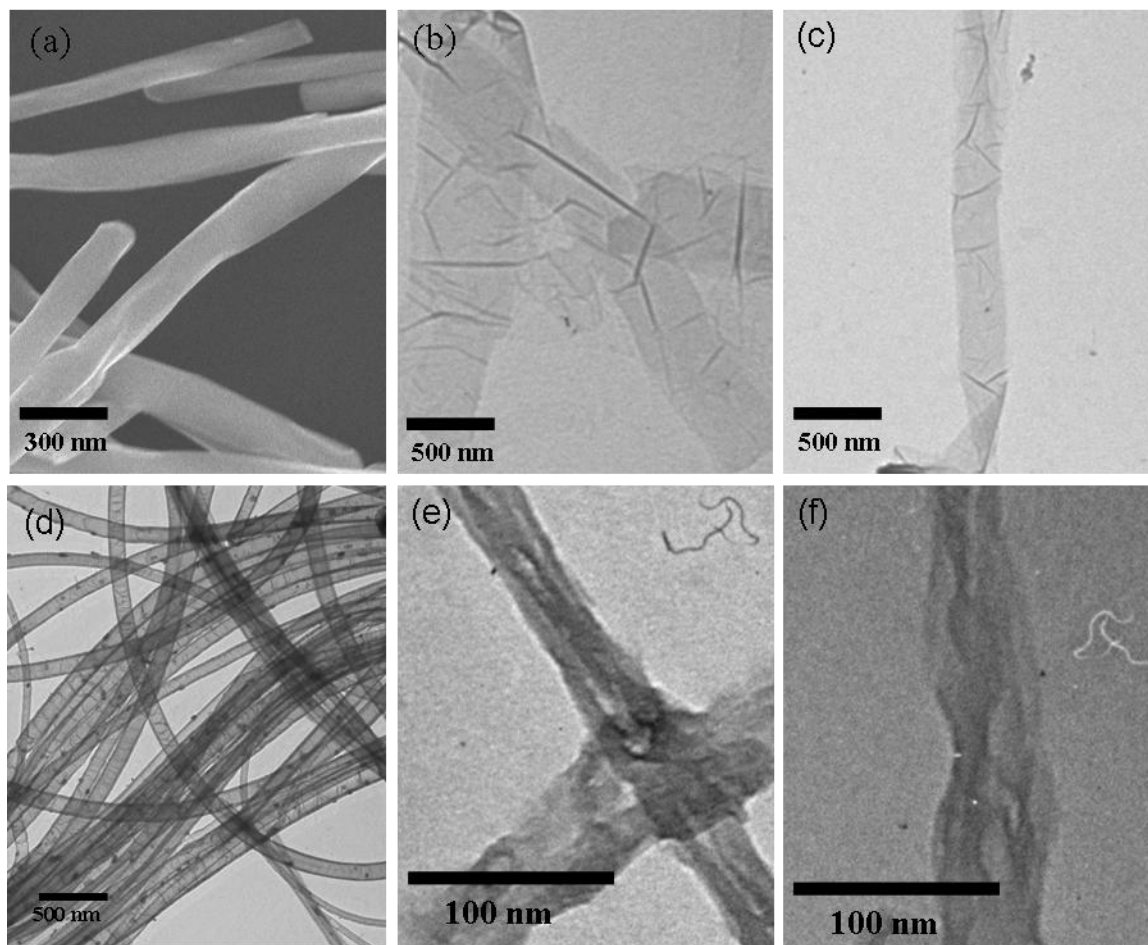


Figure 6-1 (a) The SEM image of the pristine carbon nanotubes (b, c) the TEM pictures of graphene oxide nanoribbons; (d) the TEM of home-made CN_x , and (e, f) the TEM images of nitrogen doped graphene oxide nanoribbons.

to nanosheets. Figure 6-1(b, c) shows TEM images of unzipped carbon nanotubes by oxidation process. Obviously, the graphene oxide nanoribbons strips are obtained. The typical width of the strips lies in the 300-600 nm range, while the length of the strips is about several micrometers. The simple solution-based oxidative process generates a nearly 100% yield of nanoribbon structures by lengthwise cutting and unravelling of the carbon nanotube side walls [21].

Based on the case from carbon nanotubes to graphene oxide nanoribbon, one can expect to obtain N-graphene from CN_x with different N content. Therefore N-graphene with the controlled nitrogen content can be also prepared. In the current work, CN_x (5.1% N) was

selected as the precursor [22]. Fig. 6-1(d) shows the typical TEM picture for the sample. The diameter of the CN_x is about 120 nm. It has a length of several micrometers and bamboo-like or corrugated structure. The TEM images in Figure 6-1(e, f) show clearly that the bamboo-like or corrugated structure has been destroyed by the strong oxidation process. Some long and thin N-graphene nanosheets have been produced with a diameter comprised between 40 and 50 nm. Such nanosheets show in general a tendency to stack together into overlapped layers although in some area of the TEM image (Fig. 6-1(f)) appear also as single sheets. Furthermore, some details were obtained from high resolution TEM (HRTEM) images. The pristine CN_x has about 20 graphite layers for the wall. After oxidation process, the resulting graphene nanosheets are between 4 and 9 layers. The facts provide visual evidence that the oxidative attack was effective in changing CN_x into nitrogen doped graphene nanoribbon. Importantly, it can be noticed that nitrogen doped graphene nanoribbon from CN_x has the tendency to agglomeration, but graphene nanoribbon does not. And it appears that nitrogen doped graphene nanoribbon is thicker than graphene nanoribbon. The main reason perhaps is the existence of more defects on the surface of CN_x due to the doping. From Fig. 6-2a, it can

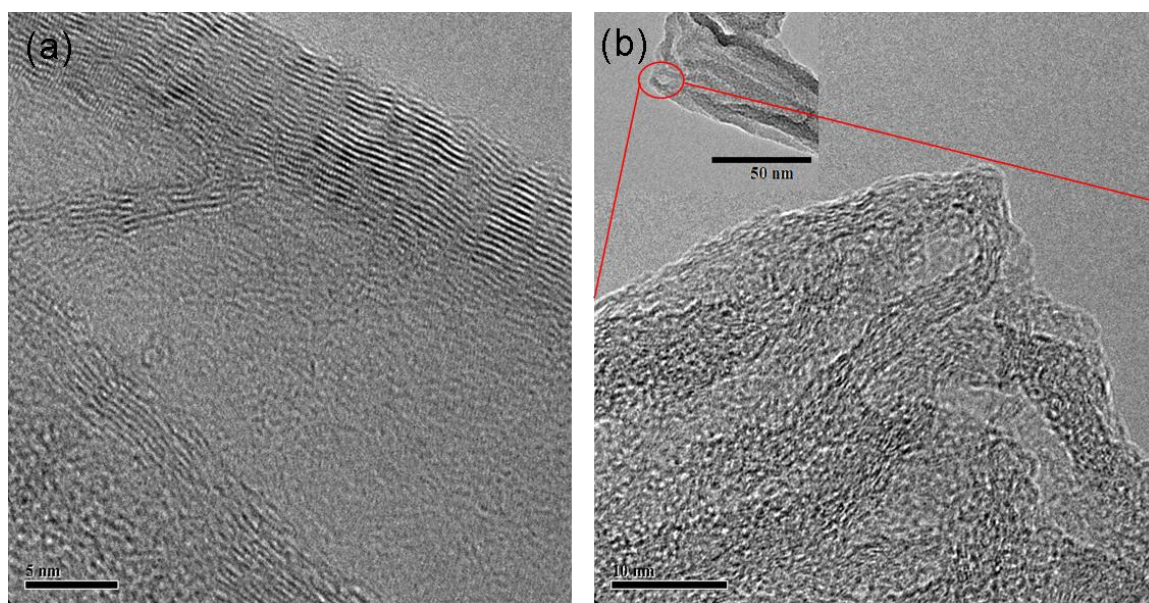


Figure 6-2 The HRTEM images of (a) the pristine CN_x and (b) nitrogen doped graphene oxide nanoribbons.

be seen that the surface morphology and atomic arrangement of the CN_x are rough and disordered. The disruptions and irregular curvatures in graphene stacking in CN_x are due to the propensity of incorporated nitrogen to form pentagonal and hexagonal defects in the graphene layers. The introduction of such defects disrupts the planar hexagonal arrangement of carbon atoms in carbon nanotubes and results in the rough surface of CN_x . However, the regular carbon nanotubes have the flat surface morphology and ordered atomic arrangement [23]. These differences resulted in that CN_x cannot be unzipped well like carbon nanotubes.

Furthermore, Fig. 6-3 shows the Raman spectra of MWCNTs and CN_x . As we know the D band, observed at approximately 1310 cm^{-1} , is disorder induced. It is attributed to structural defects on the graphitic plane. The G band, observed at approximately 1583 cm^{-1} , is commonly observed for all graphitic structures and attributed to the E_{2g} vibrational mode present in the sp^2 bonded graphitic carbons. The intensity ratio of the first peak to the second peak, namely the I_D/I_G ratio, provides the indication of the amount of structural defects and a quantitative measure of edge plane exposure. CN_x was found to have the higher I_D/I_G ratio of 0.69, obviously larger than 0.12 observed for MWCNTs [24]. So CN_x has the much more defects than MWCNTs.

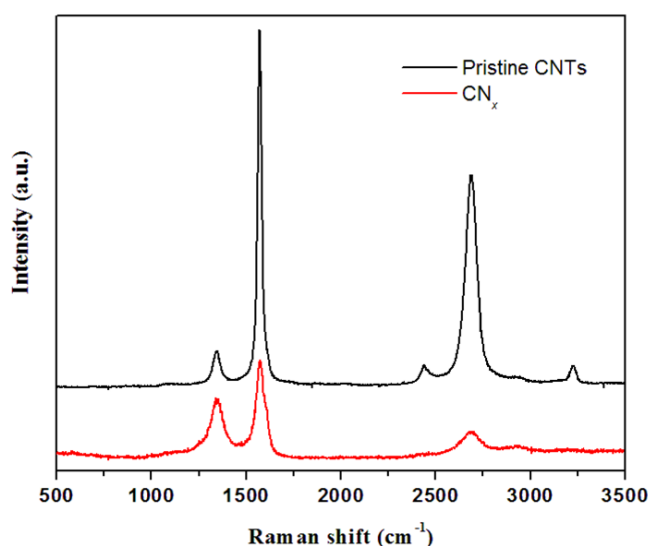


Figure 6-3 The Raman spectra of MWCNTs and CN_x .

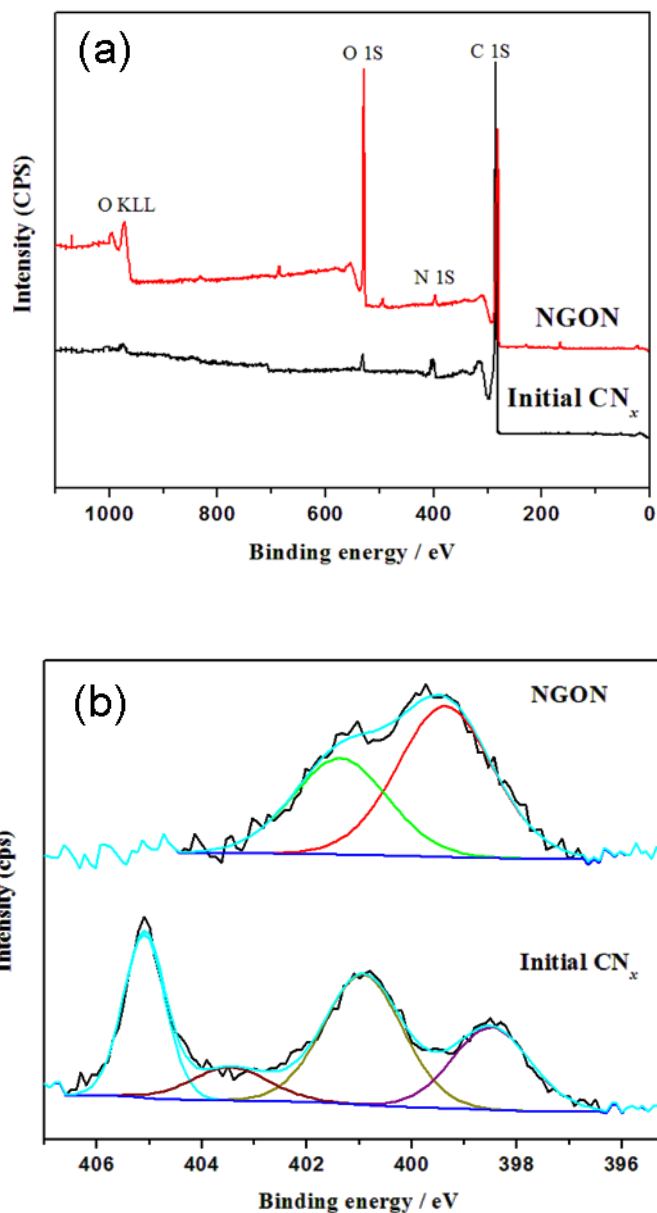


Figure 6-4 (a) XPS spectra of CN_x and NGON. (b) the high resolution N1s spectra of CN_x and NGON

What one concerns about most is the change of nitrogen content before and after oxidation process for CN_x. There is still nitrogen staying on the surface of nitrogen doped graphene nanoribbon from Fig. 6-4a. The content was changed to 2.1 at.% N from 5.1 at.% N. Fig. 6-4b showed the N1s details: there are four kinds of nitrogen existing on the

surface of initial CN_x , which are pyridine-like N (398.5 eV), graphite-like N (401.0 eV), molecular N (403.5 eV), and chemisorbed N oxide (405.1 eV), respectively. However, only graphite-like N (401.3 eV) and pyrrole-like N (399.3) were found in nitrogen doped graphene nanoribbon. Evidently, the strong oxidation process removed molecular N and chemisorbed N oxide. But why the pyrrole-like N existed in the production instead of pyridine-like N? It should also be reasonable, the strong oxidation process may break some C-C or C-N bonds of hexacyclic pyridine structure existed in initial CN_x , simultaneously some carbon atoms were oxidized and removed, thus the rest of atoms located on hexacyclic pyridine structure reorganized and formed pentacyclic pyrrole structure.

6.4 Conclusions

A simple solution-based oxidative process to produce N-graphene oxide nanoribbons has been demonstrated. The structure properties of nitrogen doped graphene oxide nanoribbons have been confirmed by TEM, the exfoliated NGON may exist as the planar structure with monolayer. But basically NGON have the 4-9 layers according to HRTEM results, and it has the tendency to agglomeration, which is different from graphene nanoribbon from MWCNTs. Importantly, there is still nitrogen staying on the surface of nitrogen doped graphene nanoribbon. The content was changed to 2.1 at.% N from 5.1 at.% N. XPS results indicated that pyrrole-like and graphite-like N are the main species in the production. The study opens a new door to synthesize nitrogen doped graphene, also the use of a low cost precursor and the solution-based procedure renders this method an attractive procedure to prepare NGON. Additional work is also needed to better understand the nature of the exfoliation process of CN_x . Such studies could allow better control of the procedure whereby perfect nitrogen doped graphene flakes could be obtained by unwrapping CN_x nanotubes.

Acknowledgments

This research was supported by Natural Sciences and Engineering Research Council of Canada (NSERC), Ballard Power Systems Inc., Canada Research Chair (CRC) Program,

Canada Foundation for Innovation (CFI), Ontario Research Fund (ORF), Ontario Early Researcher Award (ERA) and the University of Western Ontario.

References

- [1] A.K. Geim, K.S. Novoselov, The rise of graphene, *Nat Mater*, 6 (2007) 183-191.
- [2] K. Nakada, M. Fujita, G. Dresselhaus, M.S. Dresselhaus, Edge state in graphene ribbons: Nanometer size effect and edge shape dependence, *Phys Rev B*, 54 (1996) 17954-17961.
- [3] L. Yang, C.H. Park, Y.W. Son, M.L. Cohen, S.G. Louie, Quasiparticle energies and band gaps in graphene nanoribbons, *Phys Rev Lett*, 99 (2007) 186801.
- [4] K.P. Gong, F. Du, Z.H. Xia, M. Durstock, L.M. Dai, Nitrogen-Doped Carbon Nanotube Arrays with High Electrocatalytic Activity for Oxygen Reduction, *Science*, 323 (2009) 760-764.
- [5] S.U. Lee, R.V. Belosludov, H. Mizuseki, Y. Kawazoe, Designing Nanogadgets for Nanoelectronic Devices with Nitrogen-Doped Capped Carbon Nanotubes, *Small*, 5 (2009) 1769-1775.
- [6] D.S. Geng, Y. Chen, Y.G. Chen, Y.L. Li, R.Y. Li, X.L. Sun, S.Y. Ye, S. Knights, High oxygen-reduction activity and durability of nitrogen-doped graphene, *Energy Environ Sci*, 4 (2011) 760-764.
- [7] L.T. Qu, Y. Liu, J.B. Baek, L.M. Dai, Nitrogen-Doped Graphene as Efficient Metal-Free Electrocatalyst for Oxygen Reduction in Fuel Cells, *ACS Nano*, 4 (2010) 1321-1326.
- [8] A.L.M. Reddy, A. Srivastava, S.R. Gowda, H. Gullapalli, M. Dubey, P.M. Ajayan, Synthesis Of Nitrogen-Doped Graphene Films For Lithium Battery Application, *ACS Nano*, 4 (2010) 6337-6342.

- [9] X.F. Li, D.S. Geng, Y. Zhang, X.B. Meng, R.Y. Li, X.L. Sun, Superior cycle stability of nitrogen-doped graphene nanosheets as anodes for lithium ion batteries, *Electrochem Commun*, 13 (2011) 822-825.
- [10] H.B. Wang, C.J. Zhang, Z.H. Liu, L. Wang, P.X. Han, H.X. Xu, K.J. Zhang, S.M. Dong, J.H. Yao, G.L. Cui, Nitrogen-doped graphene nanosheets with excellent lithium storage properties, *J Mater Chem*, 21 (2011) 5430-5434.
- [11] L.S. Panchokarla, K.S. Subrahmanyam, S.K. Saha, A. Govindaraj, H.R. Krishnamurthy, U.V. Waghmare, C.N.R. Rao, Synthesis, Structure, and Properties of Boron- and Nitrogen-Doped Graphene, *Adv Mater*, 21 (2009) 4726-4730.
- [12] D.C. Wei, Y.Q. Liu, Y. Wang, H.L. Zhang, L.P. Huang, G. Yu, Synthesis of N-Doped Graphene by Chemical Vapor Deposition and Its Electrical Properties, *Nano Lett*, 9 (2009) 1752-1758.
- [13] X.R. Wang, X.L. Li, L. Zhang, Y. Yoon, P.K. Weber, H.L. Wang, J. Guo, H.J. Dai, N-Doping of Graphene Through Electrothermal Reactions with Ammonia, *Science*, 324 (2009) 768-771.
- [14] D.H. Deng, X.L. Pan, L.A. Yu, Y. Cui, Y.P. Jiang, J. Qi, W.X. Li, Q.A. Fu, X.C. Ma, Q.K. Xue, G.Q. Sun, X.H. Bao, Toward N-Doped Graphene via Solvothermal Synthesis, *Chem Mater*, 23 (2011) 1188-1193.
- [15] D.V. Kosynkin, A.L. Higginbotham, A. Sinitskii, J.R. Lomeda, A. Dimiev, B.K. Price, J.M. Tour, Longitudinal unzipping of carbon nanotubes to form graphene nanoribbons, *Nature*, 458 (2009) 872-876.
- [16] A.G. Cano-Marquez, F.J. Rodriguez-Macias, J. Campos-Delgado, C.G. Espinosa-Gonzalez, F. Tristan-Lopez, D. Ramirez-Gonzalez, D.A. Cullen, D.J. Smith, M. Terrones, Y.I. Vega-Cantu, Ex-MWNTs: Graphene Sheets and Ribbons Produced by Lithium Intercalation and Exfoliation of Carbon Nanotubes, *Nano Lett*, 9 (2009) 1527-1533.

- [17] D.V. Kosynkin, W. Lu, A. Sinitskii, G. Pera, Z.Z. Sun, J.M. Tour, Highly Conductive Graphene Nanoribbons by Longitudinal Splitting of Carbon Nanotubes Using Potassium Vapor, *Acs Nano*, 5 (2011) 968-974.
- [18] W.S. Kim, S.Y. Moon, S.Y. Bang, B.G. Choi, H. Ham, T. Sekino, K.B. Shim, Fabrication of graphene layers from multiwalled carbon nanotubes using high dc pulse, *Appl Phys Lett*, 95 (2009) 083103.
- [19] W.S. Hummers, R.E. Offeman, Preparation of Graphitic Oxide, *J Am Chem Soc*, 80 (1958) 1339-1339.
- [20] M. Hirata, T. Gotou, S. Horiuchi, M. Fujiwara, M. Ohba, Thin-film particles of graphite oxide 1: High-yield synthesis and flexibility of the particles, *Carbon*, 42 (2004) 2929-2937.
- [21] A.L. Higginbotham, D.V. Kosynkin, A. Sinitskii, Z.Z. Sun, J.M. Tour, Lower-Defect Graphene Oxide Nanoribbons from Multiwalled Carbon Nanotubes, *Acs Nano*, 4 (2010) 2059-2069.
- [22] J. Liu, Y. Zhang, M.I. Ionescu, R.Y. Li, X.L. Sun, Nitrogen-doped carbon nanotubes with tunable structure and high yield produced by ultrasonic spray pyrolysis, *Appl Surf Sci*, 257 (2011) 7837-7844.
- [23] Y.G. Chen, J.J. Wang, H. Liu, M.N. Banis, R.Y. Li, X.L. Sun, T.K. Sham, S.Y. Ye, S. Knights, Nitrogen Doping Effects on Carbon Nanotubes and the Origin of the Enhanced Electrocatalytic Activity of Supported Pt for Proton-Exchange Membrane Fuel Cells, *J Phys Chem C*, 115 (2011) 3769-3776.
- [24] H. Liu, Y. Zhang, R.Y. Li, X.L. Sun, S. Desilets, H. Abou-Rachid, M. Jaidann, L.S. Lussier, Structural and morphological control of aligned nitrogen-doped carbon nanotubes, *Carbon*, 48 (2010) 1498-1507.

Chapter 7

7 One-Pot Solvothermal synthesis of doped graphene with the designed nitrogen type used as a Pt support for fuel cells

Dongsheng Geng, Yuhai Hu, Yongliang Li, Ruying Li, and Xueliang Sun*

Department of Mechanical and Materials Engineering, University of Western Ontario,
1151 Richmond Street N., London, Ontario, Canada N6A 5B9 Fax: +1-519-6613020;
Tel: +1-519-6612111, Ext. 87759; E-mail: xsun@eng.uwo.ca

A version of this chapter has been published in *Electrochemistry Communications*, 2012, **22**, 65-68.

In previous chapters (Chapter 4 and 5), we have demonstrated that nitrogen doping significantly affects the structure of graphene and in turn the chemical properties. Our experimental results also proved that nitrogen doped graphene (NG) has higher electrocatalytic activity for the reduction of oxygen when it is considered as non-noble metal ORR catalyst. However, NG not only can act as the non-noble metal ORR catalyst, but also it could be the better support of Pt nanoparticles for fuel cell electrode materials. Our previous results have indicated that Pt nanoparticles can be more uniformly deposited on nitrogen-doped carbon nanotubes (CN_x) than on pristine carbon nanotubes, and it has been shown that nitrogen-doped carbon materials used as Pt supports have an enhanced catalytic activity and durability toward ORR. In this chapter, we will expand the study of NG to investigate another side (support of Pt nanoparticles).

Previous synthesis methods for NG are complex and operated at higher temperatures. They use different precursors as the carbon and nitrogen sources, resulting in uncontrollable N-doping (a mixture of pyridine-like, pyrrole-like, quaternary-like, and nitrogen oxides) and, therefore, strongly restricting the quality of NG. In this chapter, we

report a novel solvothermal method for large-scale preparation of NG by using pentachloropyridine as both the carbon source and the nitrogen source. The method features a lower synthesis temperature than previously reported. By the method, for the first time, nanoflower-like NG was obtained with pure sp^2 hybridized carbon and we realized the controllable synthesis of designed nitrogen types. More importantly, the synthesized materials exhibit much higher durability as Pt support for fuel cells than commercial carbon powder.

This work is especially important for future research and development of carbon materials for fuel cells because the synthesis concept we proposed should pave new ways for design of the doped graphene materials with the controllable doping.

Keywords: *nitrogen-doped graphene, solvothermal, fuel cell.*

7.1 Introduction

Graphene, the two-dimensional monolayer of carbon atoms arranged in a honeycomb lattice, has recently attracted great interests for both fundamental and applied research due to its unique physical and chemical properties [1]. Especially nitrogen doping affects the structure of graphene and in turn the chemical properties [2, 3]. Designing and developing new methods to synthesize nitrogen doped graphene (NG) is critical for tuning its properties. However, currently there are only limited studies on preparation of NG. So far, chemical vapor deposition [4, 5], arc-discharge [6, 7], and posttreatment methods [2, 8] have been proposed for synthesis of NG. Whereas, these methods are complex and operated at higher temperatures (800-1100 °C). Recently, solvothermal synthesis [9] and detonation processes [10] were developed to prepare NG, but these reactions usually proceed at temperatures >300 °C, which are too high for hydrothermal reactions and therefore risky. On the other hand, all of these documented methods use different precursors as the carbon and nitrogen sources, resulting in uncontrollable N-doping components (a mixture of pyridine-like, pyrrole-like, quaternary-like, and nitrogen oxides) strongly restricting the quality of the resulting NG. Herein, we report a novel solvothermal method for large-scale preparation of NG that uses pentachloropyridine as both the carbon source and the nitrogen source. The pentachloropyridine is reacted with potassium. The method features a lower synthesis temperature (~160 °C) than previously reported. Further, controllable N-doping in graphene can be realized.

Polymer electrolyte membrane (PEM) fuel cells can be high-efficiency and environmentally friendly power sources. One of the most challenging problems facing PEMFCs is the development of cost-effective, highly active, and durable electrocatalysts and their support instead of Pt nanoparticles supported on porous carbon (Pt/C). Recently, much effort has been devoted to the durability issues of support materials [11-16], demonstrating that the extent of graphitization of the carbon plays an important role in carbon support stability; more graphitic carbons are more thermally and electrochemically stable [11-14]. Graphene is really a highly graphitized carbon support with a unique graphitized basal plane [1]. Shao et al. reported that graphene is a

promising and durable electrocatalyst support for oxygen reduction in fuel cells [17]. However, there are fewer active sites for highly graphitized carbon support, which makes Pt deposition difficult. One solution to the problem is to dope nitrogen atoms to the carbon frameworks. Our previous results have indicated that Pt nanoparticles can be more uniformly deposited on nitrogen-doped carbon nanotubes (CN_x) than on pristine carbon nanotubes, due to the higher wettability, additional surface structural defects and active surface created by nitrogen doping [18]. Furthermore, it has been shown that nitrogen-doped carbon materials used as Pt supports have an enhanced catalytic activity and durability toward the oxygen reduction reaction [18-23]. Based on these features, it is of significant interest for us to focus on the electrochemical performance of Pt nanoparticles supported on nitrogen-doped graphene, a subject that has yet to be studied in detail. Therefore, in the present work, the durability of synthesized NG as a Pt support for PEM fuel cells was examined and compared with commercial Pt/C (E-TEK) and homemade Pt/C (Vulcan XC-72).

7.2 Experimental

7.2.1 Sample preparation and characterization

A solvothermal route was employed in the synthesis as described below. Typically, 200 mg of pentachloropyridine was placed in a 25 ml Teflon-lined autoclave. Then appropriate amount of metallic potassium was cut into flakes and rapidly added to the autoclave in the glove box. The autoclave was sealed and heated to the desired temperature, where it was maintained for 10 h before it was cooled to room temperature naturally. The products, dark precipitates, were filtered out and washed with acetone, absolute ethanol and water in sequence, and were then dried in a vacuum at 80 °C for 4 h.

The morphologies of the samples were characterized by Hitachi S-4800 field-emission SEM operated at 5.0 kV, high resolution TEM (HRTEM, JEOL 2010 FEG microscope) operated at 200 kV. Also the detailed structures have been also characterized by Raman spectra (HORIBA Scientific LabRAM HR Raman spectrometer system equipped with a 532.4 nm laser.). The nitrogen contents on the surface of all catalysts were also

determined by Kratos Axis Ultra Al (alpha) X-ray photoelectron spectroscopy (XPS) operated at 14 kV.

7.2.2 Electrochemical test

Autolab potentiostat/galvanostat (model PGSTAT-30 Ecochemie Brinkman Instruments) and a three-compartment cell were employed for the electrochemical measurements. The electrochemical experiments were studied using thin catalyst layers formed onto rotating ring disk electrode (RRDE). Briefly, a rotating ring disk electrode from Pine Instruments employing a glassy carbon (GC) disk ($d = 5\text{mm}$) and Au ring (6.5mm i.d., 7.5mm o.d.) was used as the working electrode. Platinum wire and Hg/Hg₂SO₄ electrode were used as the counter and the reference electrode, respectively. The potentials presented in this study are referred with respect to standard hydrogen electrode (SHE). A typical catalytic film was produced at the disk electrode according to the following procedure: 10 mg of Pt/C (E-TEK), or Pt/C (Home made), or Pt/NG was suspended in the solution (5 mL ethanol and 20 μL of 5 wt% Nafion) and ultrasonically blended for 30 min. 20 μL of this suspension was dropped on the disk electrode. Accelerated durability tests (ADT) were conducted by sweeping electrode between 0.05 ~ 1.2 V for 4000 cycles in N₂ saturated 0.5 M H₂SO₄. All the experiments were carried out at 25 °C.

7.3 Results and discussion

Figs. 7-1a and 7-1b show the morphology and structure of the synthesized NG characterized with SEM and TEM. As observed in Fig. 7-1a, the product has a flower-like structure consisting of many loose NG sheets. It can be observed from the TEM image in Fig. 7-1b that the graphene forms small particle-like structures 200-300 nm in diameter. There are a number of small flakes around the particles, indicated by arrows. High-resolution TEM (Fig. 7-1c) further revealed that the petal-like NG sheets are approximately 6-10 graphitic layers thick. The selected area electron diffraction (SAED) pattern (Fig. 7-1d) was used to identify that it is a polycrystalline structure. XPS is a commonly used technique to examine the content and features of nitrogen species in carbon materials. Using the current method, approximately 3.0

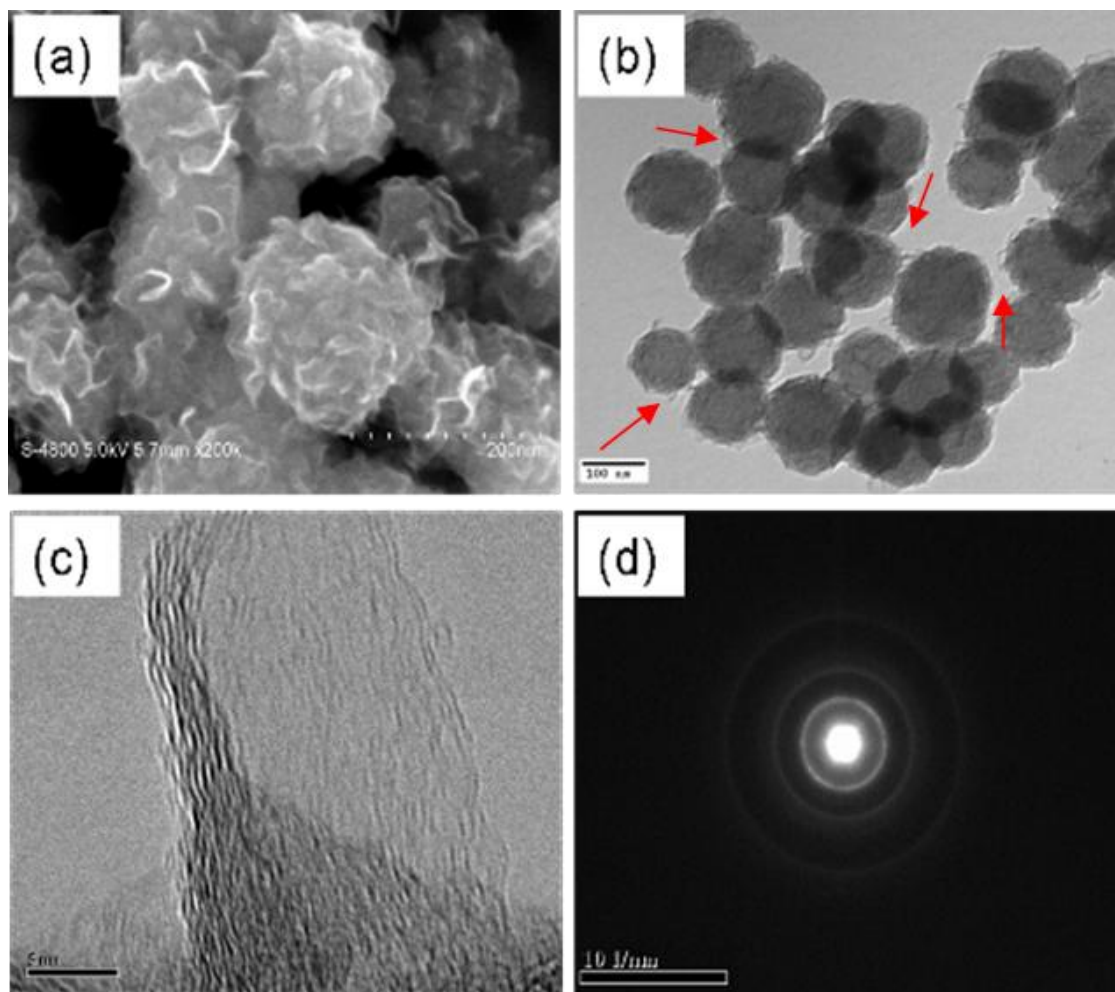


Figure 7-1 (a), (b) SEM and TEM images of the synthesized NG. (c) A high-resolution TEM micrograph of NG. (d) Electron diffraction pattern of NG.

at.% nitrogen (atomic ratio: $N/(N+C)$) was obtained in the NG based on the XPS analysis. The high-resolution XPS N1S spectrum is shown in Fig. 7-2. As expected, only pyridine-like (60.1%) and quaternary (39.9%) nitrogen are formed by the designed reaction. Accordingly, it is reasonable to conclude that flower-like NG has been synthesized successfully.

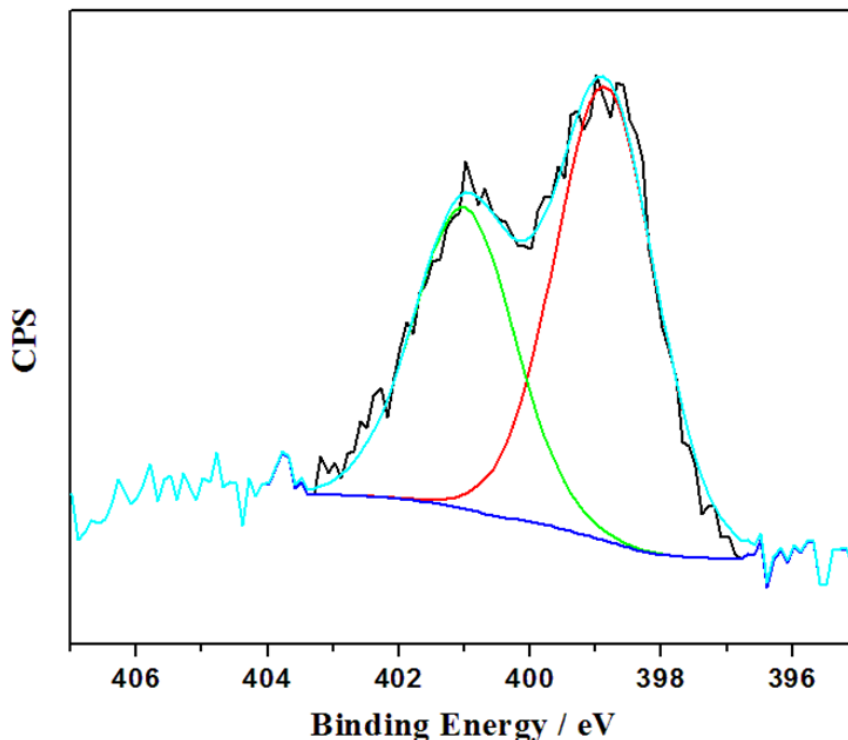


Figure 7-2 The high-resolution N1s spectrum for NG: the black and cyan lines are the raw and fitted spectra; the red and green lines correspond to pyridine-like N (398.5 eV) and quaternary N (401.3 eV), respectively.

Another goal of this work is to evaluate the durability of NG as a Pt support for PEM fuel cells. To compare its durability with the commercial Pt/C, homemade Pt/C using commercial carbon black (Vulcan XC-72) was used as the control sample. The deposition of Pt nanoparticles on NG and Vulcan XC-72 was finished by the impregnation-reduction method [24]. Figs. 7-3a and 7-3b depict the TEM images of Pt nanoparticles dispersed on NG and Vulcan XC-72. The sizes of the Pt nanoparticles range from 3 to 5 nm, similar to the sizes obtained on the commercial catalyst. Fig. 7-3c represents the change in the voltammograms during accelerated durability testing (ADT) at different cycles for Pt/NG [25-27]. Normalized by the initial scan, the degradation of the electrochemical active surface area (ECSA) is plotted in Fig. 7-3d. It can be observed that approximately 32% of the initial ECSA remained for Pt/C (E-TEK), while 36% and 50% of the initial ECSA remained for Pt/C (homemade) and Pt/NG, respectively. This suggests that homemade Pt/C has a

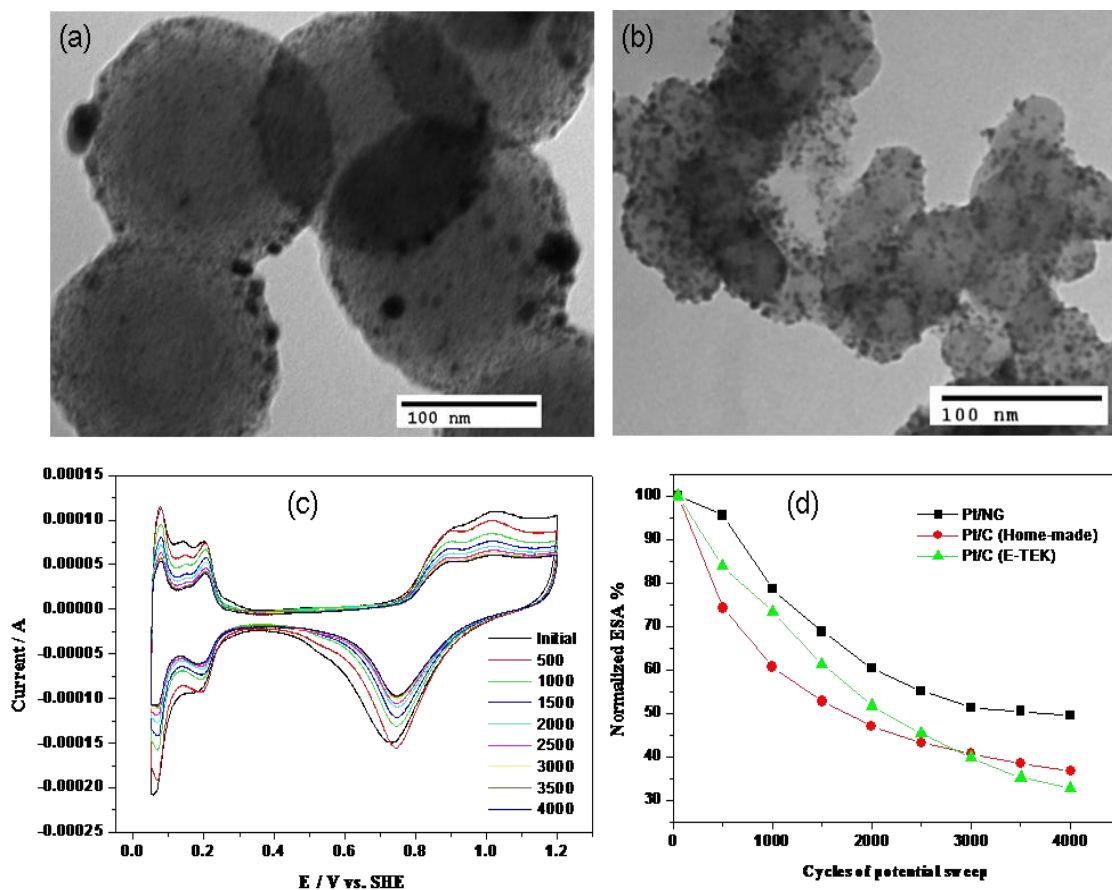


Figure 7-3 (a) and (b): TEM images of Pt/NG and Pt/C (homemade). (c) CV curves of Pt/NG for the different cycles. Scan rate: 50 mV/s. (d) Normalized ECSA of Pt/NG, Pt/C (homemade), and commercial Pt/C.

comparable durability with the commercial version; in other words, Pt deposition using the current method is feasible, and the synthesis-induced difference in the electrochemical performances can be excluded. Thus, Pt/C (homemade) should be suitable to act as the control sample. Furthermore, it can be calculated that Pt/NG retains an ECSA that is 1.5 times higher than that of Pt/C (homemade) after 4000 cycles. Based on the above discussion, we can conclude that flower-like NG has a higher stability than carbon black (Vulcan XC-72), which can be ascribed to the following three points:

- (i) The presence of nitrogen

Nitrogen doping can enhance the interaction between Pt nanoparticles and the delocalized π bond of NG. The existence of the lone electron pair in nitrogen atoms can also stabilize Pt nanoparticles. Using density functional theory, Malardier-Jugroot et al. have demonstrated that the N-doping of graphene increases the binding energy of Pt atoms to the substrate [28]. Our previous experiments also indicated that the presence of nitrogen in carbon nanotubes stabilizes Pt catalysts, resulting in better long-term performance of the catalysts [18, 23].

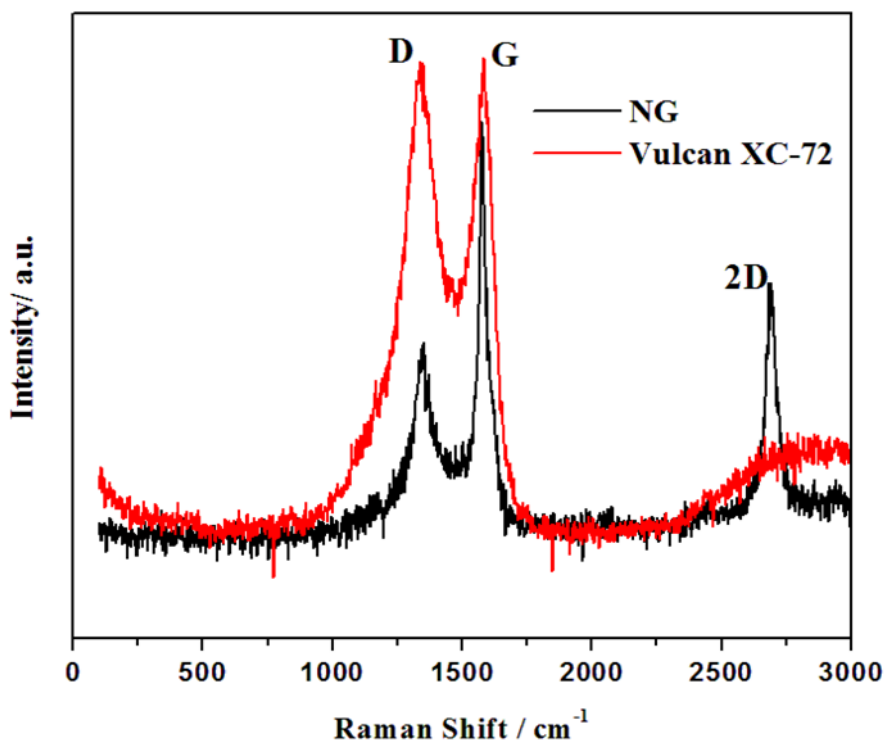


Figure 7-4 Raman spectra of NG and Vulcan XC-72.

(ii) Higher graphitized structure of NG

Many studies have shown that the greater the extent of graphitization of the carbon material, the greater its durability [11-14]. The polycrystalline structure was confirmed by the SAED pattern. To examine the degree of graphitization, Fig. 7-4 shows the Raman spectra of synthesized NG and the commercial carbon black (Vulcan XC-72). Compared with Vulcan XC-72, NG has an obvious 2D band,

indicative of the multilayer NG sheets, which is consistent with the HRTEM observations. Importantly, NG has a relatively low I_D/I_G (the peak intensity ratio of the D to G band; 0.6 vs 1.0), suggesting that the NG layer retained a higher crystalline quality. In the current synthesis, the precursor is pentachloropyridine, which contains only sp^2 -hybridized carbon. It is not difficult to conclude that the resulting graphene will consequentially contain only sp^2 -hybridized carbon (see figure 7-5). Usually, a predominance of sp^2 -hybridized carbon atoms represents a higher level of graphitization. Recently, Deng et al. also reported the solvothermal process to synthesize NG [9], but they used tetrachloromethane (CCl_4), which involves the transformation of sp^3 -hybridized carbon in CCl_4 to sp^2 -hybridized carbon in the synthesis process. Remarkably, it is more difficult to obtain pure sp^2 -hybridized carbon in the product than with our technique.

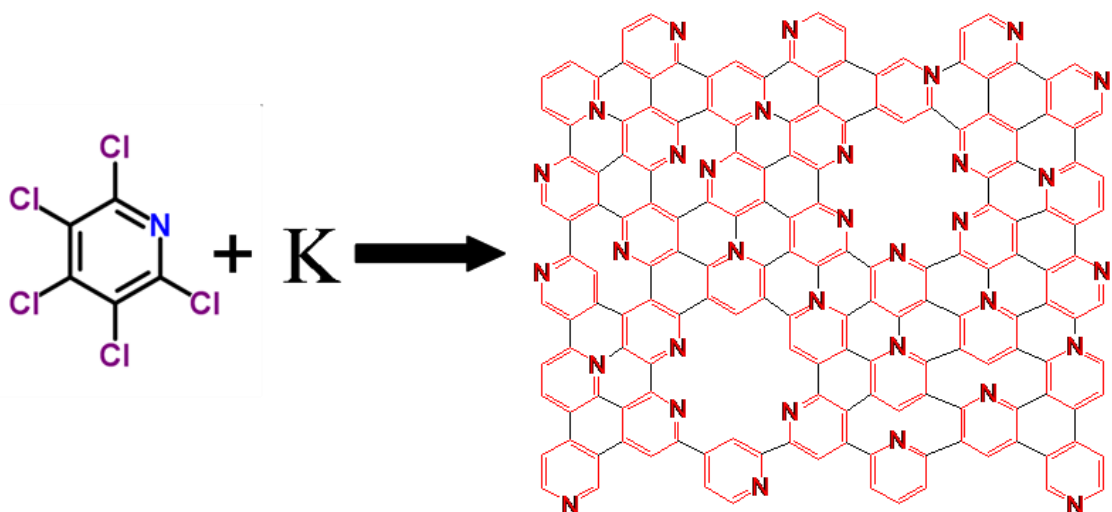


Figure 7-5 Schematic description of NG formation process.

(iii) The presence of ultra-micropores for NG

From the XPS analysis, it is known that not all nitrogen atoms form quaternary N because there is approximately 60.1% pyridine-like N in the product. As shown in Schematic 1, pyridine-like N should result in some ultra-micropores such as type-I or type-II or even others, in the synthesized NG [29]. So far, it is not clear whether the ultra-micropores are playing an important role in the durability. Further study is

necessary.

7.4 Conclusions

In summary, we have shown that nitrogen-doped graphene flowers can be synthesized through a solvothermal process. The resulting material contains sp^2 -hybridized carbon and the designed nitrogen types. This may facilitate new ways to design doped graphene materials with the controllable doping. More importantly, the synthesized NG used as support for Pt exhibited higher durability than commercial carbon black due to its special character as a promising electrocatalyst support material for PEM fuel cells.

Acknowledgements

The work was supported by the Natural Sciences and Engineering Research Council of Canada (NSERC), the Canada Research Chair (CRC) Program, the Canada Foundation for Innovation (CFI), the Ontario Research Fund (ORF), the Ontario Early Researcher Award (ERA) and the University of Western Ontario.

References

- [1] K.S. Novoselov, A.K. Geim, S.V. Morozov, D. Jiang, Y. Zhang, S.V. Dubonos, I.V. Grigorieva, A.A. Firsov, Electric field effect in atomically thin carbon films, *Science*, 306 (2004) 666-669.
- [2] X.R. Wang, X.L. Li, L. Zhang, Y. Yoon, P.K. Weber, H.L. Wang, J. Guo, H.J. Dai, N-Doping of Graphene Through Electrothermal Reactions with Ammonia, *Science*, 324 (2009) 768-771.
- [3] D.S. Geng, S.L. Yang, Y. Zhang, J.L. Yang, J. Liu, R.Y. Li, T.K. Sham, X.L. Sun, S.Y. Ye, S. Knights, Nitrogen doping effects on the structure of graphene, *Appl Surf Sci*, 257 (2011) 9193-9198.

- [4] D.C. Wei, Y.Q. Liu, Y. Wang, H.L. Zhang, L.P. Huang, G. Yu, Synthesis of N-Doped Graphene by Chemical Vapor Deposition and Its Electrical Properties, *Nano Lett*, 9 (2009) 1752-1758.
- [5] A.L.M. Reddy, A. Srivastava, S.R. Gowda, H. Gullapalli, M. Dubey, P.M. Ajayan, Synthesis Of Nitrogen-Doped Graphene Films For Lithium Battery Application, *Acs Nano*, 4 (2010) 6337-6342.
- [6] L.S. Panchokarla, K.S. Subrahmanyam, S.K. Saha, A. Govindaraj, H.R. Krishnamurthy, U.V. Waghmare, C.N.R. Rao, Synthesis, Structure, and Properties of Boron- and Nitrogen-Doped Graphene, *Adv Mater*, 21 (2009) 4726-4730.
- [7] N. Li, Z.Y. Wang, K.K. Zhao, Z.J. Shi, Z.N. Gu, S.K. Xu, Large scale synthesis of N-doped multi-layered graphene sheets by simple arc-discharge method, *Carbon*, 48 (2010) 255-259.
- [8] D.S. Geng, Y. Chen, Y.G. Chen, Y.L. Li, R.Y. Li, X.L. Sun, S.Y. Ye, S. Knights, High oxygen-reduction activity and durability of nitrogen-doped graphene, *Energ Environ Sci*, 4 (2011) 760-764.
- [9] D.H. Deng, X.L. Pan, L.A. Yu, Y. Cui, Y.P. Jiang, J. Qi, W.X. Li, Q.A. Fu, X.C. Ma, Q.K. Xue, G.Q. Sun, X.H. Bao, Toward N-Doped Graphene via Solvothermal Synthesis, *Chem Mater*, 23 (2011) 1188-1193.
- [10] L.Y. Feng, Y.G. Chen, L. Chen, Easy-to-Operate and Low-Temperature Synthesis of Gram-Scale Nitrogen-Doped Graphene and Its Application as Cathode Catalyst in Microbial Fuel Cells, *Acs Nano*, 5 (2011) 9611-9618.
- [11] Y.Y. Shao, G.P. Yin, Y.Z. Gao, Understanding and approaches for the durability issues of Pt-based catalysts for PEM fuel cell, *J Power Sources*, 171 (2007) 558-566.
- [12] X.W. Yu, S.Y. Ye, Recent advances in activity and durability enhancement of Pt/C catalytic cathode in PEMFC - Part II: Degradation mechanism and durability enhancement of carbon supported platinum catalyst, *J Power Sources*, 172 (2007) 145-154.

- [13] D.A. Stevens, M.T. Hicks, G.M. Haugen, J.R. Dahn, Ex situ and in situ stability studies of PEMFC catalysts, *J Electrochem Soc*, 152 (2005) A2309-A2315.
- [14] S.V. Selvaganesh, G. Selvarani, P. Sridhar, S. Pitchumani, A.K. Shukla, Graphitic Carbon as Durable Cathode-Catalyst Support for PEFCs, *Fuel Cells*, 11 (2011) 372-384.
- [15] E. Antolini, Carbon supports for low-temperature fuel cell catalysts, *Appl Catal B-Environ*, 88 (2009) 1-24.
- [16] A. Ignaszak, C. Teo, S.Y. Ye, E. Gyenge, Pt-SnO₂-Pd/C Electrocatalyst with Enhanced Activity and Durability for the Oxygen Reduction Reaction at Low Pt Loading: The Effect of Carbon Support Type and Activation, *J Phys Chem C*, 114 (2010) 16488-16504.
- [17] Y.Y. Shao, S. Zhang, C.M. Wang, Z.M. Nie, J. Liu, Y. Wang, Y.H. Lin, Highly durable graphene nanoplatelets supported Pt nanocatalysts for oxygen reduction, *J Power Sources*, 195 (2010) 4600-4605.
- [18] Y.G. Chen, J.J. Wang, H. Liu, R.Y. Li, X.L. Sun, S.Y. Ye, S. Knights, Enhanced stability of Pt electrocatalysts by nitrogen doping in CNTs for PEM fuel cells, *Electrochem Commun*, 11 (2009) 2071-2076.
- [19] H. Jin, H.M. Zhang, H.X. Zhong, J.L. Zhang, Nitrogen-doped carbon xerogel: A novel carbon-based electrocatalyst for oxygen reduction reaction in proton exchange membrane (PEM) fuel cells, *Energ Environ Sci*, 4 (2011) 3389-3394.
- [20] R.I. Jafri, N. Rajalakshmi, S. Ramaprabhu, Nitrogen doped graphene nanoplatelets as catalyst support for oxygen reduction reaction in proton exchange membrane fuel cell, *J Mater Chem*, 20 (2010) 7114-7117.
- [21] Y.G. Chen, J.J. Wang, X.B. Meng, Y. Zhong, R.Y. Li, X.L. Sun, S.Y. Ye, S. Knights, Atomic layer deposition assisted Pt-SnO₂ hybrid catalysts on nitrogen-doped CNTs with enhanced electrocatalytic activities for low temperature fuel cells, *Int J Hydrogen Energ*, 36 (2011) 11085-11092.

- [22] Y.G. Chen, J.J. Wang, H. Liu, M.N. Banis, R.Y. Li, X.L. Sun, T.K. Sham, S.Y. Ye, S. Knights, Nitrogen Doping Effects on Carbon Nanotubes and the Origin of the Enhanced Electrocatalytic Activity of Supported Pt for Proton-Exchange Membrane Fuel Cells, *J Phys Chem C*, 115 (2011) 3769-3776.
- [23] M.S. Saha, R.Y. Li, X.L. Sun, S.Y. Ye, 3-D composite electrodes for high performance PEM fuel cells composed of Pt supported on nitrogen-doped carbon nanotubes grown on carbon paper, *Electrochem Commun*, 11 (2009) 438-441.
- [24] D.S. Geng, D. Matsuki, J.J. Wang, T. Kawaguchi, W. Sugimoto, Y. Takasu, Activity and Durability of Ternary PtRuIr/C for Methanol Electro-oxidation, *J Electrochem Soc*, 156 (2009) B397-B402.
- [25] Y.Y. Shao, J. Wang, R. Kou, M. Engelhard, J. Liu, Y. Wang, Y.H. Lin, The corrosion of PEM fuel cell catalyst supports and its implications for developing durable catalysts, *Electrochim Acta*, 54 (2009) 3109-3114.
- [26] C. Grolleau, C. Coutanceau, F. Pierre, J.M. Leger, Effect of potential cycling on structure and activity of Pt nanoparticles dispersed on different carbon supports, *Electrochim Acta*, 53 (2008) 7157-7165.
- [27] Y. Shao-Horn, W.C. Sheng, S. Chen, P.J. Ferreira, E.F. Holby, D. Morgan, Instability of supported platinum nanoparticles in low-temperature fuel cells, *Top Catal*, 46 (2007) 285-305.
- [28] M.N. Groves, A.S.W. Chan, C. Malardier-Jugroot, M. Jugroot, Improving platinum catalyst binding energy to graphene through nitrogen doping, *Chem Phys Lett*, 481 (2009) 214-219.
- [29] M. Bieri, M. Treier, J.M. Cai, K. Ait-Mansour, P. Ruffieux, O. Groning, P. Groning, M. Kastler, R. Rieger, X.L. Feng, K. Mullen, R. Fasel, Porous graphenes: two-dimensional polymer synthesis with atomic precision, *Chem Commun*, (2009) 6919-6921.

Supporting information

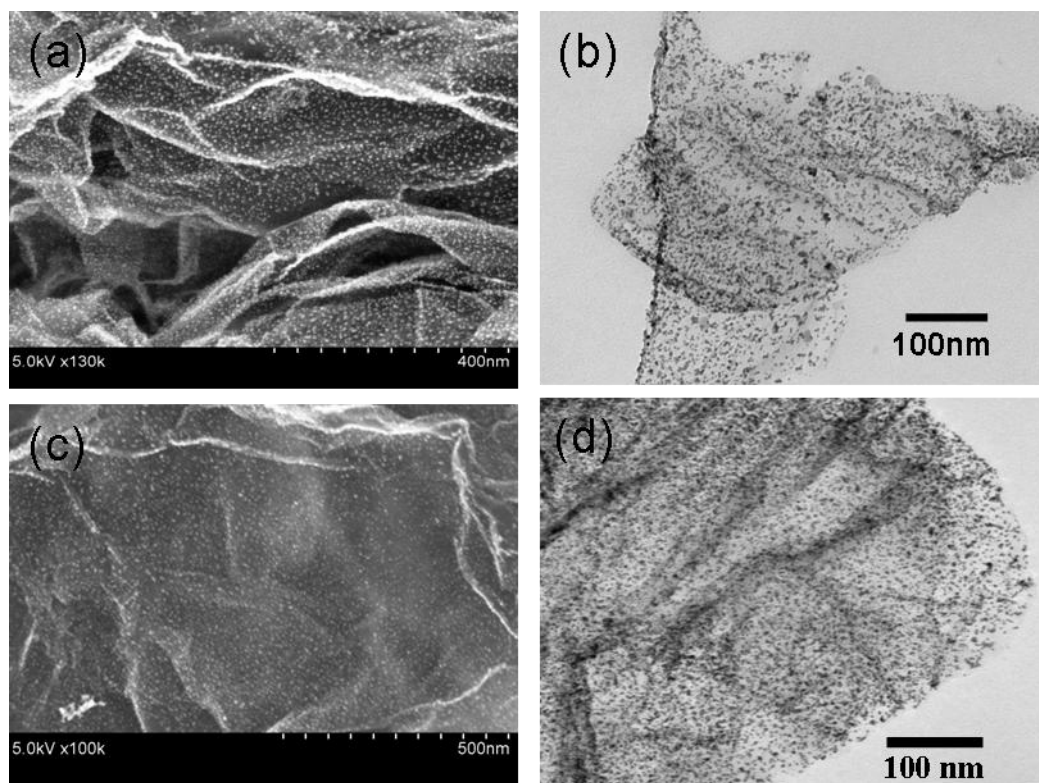


Figure 7-6 (a) SEM and (b) TEM images of Pt/graphene; (c) SEM and (d) TEM images of Pt/N-graphene. Graphene and N-graphene samples from Hummers' method (please see Chapter 4), Pt nanoparticles deposition is done based on reference 24 in this chapter.

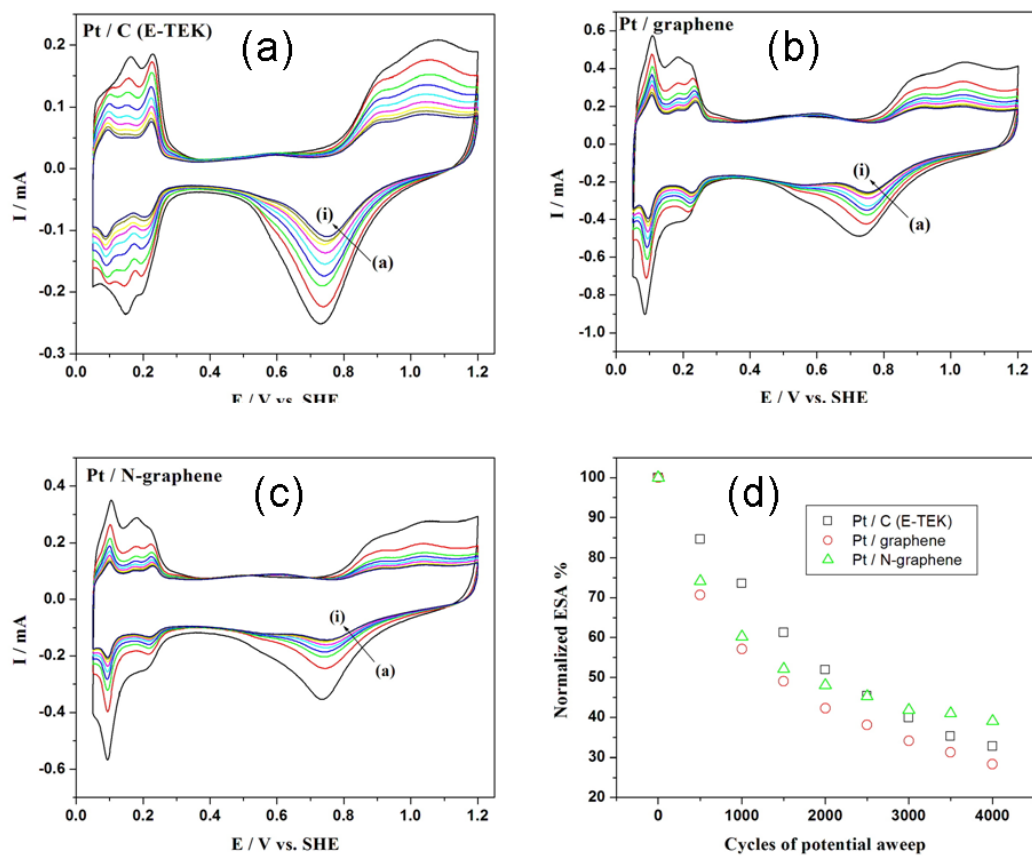


Figure 7-7 Cyclic voltammograms of: (a) Pt/C (E-TEK), (b) Pt/graphene, (c) Pt/N-graphene (2.8 at.% N) after 50, 500, 1000, 1500, 2000, 2500, 3000, 3500, 4000 cycles, and (d) the comparison of the degradations of the three catalysts. Scan rate: 50 mV/s.

Chapter 8

8 A universal method to synthesize urchin-shaped Pt nanostructures

Dongsheng Geng, Shuhui Sun, Jinli Yang, Ruying Li, Xueliang Sun*

Department of Mechanical and Materials Engineering, University of Western Ontario,
1151 Richmond Street N., London, Ontario, Canada N6A 5B9

Fax: +1-519-6613020; Tel: +1-519-6612111, Ext. 87759

E-mail: xsun@eng.uwo.ca

A version of this chapter will be submitted to publish.

As mentioned in chapter 1, there are three main research directions for developing fuel cell cathode catalysts. (i) to synthesize non-noble metal ORR catalyst; (ii) to develop novel support materials for helping decrease the dissolution of Pt; (iii) to synthesize novel nanostructured Pt with high performance and durability. In previous chapters, we have studied nitrogen doped carbon nanotubes, nitrogen doped graphene as the non-noble metal ORR catalysts for fuel cell; and also investigated nitrogen doped graphene by novel synthesis method as Pt support showing the improve durability compared with Pt/C (E-TEK). This chapter will focus on the Pt main catalyst development. Over the past decade, there has been a strong effort in developing effective strategies for improving the performance and thus reducing the cost of platinum-based ORR electrocatalysts, which involved shaping Pt nanostructures. As known, many metallic nanostructures with different shapes exhibit unique chemical and physical properties. Our previous results have shown that star-like Pt nanowires have both good catalytic activity and durability

for ORR due to the dendritic Pt nanostructures with the interconnected network made of 1D nanowires, which is believed to have the ability for making the Pt less vulnerable to dissolution, Ostwald ripening, and aggregation during fuel cell operation compared to Pt nanoparticles even Pt nanowires. However, there is a limitation in scale up for previous method. And it seems that it is difficult to control the length of Pt nanowire and the shape of star-like Pt nanostructures. Here we report a universal method to produce urchin-shaped Pt nanostructures in high yield. This is a very simple, green and efficient wet chemical route without any surfactant and template.

Keywords: *fuel cell, Pt nanowire, urchin-shaped Pt nanostructures, durability*

8.1 Introduction

The synthesis of metal nanostructures with controllable morphologies is a key goal in modern materials chemistry and has attracted considerable interest in recent years because of their importance in catalysis, photochemistry, sensors, and electronic devices [1-5]. It is generally accepted that a fine degree of morphology control for metal nanostructures can lead to the formation of materials with specific chemical and physical properties. Among various metal nanostructures, nanostructured Pt is of particular interest because of its unique catalytic properties. For example, Pt nanoparticles are playing the key role in proton exchange membrane fuel cells (PEMFCs) for oxygen reduction and hydrogen oxidation [6, 7]. Compared with Pt nanoparticles, shaped Pt nanostructures such as Pt nanowires, Pt nanotubes, three-dimensional dendritic platinum have been demonstrated to have the better electrocatalytic performance [8-11]. The manipulation of the shape of Pt nanostructures can improve its catalytic activity and contribute to lowering Pt utilization. Therefore, the synthesis of special types of Pt nanostructures is highly desirable and potentially technologically important.

Up to now, in general there are two synthetic routes to produce platinum materials with special shapes. They are template and templateless routes. Ag, Te have been used as sacrificial templates to produce 1D Pt nanowires or nanotubes [12, 13]. Also, some micelle templates such as Pluronic F127 block copolymer and Brij-35 surfactants can help to form platinum nanodendrites [14, 15]. There is still scale-up limitation due to the necessary additional procedures for preparation and removal of the templates although the route can effectively achieve the control over the shape of platinum. Regarding templateless routes, usually it is proceeded in solution with some shape-directing agents. Typically, Xia et al. have demonstrated that triggered growths by trace amount additives such as Fe^{3+} , Fe^{2+} , or NO_3^- is an effective strategy for synthesis of shaped Pt nanostructures [16, 17]. But the synthetic procedure of these methods is usually complicate involving many steps also resulting in fewer yields of Pt nanostructures.

Herein, a very simple and efficient wet chemical route was proposed to directly obtain urchin-shaped Pt nanostructures in large quantities by reducing PtCl_4^{4-} using the different

reductants (R-OH, R-CHO, or R-COOH). It seems that the process we proposed is a universal procedure for urchin-shaped Pt formation. In current study, it was possible to form urchin-shaped Pt nanostructures from K_2PtCl_4 solution as long as the reductants contain hydroxyl, aldehyde, or carboxylic. Specially, our method has the below advantages in comparison to those reported previously:

- (i) The method is very simple, which only needs Pt salt and reductants without any surfactants.
- (ii) The reaction is a green process and can be conducted very efficiently at room temperature.
- (iii) Without surfactants and templates, the products can be purified and collected easily.
- (iv) The structures of urchin-shaped Pt can be adjusted simply by the change of reductants.

8.2 Experimental

8.2.1 Materials

K_2PtCl_4 ($\geq 99.9\%$), methanol ($\geq 99.8\%$), ethanol ($\geq 99.8\%$), 2-propanol ($\geq 99.5\%$), ethylene glycol ($\geq 99\%$), formic acid ($\geq 98.0\%$), and formaldehyde (37 wt% solution in water) were purchased from Sigma-Aldrich (Canada). All the reagents were used as received without further purification. All solutions were prepared with deionized water.

8.2.2 Typical synthesis of urchin-shaped Pt nanostructures

Urchin-shaped platinum nanostructures were synthesized by the chemical reduction of Pt precursor with reductants containing -OH, -CHO, or -COOH group. All the experiments were conducted in aqueous solution, at room temperature and under ambient atmosphere. In a typical synthesis, 7.5 mg K_2PtCl_4 was dissolved into 9 mL of water, and then 1 mL of formaldehyde was quickly added. The mixture solution was stored at room temperature for 48 h. The color of the reaction solution changed with several seconds

from light pink to brown, then to opaque black. The product was collected by centrifugation and washed several times with water, and then dried in an oven at 60 °C for further use in characterization and electrochemical measurements.

8.2.3 Characterization

Transmission electron microscopy (TEM) observations were performed with a Philips CM10 microscope at an accelerating voltage of 100 kV. High-resolution TEM (HRTEM) images were obtained with a JEOL 2010F microscope, operating at 200 kV.

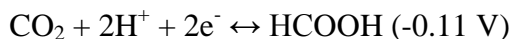
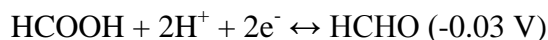
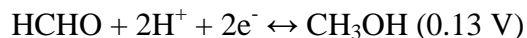
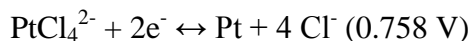
8.2.4 Electrochemical test

Electrochemical tests of urchin-shaped Pt nanostructures were performed on an Autolab potentiostat/galvanostat (Model, PGSTAT-30, Ecochemie, Brinkman Instruments) using a three-electrode system that consists of a glassy carbon (GC) rotating disk electrode (RDE), a Pt wire counter electrode, and a Hg/HgSO₄ (saturated K₂SO₄) reference electrode. For convenience, all potentials in this study are referenced to the standard hydrogen electrode (SHE). Catalyst ink was prepared by dispersing 2 mg of the electrocatalysts in 2.0 mL of ethanol and was subject to ultrasonication for 15 min. Then, 20 μL of the ink was dropped onto a glassy carbon surface with an exposed area of 0.196 cm². After drying the droplet at 60 °C, 20 μL of a 0.05 wt% Nafion alcoholic solution was further dropped on the electrode surface and heated again at 60 °C to stabilize the electrocatalysts. The working electrode was first cycled between 0.05 and 1.2 V for 50 times in an N₂-purged 0.5 M H₂SO₄ solution at room temperature, to produce a clean electrode surface. The scan rate used was 50 mV s⁻¹. Then the cyclic voltammetry (CV) measurements were conducted by cycling the potential between 0.05 and 1.2 V, with sweep rate of 50 mV s⁻¹. The electrochemical surface areas (ECSA) of platinum was calculated using the mean integral charge of the hydrogen adsorption / desorption area with double layer current corrected at 0.4 V vs. RHE and with 210 μC cm_{Pt}⁻², assuming one hydrogen atom observed to one platinum atom. The CV measurements for accelerated durability test (ADT) were conducted by potential cycling between 0.6 and 1.2 V (vs. RHE) for 4000 cycles in O₂-saturated 0.5 M H₂SO₄ solution at room

temperature, with scan rate of 50 mV s⁻¹. Meanwhile, full-scale voltammogram between 0.05 and 1.2 V in N₂-saturated H₂SO₄ solution were recorded periodically to track the degradation of Pt catalysts.

8.3 Results and discussion

In the current investigation, methanol, ethanol, 2-propanol, and ethylene glycol were selected as the reductants with hydroxyl group; formaldehyde and formic acid were selected as the reductants with aldehyde or carboxylic groups. The reduction of platinum salts by methanol, ethanol, ethylene glycol, and formaldehyde occurs in several seconds and eventually the black precipitation was obtained in the bottom of vial. For formic acid, it takes a little longer time to reduce Pt salts, but still within several seconds. However, for the 2-isopropanol system, it needs longer time (hours) for reduction occurring, which means the change of color from light pink to grey-black. From the above phenomenon, firstly it seems that all of hydroxyl, aldehyde, and carboxylic groups are able to reduce PtCl₄²⁻ to Pt metal, which is also consistent with their redox potential (see below) [18].



Secondly, the different R groups might have the effect on the different reductive rate based on the results of methanol, ethanol, 2-propanol, and ethylene glycol reductive reactions [19]. Thirdly, it appears that carboxylic group has the negative effect on the reduction of PtCl₄²⁻ when the difference is considered between formic acid and formaldehyde. Furthermore, when acetic acid is used as reductant, no any Pt precipitation and color change is found, indicating acetic acid cannot reduce PtCl₄²⁻ to Pt at room temperature at the current condition studied. Here, it is believed that either the R group (CH₃-) affects the reductive ability of carboxylic group, or essentially the reductive power of carboxylic group is not enough strong to reductive PtCl₄²⁻ to Pt at such

conditions. The real group playing the key role in reducing PtCl_4^{2-} to Pt might be its aldehyde group for formic acid.

Also the current study gives a new investigation into the old reactions. Previous results exhibited that the big Pt aggregation will be obtained without surfactants and under the condition of stir. When the reaction system is carefully adjusted and no stir is used, the exciting results are obtained. It is believed that this is a universal method to synthesize dendritic Pt structures with the various density and size.

The shape and size of the typically synthesized Pt nanostructures were characterized by TEM and the results are shown in Figure 8-1. Pt nanostructures appeared to be dendritic structures made of short Pt nanorods/nanowires and clearly uniform in shape. The very dark contrast at the body center region of nanostructures indicated that these nanostructures were rich three-dimensional (3D) structures. The particle sizes were distributed roughly from 20 to 50 nm for methanol, ethanol, ethylene glycol, and formaldehyde reductive system; whereas formic acid reductive system exhibited wider distribution for particle sizes from 20 to 80 nm. Also it should be noted that 2-propanol reductive system results in the biggest particle sizes. All these should be consistent with their reaction time mentioned above. The rapid nucleation resulting from strong reductants produces large quantity of Pt seed crystals, which will benefit the final distribution of Pt sizes. The slow nucleation process results in a broad size distribution of Pt seed crystals, in turn which will produce bigger particle sizes or the broad size distribution of the final Pt nanostructures.

High-resolution TEM images further displayed the urchin-shaped structures assembled with plentiful interconnected arms branching in various directions (Figure 8-2). The diameter of these branched Pt nanowires is about 3-4 nm. The lattice fringes are continuous from the core to the branches, revealing the high crystallinity of the nanostructures. The selected area electron diffraction (SAED) patterns exhibit the diffraction pattern corresponding to (111), (200), (220), and (311) lattice planes of fcc Pt.

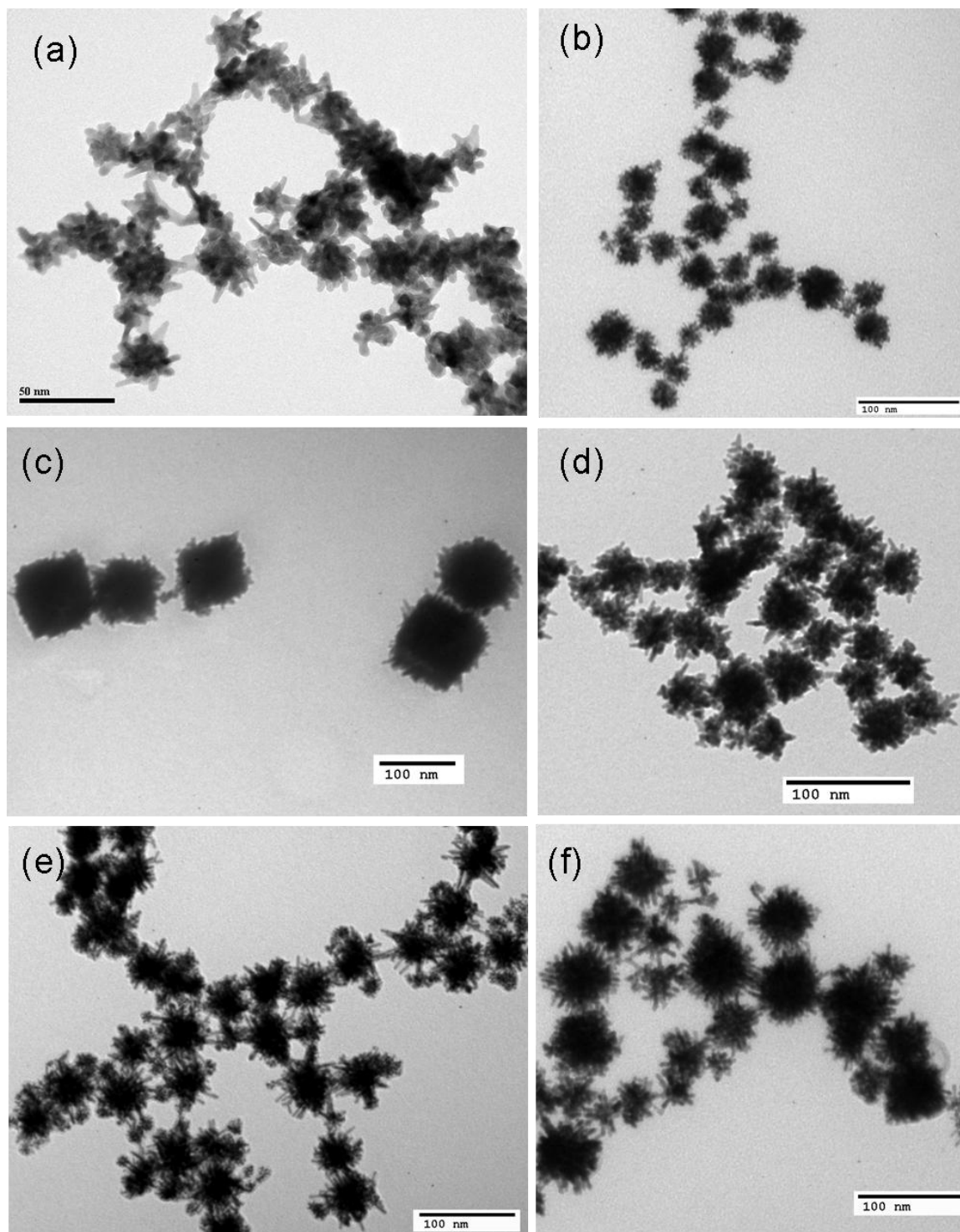


Figure 8-1 TEM images of urchin-shaped Pt nanostructures from the various reductants: (a) methanol (b) ethanol (c) 2-propanol (d) ethylene glycol (e) formaldehyde (f) formic acid.

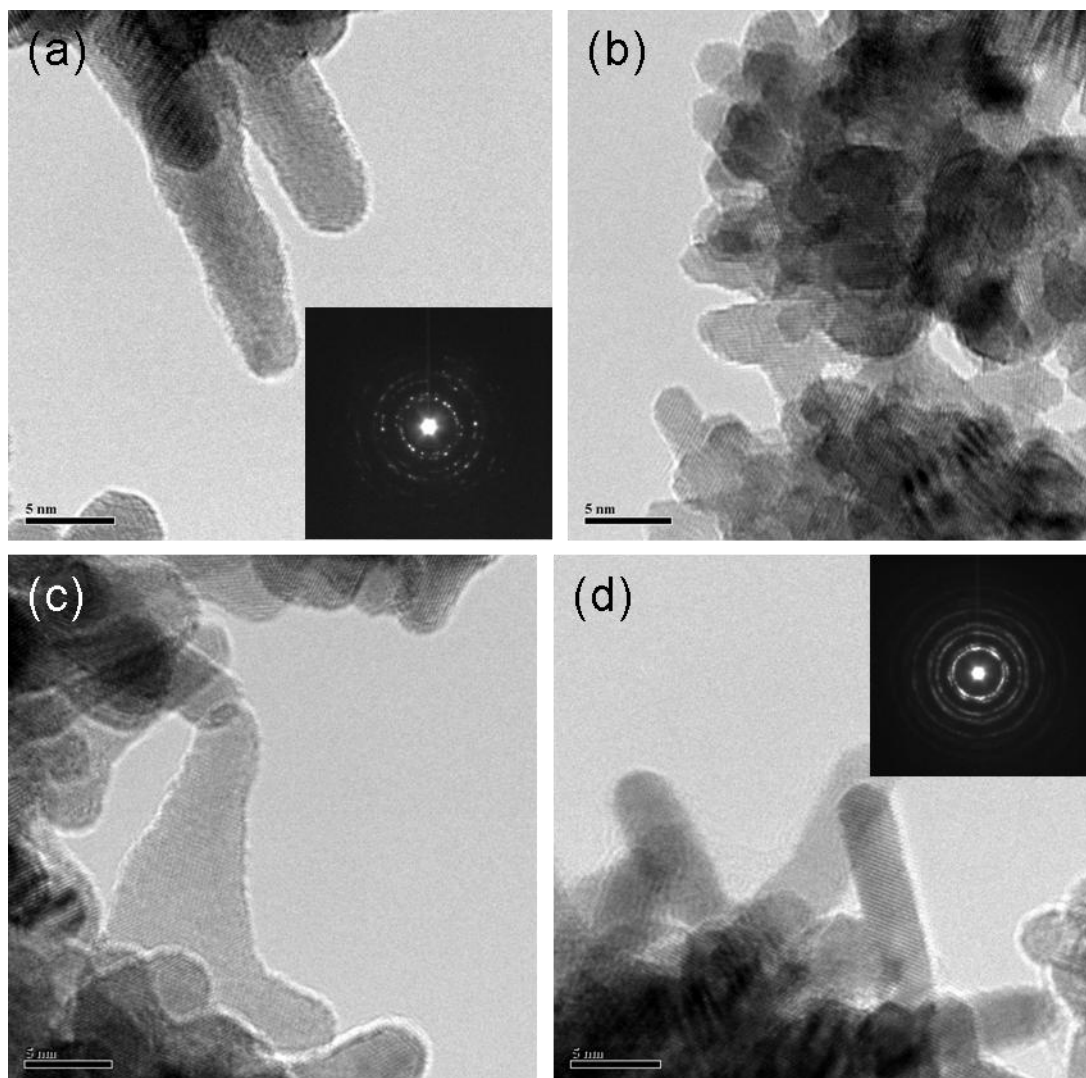


Figure 8-2 HRTEM images of urchin-shaped Pt nanostructures from the different reductants: (a) methanol (b) ethanol (c) ethylene glycol (d) formaldehyde. The insets are the corresponding SAED pictures.

And the measured lattice spacing (0.23 nm, Figure 8-2 (a-d)) corresponds to (111) lattice planes of fcc Pt. This is not difficult to understand. Usually a nucleation and auto-catalytic process are involved in the formation of Pt⁰ [20-23]. For our study system, there is the below order for the adsorption energies of -OH, -CHO, and -COOH groups on three typical Pt surfaces: Pt (110) > Pt (100) > Pt (111) [4, 20]. After Pt nucleation, the molecules with the above groups adsorbed preferentially on specific crystal surfaces, such as Pt (110) and (100) facets, restricting the growth in these two facets and resulting

in preferential growth on the Pt (111) facet. However, the detailed formation mechanism of the urchin-shaped Pt nanostructures in the synthesis is not very clear at the present time and needs further investigation.

It is highly interesting to explore the as-prepared Pt nanostructures as the fuel cell electrocatalysts. It has been very recently reported that Pt nanowires and nanotubes have shown better performance and higher stability than Pt/carbon black (the commercial catalyst). The reason might be that in comparison to zero dimensional Pt nanoparticles, single crystalline anisotropic 1D Pt possess fewer lattice boundaries, long segments of smooth crystal planes, and a low number of surface defect sites, all of which are desirable attributes for enhancing both oxygen reduction reaction (ORR) activity and long-term durability for fuel cells. Additionally, in our previous studies, it was shown that the catalytic properties of Pt metal nanocrystal can be enhanced by the combination of a multi-armed network structure and the one-dimensional shape of the arms [8]. Therefore, it is not unexpected that the current urchin-shaped Pt would improve the activity and durability.

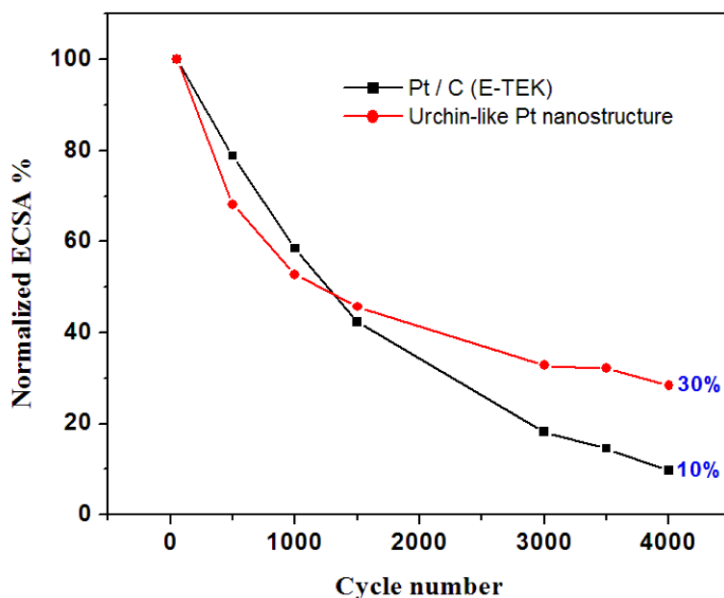


Figure 8-3 Normalized ECSA of urchin-like Pt nanostructures and commercial Pt/C.

Figure 8-3 showed the durability results of urchin-shaped Pt and commercial Pt/C catalyst. It can be observed that approximately 10% of the initial ECSA remained for Pt/C (E-TEK), while 30% of the initial ECSA remained for urchin-shaped Pt. That is, urchin-shaped Pt retains 2 times higher ECSA than that of Pt/C (E-TEK) after 4000 cycles, which can be ascribed to its special structure: interconnected 1D Pt arms.

8.4 Conclusions

A universal method to produce urchin-shaped Pt nanostructures in high yield was demonstrated by simply keeping an aqueous solution containing K_2PtCl_4 and reductant under room temperature for 48 hours. In the current study, methanol, ethanol, 2-propanol, ethylene glycol, formaldehyde, and formic acid have been demonstrated to be the effective reductive agents and the shape-directing agents. Furthermore, hydroxyl group and aldehyde group, perhaps carboxylic group should have the ability to reduce Pt salt to Pt metal, therefore which could be considered as a very general and powerful strategies for producing urchin-shaped Pt nanostructures (or dendritic Pt nanostructures).

Acknowledgements

The work was supported by the Natural Sciences and Engineering Research Council of Canada (NSERC), GM (Canada), the Canada Research Chair (CRC) Program, the Canada Foundation for Innovation (CFI), the Ontario Research Fund (ORF), the Ontario Early Researcher Award (ERA) and the University of Western Ontario.

References

- [1] Y.N. Xia, Y.J. Xiong, B. Lim, S.E. Skrabalak, Shape-Controlled Synthesis of Metal Nanocrystals: Simple Chemistry Meets Complex Physics?, *Angew Chem Int Edit*, 48 (2009) 60-103.
- [2] S.E. Skrabalak, Y.N. Xia, Pushing Nanocrystal Synthesis toward Nanomanufacturing, *Acs Nano*, 3 (2009) 10-15.

- [3] T.K. Sau, C.J. Murphy, Room temperature, high-yield synthesis of multiple shapes of gold nanoparticles in aqueous solution, *J Am Chem Soc*, 126 (2004) 8648-8649.
- [4] J. Watt, N. Young, S. Haigh, A. Kirkland, R.D. Tilley, Synthesis and Structural Characterization of Branched Palladium Nanostructures, *Adv Mater*, 21 (2009) 2288-2293.
- [5] C. Burda, X.B. Chen, R. Narayanan, M.A. El-Sayed, Chemistry and properties of nanocrystals of different shapes, *Chem Rev*, 105 (2005) 1025-1102.
- [6] M.K. Debe, Electrocatalyst approaches and challenges for automotive fuel cells, *Nature*, 486 (2012) 43-51.
- [7] Y.H. Bing, H.S. Liu, L. Zhang, D. Ghosh, J.J. Zhang, Nanostructured Pt-alloy electrocatalysts for PEM fuel cell oxygen reduction reaction, *Chem Soc Rev*, 39 (2010) 2184-2202.
- [8] S.H. Sun, G.X. Zhang, D.S. Geng, Y.G. Chen, R.Y. Li, M. Cai, X.L. Sun, A Highly Durable Platinum Nanocatalyst for Proton Exchange Membrane Fuel Cells: Multiarmed Starlike Nanowire Single Crystal, *Angew Chem Int Edit*, 50 (2011) 422-426.
- [9] S.H. Sun, F. Jaouen, J.P. Dodelet, Controlled Growth of Pt Nanowires on Carbon Nanospheres and Their Enhanced Performance as Electrocatalysts in PEM Fuel Cells, *Adv Mater*, 20 (2008) 3900-3904.
- [10] H.J. Zhou, W.P. Zhou, R.R. Adzic, S.S. Wong, Enhanced Electrocatalytic Performance of One-Dimensional Metal Nanowires and Arrays Generated via an Ambient, Surfactantless Synthesis, *J Phys Chem C*, 113 (2009) 5460-5466.
- [11] Z.W. Chen, M. Waje, W.Z. Li, Y.S. Yan, Supportless Pt and PtPd nanotubes as electrocatalysts for oxygen-reduction reactions, *Angew Chem Int Edit*, 46 (2007) 4060-4063.
- [12] Y.P. Bi, G.X. Lu, Control growth of uniform platinum nanotubes and their catalytic properties for methanol electrooxidation, *Electrochem Commun*, 11 (2009) 45-49.

- [13] H.W. Liang, S. Liu, J.Y. Gong, S.B. Wang, L. Wang, S.H. Yu, Ultrathin Te Nanowires: An Excellent Platform for Controlled Synthesis of Ultrathin Platinum and Palladium Nanowires/Nanotubes with Very High Aspect Ratio, *Adv Mater*, 21 (2009) 1850-1854.
- [14] L. Wang, Y. Yamauchi, Block Copolymer Mediated Synthesis of Dendritic Platinum Nanoparticles, *J Am Chem Soc*, 131 (2009) 9152-9153.
- [15] L. Wang, Y. Yamauchi, Synthesis of Mesoporous Pt Nanoparticles with Uniform Particle Size from Aqueous Surfactant Solutions toward Highly Active Electrocatalysts, *Chem-Eur J*, 17 (2011) 8810-8815.
- [16] B.W. Lim, X.M. Lu, M.J. Jiang, P.H.C. Camargo, E.C. Cho, E.P. Lee, Y.N. Xia, Facile Synthesis of Highly Faceted Multioctahedral Pt Nanocrystals through Controlled Overgrowth, *Nano Lett*, 8 (2008) 4043-4047.
- [17] T. Herricks, J.Y. Chen, Y.N. Xia, Polyol synthesis of platinum nanoparticles: Control of morphology with sodium nitrate, *Nano Lett*, 4 (2004) 2367-2371.
- [18] D.R. Lide, *CRC Handbook of Chemistry and Physics (87th ed.)*, CRC Press, 2006.
- [19] Y.P. Bi, G.X. Lu, Morphology-controlled preparation of silver nanocrystals and their application in catalysis, *Chem Lett*, 37 (2008) 514-515.
- [20] L. Wang, C.P. Hu, Y. Nemoto, Y. Tateyama, Y. Yamauchi, On the Role of Ascorbic Acid in the Synthesis of Single-Crystal Hyperbranched Platinum Nanostructures, *Cryst Growth Des*, 10 (2010) 3454-3460.
- [21] L.C. Ciacchi, W. Pompe, A. De Vita, Initial nucleation of platinum clusters after reduction of K_2PtCl_4 in aqueous solution: A first principles study, *J Am Chem Soc*, 123 (2001) 7371-7380.
- [22] Y.J. Song, Y. Yang, C.J. Medforth, E. Pereira, A.K. Singh, H.F. Xu, Y.B. Jiang, C.J. Brinker, F. van Swol, J.A. Shelnutt, Controlled synthesis of 2-D and 3-D dendritic platinum nanostructures, *J Am Chem Soc*, 126 (2004) 635-645.

[23] S. Cheong, J. Watt, B. Ingham, M.F. Toney, R.D. Tilley, In Situ and Ex Situ Studies of Platinum Nanocrystals: Growth and Evolution in Solution, *J Am Chem Soc*, 131 (2009) 14590-14595.

Supporting information

The effect of pH, NO_3^- , and Fe^{3+} on the morphologies of Pt nanostructures.

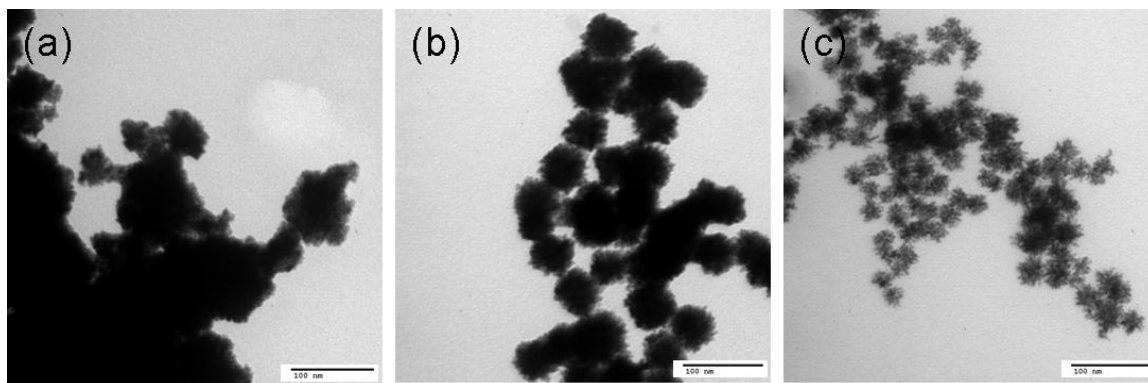


Figure 8-4 TEM images of Pt nanostructures from the various reductants and under pH = 2: (a) methanol (b) formaldehyde (c) formic acid.

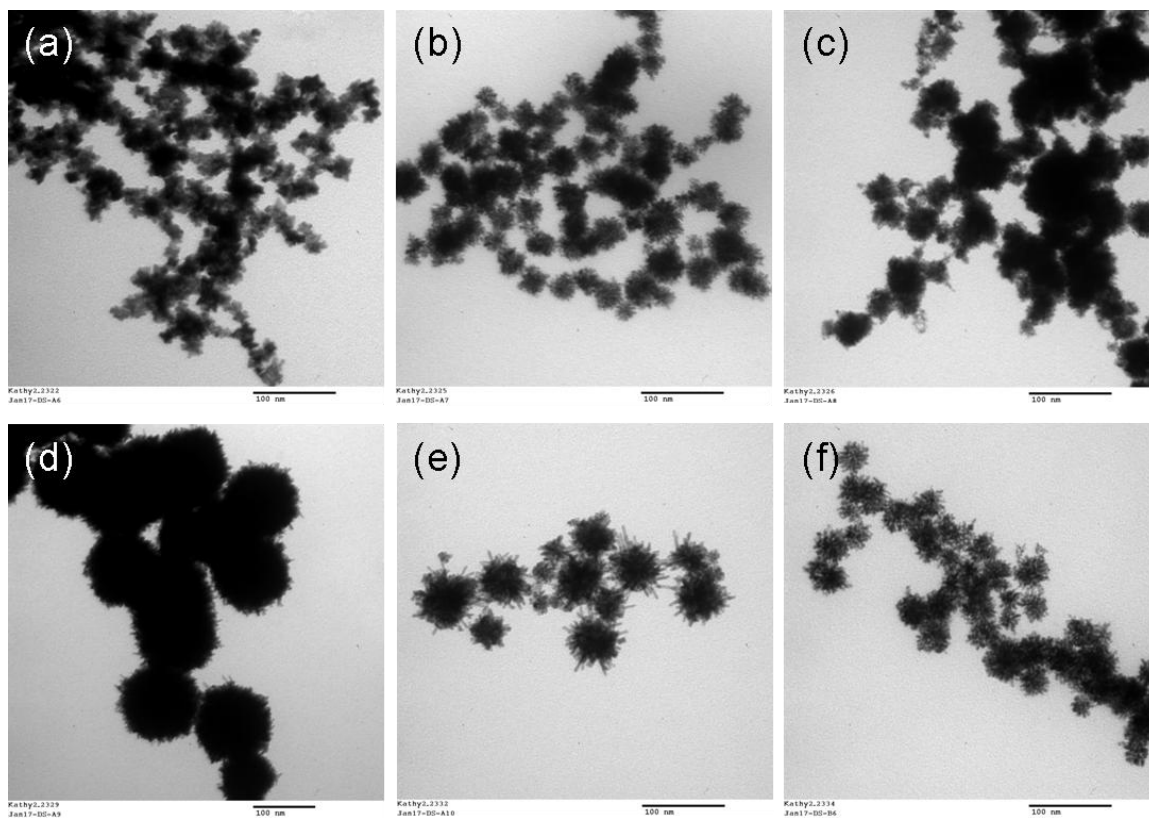


Figure 8-5 TEM images of Pt nanostructures from the various reductants under the existence of NO_3^- ($[\text{Pt}]:[\text{NO}_3^-] = 1:10$): (a) methanol (b) ethanol (c) 2-propanol (d) ethylene glycol (e) formaldehyde (f) formic acid.

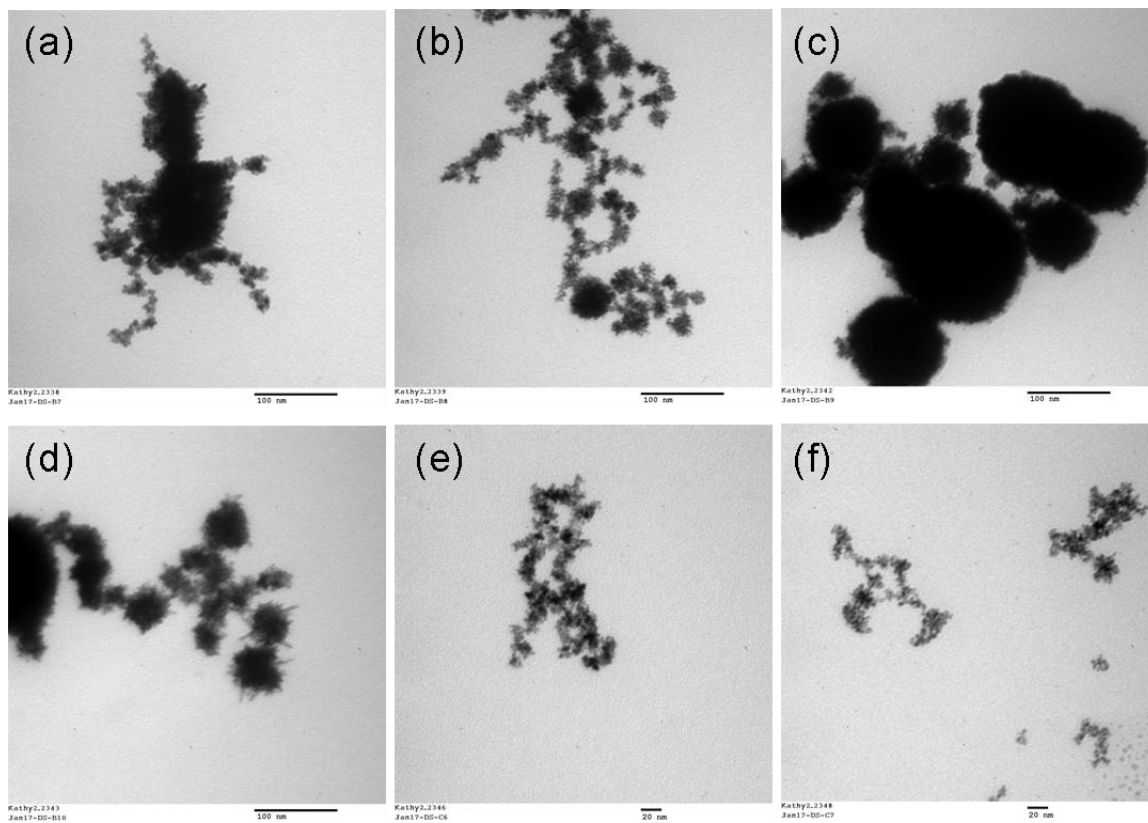


Figure 8-6 TEM images of Pt nanostructures from the various reductants under the existence of Fe³⁺ ([Pt]:[Fe³⁺] = 1 :10): (a) methanol (b) ethanol (c) 2-propanol (d) ethylene glycol (e) formaldehyde (f) formic acid.

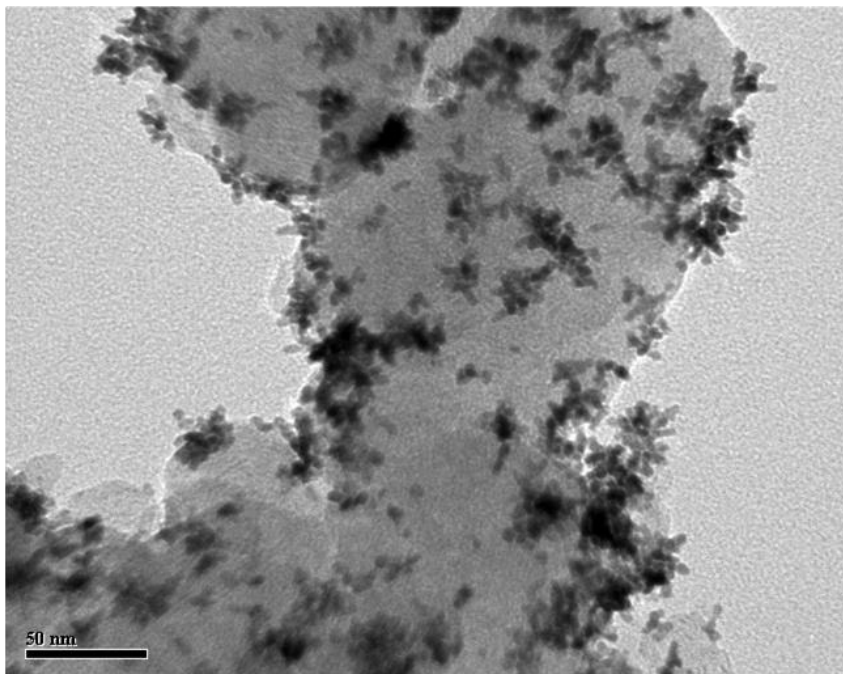


Figure 8-7 Urchin-shaped Pt nanostructures growth on carbon black (Vulcan XC-72); the reductant is formaldehyde.

Chapter 9

9 Conclusions and Suggestions

Currently, cost and durability are still the two major barriers for large-scale manufacturing and full commercialization of PEMFCs. Developing high-performance, low-cost and high durable electrocatalysts is the number one set of priorities for PEMFCs research and development. In the thesis, a series of experiments was conducted to synthesize novel nanostructured materials as cathode materials of fuel cells. Emphasis was put on three ways: (i) development of nitrogen doped carbon nanotube and graphene as non-noble metal ORR catalysts (ii) development of novel method to synthesize nitrogen doped graphene as Pt support (iii) synthesis of novel dendritic Pt nanostructures by green, simple method, which includes material synthesis, characterization, and performance test. The results and contributions of the thesis work are summarized below, and some personal opinions and suggestions for future work are provided.

9.1 Conclusions

Nitrogen doped carbon nanotubes (CN_x) with the controllable nitrogen content have been prepared via a floating catalyst chemical vapor deposition method using precursors consisting of ferrocene and melamine. The relationship between structures of CN_x and ORR activity has been investigated in detail. The active site involving nitrogen, iron, carbon is further identified by the study. The work for the first time disclosed the promoting effect of nitrogen on the ORR activity systematically. It is believed that the higher the nitrogen content is, the higher the oxygen reduction activity. And CN_x has the potential to replace the costly Pt/C catalyst in alkaline fuel cells.

Further, the study about non-noble metal ORR catalyst was extended to 2D nitrogen doped carbon materials --- N-graphene from the 1D nitrogen doped carbon nanotubes. We reported the synthesis of nitrogen-doped graphene as a metal-free catalyst for oxygen reduction by heat-treatment of graphene using ammonia. As a consequence, it was revealed that the catalyst has the comparable or better activity and stability than the

commercial Pt/C towards ORR, and the quaternary type nitrogen species seem to play the most important role for ORR activity. This is a very important finding, which will not only help to identify the active site, but also benefit to the designing of this kind of catalyst for the next generation.

Moreover, based on the better ORR activity and durability of carbon materials after doping, nitrogen doping effect on carbon structure was investigated systematically using many characterization techniques by taking the example of graphene and N-graphene. It was found that more defects are present on nitrogen doped graphene, especially XANES results reveal that N doping decreases the surface oxygen-containing groups.

It is always the challenge to develop new way to prepare nitrogen doped graphene. A simple one-step solution-based oxidative process to produce N-graphene oxide nanoribbons (NGON) has been developed. As a consequence, the method generates a nearly 100% yield of nanoribbon structures by lengthwise cutting and unravelling of the nitrogen doped carbon nanotube side walls. The work should open a new door to synthesize nitrogen doped graphene, also the study for the first time demonstrated the possibility of transformation from nitrogen doped carbon nanotubes to nitrogen doped graphene oxide nanoribbons directly.

Nitrogen doped graphene has been prepared by a novel solvothermal method at the large scale. The method features a lower synthesis temperature than previously reported. The results indicated that nanoflower-like N-graphene was obtained with pure sp^2 hybridized carbon and the designed nitrogen types. More importantly, the synthesized materials exhibit much higher durability as Pt support for fuel cells than commercial carbon powder due to its special characters.

A very simple, green and efficient wet chemical route has been developed to produce urchin-shaped Pt nanostructures in high yield without any surfactant and template. Again the study gains an insight into the old reductive reactions. It is revealed that hydroxyl group and aldehyde group, perhaps carboxylic group should have the ability to reduce $PtCl_4^-$ to Pt metal even with the uniform morphology distribution under the stationary conditions (without stir). More importantly, urchin-shaped Pt indicates 2 times higher

stability than that of Pt/C (E-TEK) under the current test condition due to its special interconnected 1D Pt arms structure.

9.2 Suggestions

The thesis exploited the ORR activity and durability of nitrogen doped carbon nanotubes and graphene. However, in comparison to commercial Pt/C, the performance is still poor in acid condition. The development of non-noble metal ORR catalyst is facing the big challenge. For nitrogen doped carbon materials, in order to further improve their performance, it is necessary to find new synthesis methods for increasing nitrogen content and controlling the nitrogen doping form.

The thesis also tried to investigate the performance of nitrogen doped graphene as a support of Pt showing the improve durability compared with the Pt nanoparticles supported on carbon black. However, the relationship between performance improvement, the structure of support, and the degradation is still unclear. For a better understanding and therefore for further increasing the stability of support, more fundamental investigation is required such as the relationship of pore size, specific surface area, graphitic structure and stability. This topic will remain a challenge. In addition, a recent study indicated that ITO-graphene hybrid material as Pt support exhibited greatly enhanced stability and activity. It is expected that metal oxide-graphene based hybrid materials could be even more stable.

This thesis also exploited a new type of dendritic Pt nanostructures which showed much improved durability than the particle Pt. Recently, the focus is put on Pt-alloy nanoparticles on carbon, which have historically been observed to increase ORR activity over pure Pt/C by about a factor of 2 to 2.5. It is expected that the activities and durability could be further increased if dendritic Pt alloy nanostructures could be synthesized and used in fuel cells.

APPENDICES

Supporting information

(The detailed process for electrode preparation and durability test)

Taking Pt/C catalyst as an example, the electrochemical characterizations of the catalysts were conducted in a standard three-compartment electrochemical cell using a glassy carbon (GC) rotating ring disk electrode. Here, a Pt wire was used as the counter electrode and Hg/HgSO₄ (saturated K₂SO₄) was used as the reference electrode. 10 mg of Pt/C was suspended in the solution (5 mL ethanol and 20 μ L of 5 wt% Nafion) and ultrasonically blended for 30 min. 20 μ L of this suspension was dropped on the disk electrode and dried at 60 °C.

The electrodes were first pretreated to remove surface contamination by cycling the electrode from 0.05 to 1.2 V vs SHE at 50 mV s⁻¹ for 50 cycles in nitrogen saturated electrolyte. Then the quasi-steady-state voltammograms can be obtained and used to calculate the initial ECSA of Pt/C. Accelerated durability tests (ADT) were conducted by sweeping electrode between 0.05 ~ 1.2 V for 4000 cycles. The durability was evaluated by comparing the change of ECSA. Here, figure A-1 (a) shows the initial CV curves for three samples of Pt/C, figure A-1 (b) shows the CV curves after 4000 cycles for the corresponding samples.

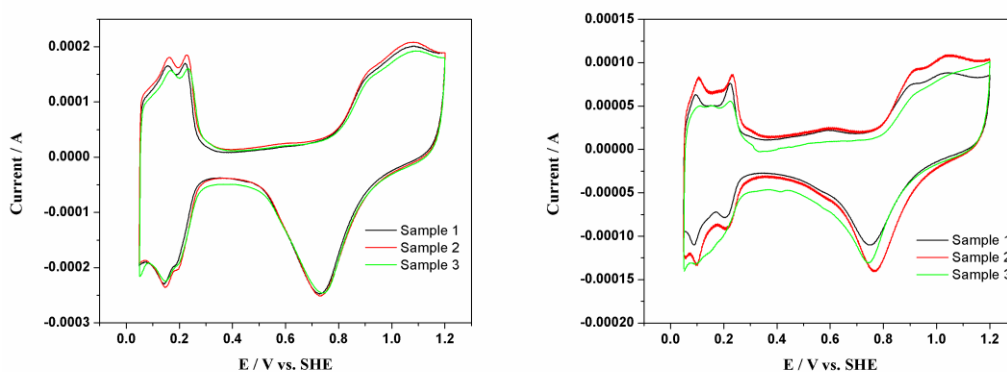


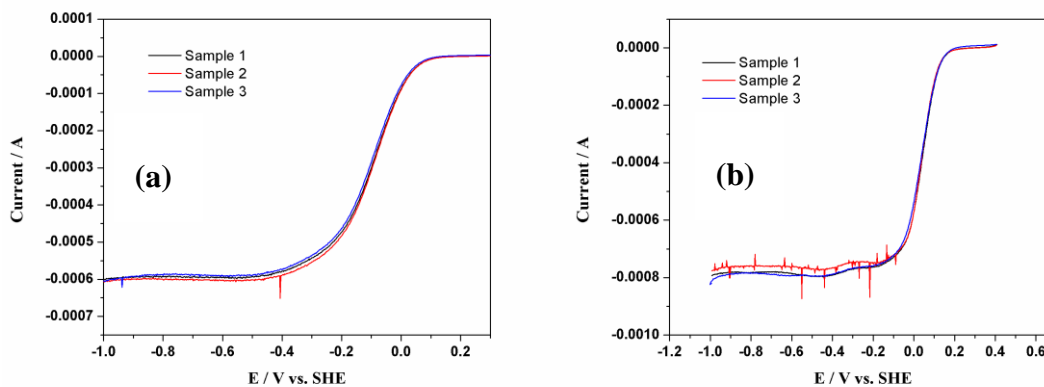
Fig. A-1 (a) The initial CV curves of Pt/C and (b) the CV curves of Pt/C after 4000 cycles from 0.05 – 1.2 V in 0.5 M H₂SO₄ solution with saturated N₂, Scan rate: 50 mV s⁻¹.

As seen, there is good repeatability for our samples. After 4000 cycles' degradation, it can be calculated that approximately 30.4%, 32% and 33.2% of the initial ECSA remained for sample 1, sample 2 and sample 3, respectively.

(The detailed process for ORR test and the electrode preparation)

Autolab potentiostat/galvanostat (model PGSTAT-30 Ecochemie Brinkman Instruments) and a three-compartment cell were employed for the electrochemical measurement. The electrocatalytic activities of CN_x and N-graphene were studied using RRDE technique. A typical catalytic film was produced at the disk electrode according to the following procedure: 5 mg of CN_x or N-graphene were suspended in the solution (1080 μL ethanol and 180 μL of 5 wt % Nafion) and ultrasonically blended for 30 min. 10 μL of this suspension was dropped on the disk electrode. CV curves of ORR were recorded by scanning the disk potential from 0.4 to -1.0 V (0.1 M KOH solution) vs SHE at a scan rate of 5 mV s^{-1} with the rotating speed of 1600 rpm.

In order to further demonstrate the repeatability of our samples' activities, here we provide three times data about ORR activity for CN_x (7.7%), N-graphene (900), and Pt/C, respectively.



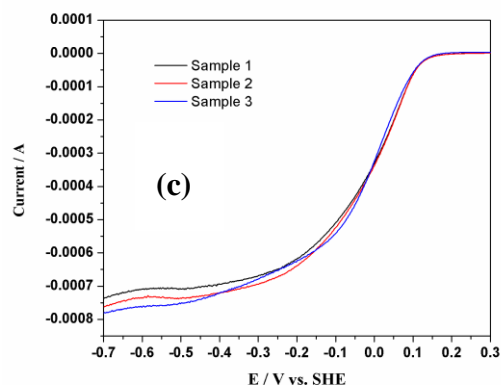


Fig.A-2 (a) The polarization curves of oxygen reduction on CN_x (7.7%) catalyst; (b) N-graphene (900) catalyst; (c) Pt/C catalyst. Electrolyte: 0.1 M KOH, scan rate: 5 mV s^{-1} , and rotation speed: 1600 rpm.

As we can see, CN_x (7.7%) has the perfect repeatability for ORR activity not only at current density but also onset potential. Although there is a little bit difference at the current density for N-graphene (900) and Pt/C, usually the ORR activities are evaluated by comparing the onset potential; basically we cannot find any difference at the onset potential for three samples.

**APPENDIX I: PERMISSION FROM ROYAL SOCIETY OF CHEMISTRY (RSC)
FOR PUBLISHED ARTICLE**

Published paper: High oxygen-reduction activity and durability of nitrogen-doped graphene, *Energy & Environmental Science*, 2011, **4**, 760-764.

RSC Copyright Policy

(<http://www.rsc.org/AboutUs/Copyright/RightsRetainedbyJournalsauthors.asp>):

Rights retained by journal authors

When the author signs the exclusive Licence to Publish for a journal article, he/she retains certain rights that may be exercised without reference to the RSC. He/she may:

- ***Reproduce/republish portions of the article (including the abstract)***
- *Photocopy the article and distribute such photocopies and distribute copies of the PDF of the article that the RSC makes available to the corresponding author of the article upon publication of the article for personal or professional use only, provided that any such copies are not offered for sale.*

APPENDIX II: PERMISSION FROM ELSEVIER FOR PUBLISHED ARTICLES

Published paper:

- (1) Nitrogen doping effects on the structure of graphene, *Applied Surface Science*, 2011, **21**, 9193-9198.
- (2) One-pot solvothermal synthesis of doped graphene with the designed nitrogen type used as a Pt support for fuel cells, *Electrochemistry Communications*, 2012, **22**, 65-68.
- (3) Non-noble metal oxygen reduction electrocatalysts based on carbon nanotubes with controlled nitrogen contents, *Journal of Power Sources*, 2011, **196**, 1795-1801.

Elsevier Copyright Policy

(<http://www.elsevier.com/wps/find/authorsview.authors/rights>):

*As a journal author, you retain rights for a large range of author uses of your article, including use by your employing institute or company. **These rights are retained and permitted without the need to obtain specific permission from Elsevier.***

What rights do I retain as a journal author*?

- the right to make copies (print or electronic) of the journal article for your own personal use, including for your own classroom teaching use;
- the right to make copies and distribute copies of the journal article (including via e-mail) to research colleagues, for personal use by such colleagues for scholarly purposes*;
- the right to post a pre-print version of the journal article on Internet websites including electronic pre-print servers, and to retain indefinitely such version on such servers or sites for scholarly purposes* (with some exceptions such as The Lancet and Cell Press. See also our information on [electronic preprints](#) for a more detailed discussion on these points)*;

- the right to post a revised personal version of the text of the final journal article (to reflect changes made in the peer review process) on your personal or institutional website or server for scholarly purposes*, incorporating the complete citation and with a link to the Digital Object Identifier (DOI) of the article (but not in subject-oriented or centralized repositories or institutional repositories with mandates for systematic postings unless there is a specific agreement with the publisher. [Click here](#) for further information);
- the right to present the journal article at a meeting or conference and to distribute copies of such paper or article to the delegates attending the meeting;
- for your employer, if the journal article is a ‘work for hire’, made within the scope of the author’s employment, the right to use all or part of the information in (any version of) the journal article for other intra-company use (e.g. training);
- patent and trademark rights and rights to any process or procedure described in the journal article;
- the right to include the journal article, in full or in part, in a thesis or dissertation;
- the right to use the journal article or any part thereof in a printed compilation of your works, such as collected writings or lecture notes (subsequent to publication of the article in the journal); and
- the right to prepare other derivative works, to extend the journal article into book-length form, or to otherwise re-use portions or excerpts in other works, with full acknowledgement of its original publication in the journal.

CURRICULUM VITAE

Name: Dongsheng Geng

Education: Department of mechanical and material engineering
The University of Western Ontario, London, ON, Canada
2010-2013, Ph.D.

Lanzhou Institute of Chemical Physics
Chinese Academy of Sciences, China
2002-2007, M.S./Ph.D.

Department of Chemical and Environmental Engineering
Hebei University, China
1997-2001, B.S.

Work experience: Teaching & Research Assistant (2010-2012)
The University of Western Ontario, ON, Canada

Postdoctoral fellow (2008-2010)
The University of Western Ontario, ON, Canada

Postdoctoral fellow (2007-2008)
Shinshu University, Ueda, Japan

Research Assistant (2002-2007)
Lanzhou Institute of Chemical Physics
Chinese Academy of Sciences, China

Researcher (2001-2002)
Hebei Zhongrun Pharmaceutical Co., Ltd., China

Relevant Publications:

(A) Patent

X. Sun, H. Yang, X. Li, **D. Geng**. (2010) Secondary lithium batteries having novel anodes field of the invention. US patent, pending, Dec. 2010.

*(B) Peer-reviewed Journal papers based on This Thesis
(First Author)*

1. **D. Geng**, Y. Hu, Y. Li, R. Li, X. Sun, (2012) One-pot Solvothermal Synthesis of Doped Graphene with the Designed Nitrogen Type Used as a Pt Support for Fuel Cells. *Electrochem. Commun.* 22: 65-68.
2. **D. Geng**, Y. Chen, Y. Chen, Y. Li, R. Li, X. Sun, S. Ye, S. Knights. (2011) High oxygen-reduction activity and durability of nitrogen-doped graphene. *Energy. Environ. Sci.* 4: 760-764. [Highlighted by "[*Materials Today*](#)", **ten most downloaded articles in Feb. 2011**]
3. **D. Geng**, S. Yang, Y. Zhang, J. Yang, J. Liu, R. Li, T.K. Sham, X. Sun, S. Ye, S. Knights. (2011) Nitrogen doping effects on the structure of graphene. *Appl. Surf. Sci.* 257: 9193-9198.
4. **D. Geng**, H. Liu, Y. Chen, R. Li, X. Sun, S. Ye, S. Knights. (2011) Non-Noble Metal Oxygen Reduction Electrocatalysts Based on Carbon Nanotubes with Controlled Nitrogen Contents. *J. Power Sources* 196: 1795-1801.
5. **D. Geng**, S. Sun, J. Yang, R. Li, X. Sun, A universal method to synthesize urchin-shaped Pt nanostructures. To be submitted.

6. **D. Geng**, Y. Hu, J. Liu, R. Li, X. Sun, S. Ye, S. Knights, Nitrogen doped graphene oxide nanoribbons from nitrogen doped carbon nanotubes. To be submitted.

(C) *Peer-reviewed Journal Papers Related with This Thesis*
(Coauthor)

7. D. Wang, X. Li, J. Wang, J. Yang, **D. Geng**, R. Li, M. Cai, T.-K. Sham, X. Sun, (2012) Defect-Rich Crystalline SnO₂ Immobilized on Graphene Nanosheets with Enhanced Cycle Performance for Li Ion Batteries. *J. Phys. Chem. C*. Accepted.
8. J. Liu, X. Meng, Y. Hu, **D. Geng**, M. Banis, M. Cai, R. Li, X. Sun, (2012) Controlled synthesis of Zirconium Oxide on graphene nanosheets by atomic layer deposition and its growth mechanism. *Carbon*. In press.
9. Y. Li, J. Wang, X. Li, **D. Geng**, M. Banis, Y. Tang, D. Wang, R. Li, T.-K. Sham, X. Sun, (2012) Discharge product morphology and increased charge performance of lithium–oxygen batteries with graphene nanosheet electrodes: the effect of sulphur doping. *J. Mater. Chem.* 22: 20170-20174.
10. J. Yang, J. Wang, X. Li, D. Wang, J. Liu, G. Liang, M. Gauthier, Y. Li, **D. Geng**, R. Li, X. Sun, (2012) Hierarchically Porous LiFePO₄/Nitrogen-doped Carbon Nanotube Composite for Lithium Ion Batteries Cathodes. *J. Mater. Chem.* 22: 7537-7543.
11. J. Yang, J. Wang, D. Wang, X. Li, **D. Geng**, G. Liang, M. Gauthier, R. Li, X. Sun, (2012) 3D Porous LiFePO₄-

- graphene Hybrid Electrodes with Enhanced Performance for Li-ion Batteries. *J. Power Sources* 208: 340-344.
12. X. Li, **D. Geng**, Y. Zhang, X. Meng, R. Li, X. Sun. (2011) Superior cycle stability of nitrogen-doped graphene nanosheets as anodes for lithium ion batteries. *Electrochem. Commun.* 13: 822-825.
 13. X. Li, J. Liu, Y. Zhang, Y. Li, H. Liu, X. Meng, J. Yang, **D. Geng**, D. Wang, R. Li, X. Sun, (2012) High Concentration Nitrogen Doped Carbon Nanotube Anodes with Superior Li⁺ Storage Performance for Lithium Rechargeable Battery Application. *J. Power Sources* 197: 238-245.
 14. X. Meng, **D. Geng**, J. Liu, R. Li, X. Sun. (2011) Controllable synthesis of graphene-based titanium dioxide nanocomposites by atomic layer deposition. *Nanotechnology* 22: 165602
 15. X. Meng, **D. Geng**, J. Liu, M. Banis, Y. Zhang, R. Li, X. Sun. (2010) A non-aqueous approach to synthesize amorphous/crystalline metal oxide-graphene nanosheet hybrid composites. *J Phys. Chem. C* 43: 1830-18337.
 16. H. Ismaili, **D. Geng**, A. Sun, T. T. Kantzas, M. S. Workentin, (2011) Light-Activated Covalent Formation of Gold Nanoparticle–Graphene and Gold Nanoparticle–Glass Composites, *Langmuir* 27: 13261-13268.
 17. Y. Li, J. Wang, X. Li, **D. Geng**, R. Li, X. Sun. (2011) Superior energy capacity of graphene nanosheets for a nonaqueous lithium-oxygen battery. *Chem. Commun.* 47: 9438-9440.

18. Y. Li, J. Wang, X. Li, J. Liu, **D. Geng**, J. Yang, R. Li, X. Sun, (2011) Nitrogen-doped Carbon Nanotubes as Cathode for Lithium-Air Batteries. *Electrochem. Commun.* 13: 668-672.
19. X. Li, X. Meng, J. Liu, **D. Geng**, Y. Zhang, M. Banis, Y. Li, R. Li, X. Sun, M. Cai, M. Verbrugge, (2012) Tin Oxide with Controlled Morphology and Crystallinity by Atomic Layer Deposition onto Graphene Nanosheets for Enhanced Lithium Storage. *Adv. Funct. Mater.* 22: 1647-1654.
20. Y. Li, J. Wang, X. Li, **D. Geng**, M. Banis, R. Li, X. Sun, (2012) Nitrogen-doped Graphene Nanosheets as Cathode Materials with Excellent Electrocatalytic Activity for High Capacity Lithium-oxygen Batteries. *Electrochem. Commun.* 18: 12-15.
21. S. Sun, G. Zhang, **D. Geng**, Y. Chen, R. Li, M. Cai, X. Sun. (2011) A new highly durable Pt nanocatalyst for PEM fuel cells: the multiarmed star-like nanowire single crystal. *Angew. Chem. Int. Ed.* 50: 422-426.
22. Y. Chen, Y. Zhang, **D. Geng**, R. Li, H. Hong, J. Chen, and X. Sun, (2011) One-pot Synthesis of MnO₂/Graphene/Carbon nanotube Hybrid by Chemical Method. *Carbon* 49: 4434-4442.
23. H. Li, H. Liu, Z. Jong, W. Qu, **D. Geng**, X. Sun, H. Wang, (2011) Nitrogen-doped Carbon Nanotubes with High Activity for Oxygen Reduction in Alkaline Media. *Int. J Hydrogen Energy* 36: 2258-2265.

(D) Previous Publications

24. S. Sun, G. Zhang, **D. Geng**, Y. Chen, R. Li, M. Cai, X. Sun, (2010) Direct Growth of Single-Crystal Pt Nanowires on Sn@CNT Nanocable: 3D Electrodes for Highly Active Electrocatalysts. *Chem. Eur. J.* 16: 829-835.
25. Y. Zhang, **D. Geng**, H. Liu, M.N. Banis, M.I. Ionescu, R. Li, M. Cai, X. Sun. (2011) Designed growth and characterization of radially aligned Ti(5)Si(3) nanowire architectures. *J. Phys. Chem. C* 115: 15885-15889.
26. **D. Geng**, D. Matsuki, J. Wang, T. Kawaguchi, W. Sugimoto, Y. Takasu. (2009) Activity and Durability of Ternary PtRuIr/C for Methanol Electro-oxidation. *J. Electrochem. Soc.* 156: B397-B402. [Selected for the January 26, 2009 issue of *Virtual Journal of Nanoscale Science & Technology*]
27. **D. Geng**, G. Lu. (2007) The dependence of onset potential for methanol electrocatalytic oxidation on steric location of active center in multi-component electrocatalysts. *J. Phys. Chem. C* 111: 11897-11902.
28. **D. Geng**, L. Chen, G. Lu. (2007) pH induced size-selected synthesis of PtRu nanoparticles, their characterization and electrocatalytic properties. *J. Mol. Catal. A* 265: 42-49.
29. **D. Geng**, G. Lu. (2007) Size effect of gold nanoparticles on the electrocatalytic oxidation of carbon monoxide in alkaline solution. *J. Nano. Res.* 9: 1145-1151.
30. **D. Geng**, G. Lu, Y. Bi, Y. Bi. (2005) Particle size effect of alumina-supported platinum catalysts synthesized by microemulsion on the electrocatalytic oxidation of CO. *Acta Chimica Sinica*, 6: 658-662.

31. Z. Tang, **D. Geng**, G. Lu. (2005) Size-controlled synthesis of colloidal platinum nanoparticles and their activity for the electrocatalytic oxidation of carbon monoxide. *J. Colloid Interface Sci.* 287: 159-166.
32. Z. Tang, **D. Geng**, G. Lu. (2006) Electrocatalytic oxidation of carbon monoxide on platinum-modified polyaniline film electrodes. *Thin Solid Films*, 497: 309-314.
33. Z. Tang, **D. Geng**, G. Lu. (2005) A simple solution-phase reduction method for the synthesis of shape-controlled platinum nanoparticles. *Mater. Lett.* 59: 1567-1570.
34. Y. Bi, **D. Geng**, Y. Bi, G. Lu. (2005) Investigation of Nano-Pt/Al₂O₃ Preparation via Room Temperature Reduction and Its Catalytic Properties. *J. Mol. Catal. (China)* 19: 98-103.
35. Y. Bi, G. Lu, **D. Geng**, Y. Bi. (2005) Correlation of Activity and Size of Pt Nanoparticles for Methanol Steam Reforming over Pt/Y-Al₂O₃ Catalysts. *Acta Chimica Sinica*, 63: 802-808.

(E) Conference Presentations

1. **D. Geng**, S. Sun, Y. Hu, R. Li, X. Sun, S. Ye, S. Knights. (2011) Synthesis and application of doped graphene as non-noble metal electrocatalysts for fuel cells. 61st Canadian Chemical Engineering Conference, London, Ontario, Canada.
2. **D. Geng**, H. Liu, Y. Chen, R. Li, X. Sun, S. Ye, S. Knights. (2010) Non-Noble Metal Oxygen Reduction Electrocatalysts Based on Carbon Nanotubes with

Controlled Nitrogen Contents. ECS Canadian Section Fall Symposium, London, Canada.

3. **D. Geng**, Y. Chen, Y. Chen, R. Li, X. Sun. (2010) Graphene: Synthesis and Application in Fuel Cells. Ontario Nanoscience and Nanotechnology Workshop, London, Canada.
4. **D. Geng**, G. Lu. (2006) Enhanced activity for methanol electro-oxidation on Pt/C+NaZSM-5 composite support catalysts. The 13th National Catalysis Conference, China.
5. X. Meng, X. Li, Y. Chen, **D. Geng**, Y. Zhong, R. Li, X. Sun, (2010) Atomic layer deposition (ALD): a new technique to synthesize nanostructured composites for energy conversion and storage, **The Electrochemical Society Inc. (Canadian Section)**, London, ON, Canada.
6. X. Li, X. Meng, **D. Geng**, J. Liu, J. Wang, Y. Zhang, Y. Zhong, D. Wang, Y. Li, J. Yang, R. Li, X. Sun, (2010) Nitrogen doped CNTs and SnO₂/graphene as anode materials for high performance lithium ion batteries, **The 15th International Meeting on Lithium Batteries (IMLB 2010)**, Montreal, QC, Canada.
7. X. Li, **D. Geng**, X. Meng, J. Wang, J. Liu, Y. Li, D. Wang, J. Yang, R. Li, X. Sun, (2010) Graphene and SnO₂/graphene as anodes of lithium-ion batteries, **The 15th International Meeting on Lithium Batteries (IMLB 2010)**, Montreal, QC, Canada.
8. X. Li, J. Yang, J. Liu, D. Wang, Y. Li, J. Wang, Y. Zhang, D. Geng, **X. Meng**, R. Li, X. Sun, (2010) Nanostructured cathodes and anodes of high performance lithium ion

batteries for EVs and HEVs applications, **NanoOntario**, London, ON, Canada.

9. S. Sun, N. Gauquelin, G. X. Zhang, X. B. Meng, **D. Geng**, R. Li, G. Botton, S. Y. Ye, S. Knights, X. L. Sun, (2011) Atomic Layer Deposition of Pt Nanocatalyst on Graphene and N-doped Graphene for PEM Fuel Cells. **61st Canadian Chemical Engineering Conference**, London, Canada.
10. S. Sun, G. Zhang, X. Meng, **D. Geng**, R. Li, X. Sun, (2011) Atomic Layer Deposition of Pt Nanocatalyst on Graphene Nanosheet for PEM Fuel Cell Applications. **219th Meeting of the Electrochemical Society**. Montreal, Canada.
11. S. Sun, G. Zhang, R. Li, **D. Geng**, Y. Zhong, X. Sun, (2010) Single-Crystal Pt Nanowire-based 3D Electrodes for PEM Fuel Cell Applications. **The International Green Energy Conference (IGEC)**. Waterloo, Canada.
12. S. Sun, G. Zhang, R. Li, **D. Geng**, Y. Zhong, X. Sun, (2010) “Synthesis of Ultrathin Pt Nanowire-based 3D Hierarchical Nanostructures and Their Enhanced Performance as Electrocatalysts in Fuel Cells. **Ontario Nanoscience and Nanotechnology Workshop**. London, Canada.

Awards and Honors:

1. **Western Engineering Scholarship** from 2010-2013, The University of Western Ontario.

2. **Students' Scholarship** for three times 2002-2007
(Awarded by Graduate School of Chinese Academy of
Sciences)